UNIVERSITY OF OKLAHOMA

GRADUATE COLLEGE

THE ROLE OF CELL DEFORMATION DURING SELECTIN-MEDIATED NEUTROPHIL ROLLING

A DISSERTATION

SUBMITTED TO THE GRADUATE FACULTY

in partial fulfillment of the requirements for the

Degree of

DOCTOR OF PHILOSOPHY

By

PHILLIP A. COGHILL
Norman, Oklahoma
2012

Downloaded from SHAREOK. Persistent Handle URL: https://hdl.handle.net/11244/319226

THE ROLE OF CELL DEFORMATION DURING SELECTIN-MEDIATED NEUTROPHIL ROLLING

A DISSERTATION APPROVED FOR THE
SCHOOL OF CHEMICAL, BIOLOGICAL AND MATERIALS ENGINEERING

BY

_____
Dr. David Schmidtke, Chair

_____
Dr. Binil Starly

_____
Dr. Edgar O'Rear

_____
Dr. Matthias U. Nollert

_____
Dr. Rodger McEver

©Copyright by PHILLIP A. COGHILL 2012
All Rights Reserved.

ACKNOWLEDGEMENTS

I would like to extend my sincerest thanks to my advisor, Dr. David Schmidtke. Without his expertise, training and guidance, I certainly would not have been able to attain this monumental achievement. I would also like to thank my committee members: Dr. Matthias U. Nollert, Dr. Edgar A. O'Rear, Dr. Binil Starly and Dr. Rodger McEver for their time and advice both in the classroom and in regard to this dissertation. In addition, I would like to gratefully acknowledge Dr. McEver's contributions to this project by graciously providing me with various reagents and evaluating my work during technical presentations at his weekly laboratory meetings.

I am thankful for the assistance I received from other members of Dr. Schmidtke's group, specifically Dr. Zackary Taylor, Jeffrey Fontenot, Travis Spain and Eddie Shimp. Special thanks are due to Sandra Bryant and Dr. Alexander Christov who taught me a number of the laboratory and microscopy techniques when I first began working in the lab. Furthermore, there are many members of Dr. McEver's research group at the Oklahoma Medical Research Foundation who gave their time to help me with specific analytical techniques. I am especially grateful to Dr. Hendra Setiadi for his help with site density measurements, Dr. Tadayuki Yago and Dr. Bojing Shao for their assistance with the flow cytometer and Cindy Carter for sharing her cell culture expertise. Also, I would like to thank Dr. Damir Khismatullin for running the VECAM simulations that supplemented some of my experimental microfluidic data.

Last but not least, I dedicate this work to my wife, Courtney, and my daughter, Jillian. They brighten my life on the most difficult days and remind me that through perseverance, I can achieve everything to which I set my mind. Also, I thank my parents, Jim and Darla Coghill, my wife's parents, Chaz and Janet Ruark, and my brother and his wife, Mike and Jessica Coghill. All of these family members provided me with tremendous support and encouragement.

Finally, I thank God for placing all of these people in my life and blessing me with the talents to achieve this milestone. "To the only God our Savior be glory, majesty, power and authority, through Jesus Christ our Lord, before all ages, now and forevermore! Amen." –Jude 1:25

TABLE OF CONTENTS

ACKNOWLEDGEMENTS **iv**

TABLE OF CONTENTS **vi**

LIST OF TABLES **xi**

LIST OF FIGURES **xii**

ABSTRACT **xv**

CHAPTER 1: AN INTRODUCTION TO CELL DEFORMATION AND P-SELECTIN MEDIATED NEUTROPHIL ADHESION **1**

Leukocyte Adhesion in Inflammation and Cardiovascular Disease 1

The Inflammation Cascade 2

The Biology of Leukocyte Adhesion 3

The Role of Shear Stress in Cardiovascular Disease 5

Effects of Shear Stress on Molecular Interactions during Leukocyte Rolling 7

Effects of Shear Stress on Cell Deformation 9

Influence of Selectin/Ligand Site Densities on Leukocyte Rolling 12

In Vitro Models of Leukocyte Rolling 13

Cell Size versus Channel Height in Microfluidic Chambers 17

Microfluidic Studies Involving Channel Geometry 18

Overview and Significance 21

CHAPTER 2: REFLECTIVE INTERFERENCE CONTRAST IMAGING OF ROLLING NEUTROPHIL CONTACT AREAS AND MEMBRANE TETHERS **24**

INTRODUCTION 24

METHODS 27

Antibodies and Reagents 27

Neutrophil Isolation 27

Substrates 28

Cell/Substrate Treatments 28

Flow Assay and Metamorph Analysis 28

Image Analysis 29

Ficoll Experiments 30

RESULTS 31

Neutrophil contact area during rolling is dependent on cell/substrate separation distance and shear stress 31

Neutrophil contact area is dynamic and relates to instantaneous rolling velocity 34

RICM images the formation and breakage of membrane tethers during rolling 39

Membrane tether formation and breakage correlate with elevated wall shear stress levels 41

Overall contact area and membrane tether formation correlate with shear stress rather than shear rate 43

DISCUSSION 46

CHAPTER 3: THE INFLUENCE OF LIGAND DENSITY AND LIGAND TYPE ON NEUTROPHIL MEMBRANE TETHER FORMATION DURING ROLLING 53

INTRODUCTION 53

METHODS 58

Antibodies and Reagents 58

Human Neutrophil Isolation 58

Substrates 59

Parallel Plate Flow Assay 59

Tether Analysis 60

RESULTS 61

Elevated P-selectin concentration increases tether lifetime but not tether length 61

Membrane tethers stabilize rolling on high P-selectin concentrations but grow at slower rates 63

Membrane tether lengths and lifetimes are unchanged on a P-selectin-Fc chimera 67

Membrane tether lengths are unchanged on rhE-selectin but lifetimes are significantly longer than on rhP-selectin 70

Membrane tethers formed during rolling on rhE-selectin last longer compared to rhP-selectin at equivalent rolling velocities 72

Multiple leukocyte ligands mediate membrane tether formation on E-selectin 74

DISCUSSION 76

CHAPTER 4: EFFECTS OF MICROFLUIDIC CHANNEL GEOMETRY ON LEUKOCYTE ROLLING ASSAYS 84

INTRODUCTION 84

METHODS 89

Proteins and Reagents 89

Fabrication of Microfluidic Chambers 89

Flow Characterization in Microfluidic Chambers 90

PSGL-1 Coated Beads 91

Neutrophil Isolation 91

Rolling Velocity and Contact Area Experiments 92

Numerical Model 93

RESULTS 96

Microfluidic channel fabrication and Characterization 96

Effects of D_c/H on neutrophil rolling behavior 100

Numerical simulation of the effects of D_c/H on neutrophil rolling behavior 103

Rolling differences are correlated to cell rigidity 104

Effects of D_c/H on neutrophil contact area during rolling 106

DISCUSSION 110

CHAPTER 5: SHEAR STRESS AT BIFURCATIONS AND ITS EFFECTS ON NEUTROPHIL ADHESION 119

INTRODUCTION 119

METHODS 123

Proteins and Reagents 123

Fabrication of Microfluidic Chambers 123

Neutrophil Isolation 123

Perfusion Experiments 124

Analysis of Adhesion Pattern 125

RESULTS 126

Leukocyte Aggregate Formation is Dependent on Channel Cross-Sectional Dimensions 126

Cells adhere at bifurcation apex at high shear but not in the main channel 128

Antibody control experiments 130

Apex adhesion decreases with paraformaldehyde fixation and L-selectin blocking 132

Adhesion at the bifurcation apex decreases with decreasing P-selectin concentration 134

Adhesion at the bifurcation apex decreases with decreasing bifurcation angle 137

DISCUSSION 140

CHAPTER 6: CONCLUSIONS AND FUTURE DIRECTIONS 148

REFERENCES 155

APPENDICES 178

Appendix A: Mathematical description of flow in a rectangular channel 178

Appendix B: Neutrophil Isolation Protocols 182

Appendix C: Photolithography Protocol 184

LIST OF TABLES

Table 1: The Selectins and Their Ligands 4

Table 2: Flow Rate Comparison for Microfluidic vs. Glycotech Chamber 16

Table 3: Published Studies on Membrane Tether Extraction from Neutrophils 57

Table 4: Comparison of Recent Leukocyte Studies Using Microfluidic Devices 86

LIST OF FIGURES

Figure 1: The Inflammation Cascade 3

Figure 2: Schematic of Neutrophil Membrane Tether Formation 11

Figure 3: Illustration of Parallel-Plate Flow Chambers 14

Figure 4: Vertical Step Sudden Expansion Flow Chamber 19

Figure 5: RICM Visualizes Neutrophil "Footprints" During Rolling 32

Figure 6: Instantaneous Velocities and Contact Areas of Neutrophils at 1 dyne/cm^2 33

Figure 7: Instantaneous Velocities and Contact Areas of Neutrophils at 8 dynes/cm^2 34

Figure 8: Instantaneous Velocity Plotted Against Contact Area for Neutrophils at 1 dyne/cm^2 36

Figure 9: Instantaneous Velocity Plotted Against Contact Area for Neutrophils at 8 dynes/cm^2 37

Figure 10: Estimated Number of Microvilli Interacting with the Substrate at $z < 50$ nm 38

Figure 11: Average Neutrophil Contact Area Based on Separation Distance 38

Figure 12: Visualization of Neutrophil Membrane Tether Formation with RICM 40

Figure 13: Membrane Tether Breakage Results in the Deposition of Microparticles and Microfragments 41

Figure 14: Membrane Tether Formation and Microparticle/Microfragment Deposition Correlate with Elevated Shear Stress 42

Figure 15: Membrane Tether Formation and Neutrophil Contact Area are Dependent on Shear Stress Rather than Shear Rate 44

Figure 16: Schematic of the Forces Involved in Neutrophil Membrane Tether Formation 54

Figure 17: Schematic of mP-selectin and rhP- and rhE-selectin-Fc Chimeras 58

Figure 18: Effects of Ligand Density on Neutrophil Membrane Tether Formation During Rolling on mP-selectin 62

Figure 19: Presence of Membrane Tethers Correlate with Decreased Rolling Velocities on a Wide Range of Ligand Densities 64

Figure 20: Effects of Ligand Density on Membrane Tether Growth Rate 65

Figure 21: Instantaneous Velocity Profiles of Neutrophils Rolling on mP-, rhP- and rhE-selectin 67

Figure 22: Comparison of Membrane Tether Formation on mP- and rhP-selectin 69

Figure 23: Comparison of Membrane Tether Formation on rhP- and rhE-selectin 71

Figure 24: Membrane Tether Formation on rhP- and rhE-selectin at Equivalent Neutrophil Rolling Velocities 73

Figure 25: Effects of PSGL-1 Blocking on Tether Formation on rhE-selectin 74

Figure 26: Flow Characterization in Microfluidic Channels 98

Figure 27: Instantaneous Rolling Velocities of Neutrophils on P-selectin in Microfluidic Channels 100

Figure 28: Effects of D_c/H on Average Neutrophil Rolling Velocity and Velocity Variance 102

Figure 29: VECAM Predictions of Instantaneous Neutrophil Rolling Velocities on P-selectin in Microfluidic Channels 104

Figure 30: VECAM Predictions of the Effects of D_c/H on Average Neutrophil Rolling Velocity 105

Figure 31: Effects of D_c/H on the Rolling Velocities of Paraformaldehyde-Fixed Neutrophils and PSGL-1 Coated Microspheres 106

Figure 32: Effects of D_c/H on Neutrophil Contact Area 107

Figure 33: Illustration of the Effect of Channel Height on the Vertical Shear Stress Gradient 113

Figure 34: Images of Diamond Shaped Microfluidic Devices Used to Study Neutrophil Adhesion at Bifurcations 122

Figure 35: Neutrophil Aggregate Formation in a Symmetric Bifurcation 127

Figure 36: Neutrophil Adhesion in a Bifurcated Microfluidic Device with Enlarged Cross-Sectional Dimensions 128

Figure 37: Neutrophil Adhesion Patterns in the Inlet Channel and at the Bifurcation Apex 129

Figure 38: Neutrophil Adhesion at the Bifurcation Apex is Dependent on P-selectin/PSGL-1 Interactions 131

Figure 39: Effects of L-selectin Blocking and Paraformaldehyde Fixation on Neutrophil Adhesion at the Bifurcation Apex 133

Figure 40: Effects of P-selectin Coating Concentration on Neutrophil Adhesion at the Bifurcation Apex 135

Figure 41: Effects of Bifurcation Angle on Neutrophil Adhesion at the Bifurcation Apex 138

Figure 42: Schematic of Flow Deflection at a Bifurcation 141

ABSTRACT

Selectin-mediated neutrophil rolling on endothelial cells is an important step in the biological processes of inflammation and thrombosis. Conversely, it has also been implicated in the pathogenesis of various cardiovascular diseases. While there are many factors that affect this phenomenon, shear stress is among the most significant. Previous studies have demonstrated the effects of shear stress on the selectin/ligand interactions that sustain neutrophil rolling. However, the effects of cell deformation on neutrophil rolling are still under investigation. In this study, the effects of cell deformation on selectin-mediated rolling are investigated on two scales: (I)deformation on a local scale such as contact zone deformation or membrane tether formation and (II)deformation of the cell body on a global scale.

We present reflective interference contrast microscopy (RICM) as a low-cost alternative to current microscopy techniques used to visualize cell footprints during rolling (i.e. quantitative dynamic footprinting). RICM visualized neutrophil contact areas similar to those reported by qDF and also visualized the formation of membrane tethers from distinct adhesion points. We also use RICM to show that membrane tether formation and neutrophil contact area are dependent on shear stress rather than shear rate.

Alternatively, using differential interference contrast (DIC) microscopy we demonstrate that increased membrane tether lifetime correlates with increasing P-selectin density while increased tether length correlates with increased shear stress. We also report the characterization of membrane tether formation on recombinant human P- and E-selectin-Fc chimeras.

Cellular deformation on a global scale has been suggested to occur as a result of the shearing force applied to an adherent cell by hemodynamic flow. Previous computational studies have related this shear effect to the ratio between the diameter of the cell (D_c) and the height of the channel being perfused (H). Although this D_c/H ratio can be large for neutrophils in post-capillary venules where leukocyte rolling typically occurs, many in vitro studies have used flow chambers where D_c/H is small (< 0.1).

To investigate leukocyte rolling in chambers with dimensions similar to post-capillary venules, we fabricated microfluidic chambers with various cross-sectional dimensions that required perfusion rates as low as 40 nL/min. We observed a significant decrease in neutrophil rolling velocity on P-selectin that correlated with decreasing chamber height (increasing D_c/H). Comparable studies with fixed cells and PSGL-1 coated microspheres, as well as contact area measurements made with RICM, demonstrated this velocity decrease was related to cell deformability.

Likewise, we fabricated bifurcated microfluidic chambers to investigate the impact of chamber geometry on neutrophil adhesion. Neutrophils accumulated at the bifurcation apex in P-selectin coated chambers at shear stresses as high as 100 dynes/cm^2. Similarly, we used fixed cells to demonstrate that this accumulation is related to cellular deformation. We also report that adherent cell accumulation is dependent on specific molecular interactions, P-selectin coating concentration and the geometric properties of the chambers (e.g. bifurcation angle and channel cross-section dimensions).

Chapter 1: An Introduction to Cell Deformation and Selectin-Mediated Neutrophil Adhesion

Leukocyte Adhesion in Inflammation and Cardiovascular Disease

Inflammation and hemostasis are important biological processes that help the body maintain its natural state. These processes involve a number of cellular and sub-cellular components of the circulatory system including leukocytes, endothelial cells, platelets and various circulating plasma proteins. Leukocytes play an important role in these processes by interacting with and rolling on endothelial cells or platelets through specific molecular interactions[78, 151, 178]. Although some of these interactions can take place under static conditions, the normal circulation of blood flow in the body creates a shear force that these interactions must be able to withstand. This leads to the phenomenon of leukocyte rolling, which is an important first step in the overall migration of leukocytes to sites of inflammation and injury.

Although inflammation is an important defense mechanism, inflammatory cells have been implicated in the pathogenesis of a number of cardiovascular diseases including thrombosis[60, 179], stroke[117], sepsis[6], cardiovascular complications from diabetes[26, 141] and myocardial infarction[75]. Leukocyte interactions with the endothelium also play a role in the infiltration of these cells into atherosclerotic lesions[92] as well as in atherosclerotic plaque rupture[247]. While shear stress is extremely influential in promoting leukocyte-endothelial interactions during the early stages of inflammation, it has also been shown to promote the formation of leukocyte-leukocyte and leukocyte-platelet aggregates that can disrupt the overall consistency of circulation in the vasculature[12, 93, 99, 116]. Such changes in shear stress can also influence the regulation of adhesive proteins

expressed by endothelial cells through a process known as mechanotransduction. Further investigation of the effects of shear on inflammatory cells will lead to a better understanding of the role these cells play in the pathogenesis of cardiovascular diseases.

The Inflammation Cascade

During inflammation, leukocytes are recruited to and extravasate through the endothelial cell layer that lines the inside of the vasculature. This process, known as the inflammation cascade, occurs through a series of steps that involve specific molecular interactions. These steps include capture, initial rolling, slow rolling, firm adhesion and extravasation (Figure 1) [136, 233]. Leukocyte rolling is initiated when transmembrane proteins expressed on the tips of leukocyte microvilli interact with E-selectin expressed by activated endothelial cells[14], P-selectin expressed by activated platelets and endothelial cells[107] or L-selectin expressed by other leukocytes[238]. As these selectin-ligand interactions reduce the velocity of a circulating leukocyte, the surrounding blood flow imposes a shear stress on the captured cell causing it to translocate downstream.

When imposed upon by a certain level of shear stress, selectin-ligand bonds have been shown to have transient lifetimes with very high k_{off} rates compared to static conditions[5]. At the leading edge of the cell, however, cell surface ligand interactions with selectins correlate with shear rate rather than shear stress leading to rapid bond formation[36]. This continuous formation and dissociation of bonds results in a rolling-like motion. It is this rolling mechanism that allows the cell to sample chemokine signals expressed by the endothelium[105, 134], which in turn

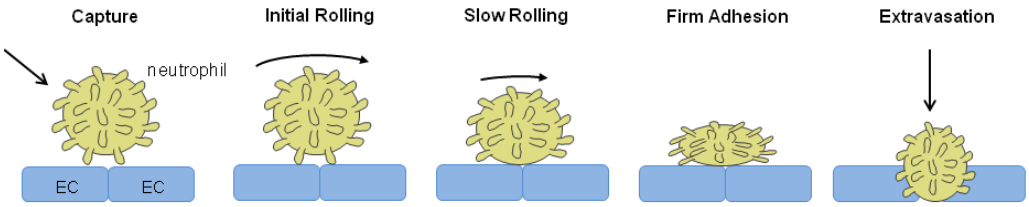


Figure 1: A Schematic of the Leukocyte Adhesion Cascade

activate the integrin proteins expressed on the leukocyte membrane[65, 79, 128]. Integrin-mediated interactions have longer lifetimes under shear than those mediated by selectins. Thus, these interactions lead to slower rolling and arrest before the cell ultimately leaves the blood stream to migrate to the inflammation site.

The Biology of Leukocyte Adhesion

Selectin proteins have a very unique structure that makes them well suited to inflammatory adhesion. Their structure consists of an extracellular domain, a transmembrane domain and a short cytoplasmic domain[154, 248]. At the NH_2 terminus of each selectin is a lectin domain by which the selectin is able to bind to its various ligands. This domain is followed by an epidermal growth factor (EGF)-like domain and a specific number of short consensus repeats[259]. These repeats have been suggested to be necessary in order to extend the lectin domain to a sufficient length above the plasma membrane[185]. The transmembrane domain and the cytoplasmic domain play an important role in targeting P-selectin to Weibel-Palade bodies[48, 64]. From these bodies, P-selectin is then up-regulated to the cell surface in response to certain chemical signals[151].

Table 1: The Selectins and Their Ligands

Selectin	Cell Type	Ligand	Cell Type
P-selectin	Platelets/Endothelial Cells	PSGL-1	Leukocytes
		CD-24	Leukocytes
E-selectin	Endothelial Cells	PSGL-1	Leukocytes
		CD-44	Leukocytes
		ESL-1	Leukocytes
L-selectin	Leukocytes	PSGL-1	Leukocytes
		PNAd	Endothelial Cells

While several ligands to selectin proteins have been shown to exist (Table 1), there is one of significant physiological relevance. P-selectin glycoprotein ligand-1 (PSGL-1) is a homodimeric mucin expressed on the microvilli of nearly all leukocytes[151]. PSGL-1 is the key ligand that mediates leukocyte adhesion to P-selectin on activated platelets and endothelial cells[162, 174] as well as L-selectin on other leukocytes[55, 161]. It should be noted that tumor cells expressing CD-24 have also been reported to roll on P-selectin[1]. Although PSGL-1 also mediates neutrophil rolling on E-selectin, it has been suggested that neutrophils may express other ligands to E-selectin such as E-selectin ligand-1 (ESL-1) and CD-44[96]. Indeed, previous studies have demonstrated that leukocytes can roll on E-selectin in the absence of PSGL-1, however this function is significantly impaired[258, 262]. The role of these additional ligands in neutrophil rolling on E-selectin is still under investigation.

PSGL-1 mediated adhesion occurs because the lectin domains of the selectins have a low affinity for O-glycans expressed along the backbones of mucin proteins. Using recombinant forms of PSGL-1 and various biochemical assays, the binding of PSGL-1 and P-selectin has been thoroughly studied. Leppanen et al

showed that P-selectin achieves optimal binding with PSGL-1 when a modified core-2 O-glycan is present at residue Thr-44 along with sulfation of the tyrosine residues at Tyr-46, Tyr-48 and Tyr-51[133]. Post-translational modification of the O-glycan at Thr-44 includes the addition of the tetrasaccharaide, sialyl Lewis^x (sLe^x), which is necessary for binding with P-selectin[138]. It has been shown previously that selectins can bind sLe^x alone both under static[13, 67, 191] and low shear stress conditions ($\tau \leq 2$ dyn/cm^2) [4, 24, 206, 259].

In addition to leukocyte-endothelial cell interactions, there are several ways that leukocytes can interact with platelets during thrombus formation and vascular repair. Specifically, monocytes have been shown to express both PSGL-1, which can interact with platelet P-selectin, and tissue factor (TF) which plays an important role in thrombus formation by working with factor VIIa to convert factor X into factor Xa[164-165]. Weber and Springer also observed that polymorphonuclear leukocytes can arrest on platelet layers through interactions between leukocyte Mac-1 and fibrinogen bound to platelets via the integrin αIIbβ3[253]. Indeed, the absence of Mac-1 has been shown to significantly impair leukocyte accumulation at sites of vascular injury[226]. Also, Mac-1 has been observed to bind to GPIbα[225].

The Role of Shear Stress in Cardiovascular Disease

Although inflammatory cell adhesion depends heavily on interactions between specific adhesion molecules, shear stress has also been shown to influence leukocyte adhesion in various cardiovascular diseases. Atherosclerotic lesion formation has been observed to localize in regions of unsteady shear throughout the arterial tree such as those found at bifurcations[127, 170, 183]. Several studies have

examined the role of shear stress in the progression of atherosclerosis[81, 121, 176], and a recent computational study has suggested that vascular remodeling, which can be tied in part to atherosclerotic plaque development, can cause changes in wall shear stress consistency[76]. These changes can have detrimental effects both in terms of cell adhesion and also the vascular wall itself.

Changes in shear stress not only result in the continuous build up of adherent cells in unsteady shear zones; they can also affect the endothelium through a process known as mechanotransduction. Mechanotransduction occurs through physical stimuli caused by shear stress and can result in physical changes (e.g. vascular remodeling[126, 157] and the alteration of cell morphology[145]) or biochemical changes where forces exerted on a cell can up-regulate proinflammatory adhesion molecules[37, 169] (for an in-depth review of mechanotransduction, see [44]). Brakemeier et al showed that the regulation of gene IKCa1, which is responsible for the activation of potassium channels leading to cell hyperpolarization, is governed by shear stress[20]. The hyperpolarization induced by IKCa1 has been shown to be important to overall endothelial cell function during inflammation. Also, shear stress has been shown to cause changes in cell morphology through mechanisms involving the remodeling of the cytoskeleton that are dependent on tyrosine kinase, intracellular calcium and the cytoskeletal network itself.

Other studies have shown that the production of prostacyclin, a potent vasodilator and inhibitor of platelet aggregation, is also linked to shear. Frangos et al showed that endothelial cells exposed to pulsatile shear produced prostacyclin at a rate more than twice that of cells exposed to steady shear and 16 times greater than

cells in stationary culture[69]. This suggests that areas of the vasculature that experience less pulsatile stress could be more vulnerable to atherosclerotic plaque build-up. Ranjan et al also observed an increase in constitutive nitric oxide synthase (cNOS) mRNA and protein levels in endothelial cells exposed to arterial shear stress levels but not in cells subjected to venous shear stresses[199]. This study demonstrated that endothelial cell production of vasodilators can be linked to elevated shear stress levels. Conversely, increased shear can also lead to the increased expression of endothelial adhesion molecules. Nagel et al showed that HUVECs exposed to a shear stress of 10 dynes/cm^2 expressed ICAM-1 at significantly greater levels over time than cells in static conditions[169]. While these studies have shown that shear stress can have a profound impact on endothelial cells, its effects on leukocyte rolling and adhesion during inflammation are still being investigated.

Effects of Shear Stress on Molecular Interactions during Leukocyte Rolling

Shear stress has been shown to significantly influence leukocyte rolling by affecting the kinetics of selectin-ligand interactions. In 1978, George Bell proposed that the net dissociation rate for lectin-carbohydrate bonds that mediate adhesion between two cells could be determined as:

$$k = k_o exp(\frac{\gamma f}{k_B T}) \quad (1)$$

where k_o is the unstressed dissociation rate, γ relates the ability of two molecules to interact to the distance separating them, $k_B T$ is the thermal energy and f is the force applied to the bond[11]. This model suggests that the bond is more likely to dissociate when increasing tensile force is applied to it, thereby describing what is

known as a slip bond. In most cases, the bonds that form and dissociate during leukocyte rolling adhere to slip bond kinetics. Indeed, Alon et al observed that while the unstressed off-rate of a PSGL-1/P-selectin bond averaged approximately 1 s^{-1}, the application of 1.1 dynes/cm^2 of shear stress (equivalent force loading of 112 pN) more than tripled k_{off} to 3.5 s^{-1}[5].

In contrast, the peeling model during the disruption of cell adhesion presented by Dembo et al suggested that there are potential cases where tension applied to a bond may help lock the bond into place rather than disrupt it[46]. This provided the theoretical basis for catch bonds, which display a positive correlation between bond lifetime and force loading. Finger et al reported that at low shear stresses, leukocytes rolling on peripheral node addressin (PNAd) through L-selectin-mediated binding required a minimum threshold shear stress to initiate rolling interactions[62]. Further studies also demonstrated that P- and E-selectin-mediated leukocyte rolling also displayed this minimum threshold shear behavior; however, this behavior was also dependent upon the site densities of the immobilized selectins[129].

In 2003, Marshall et al reported the first direct observation that increasing force could prolong the lifetimes of P-selectin/PSGL-1 complexes[148]. The AFM and flow chamber measurements in this study elucidated a transition mechanism where P-selectin/PSGL-1 bonds exhibited catch bond behavior at low force loading but transitioned to slip bond behavior as force was increased. Further work by Evans et al showed that P-selectin/PSGL-1 complexes exhibit a two-pathway mechanism for dissociation where the bonds dissociate quickly when the force loading is slowly

ramped up but actually strengthen when quickly loaded with a jump in force[57]. While these studies demonstrated the existence of catch bonds, they did not clarify the role that catch bonds play in leukocyte rolling. That role was defined, however, through experiments performed by Yago et al which showed that catch bonds stabilize L-selectin-mediated neutrophil rolling at threshold shear[260]. Recently, Wayman et al also reported a role for catch bonds in E-selectin-mediated cell adhesion[252]. These studies clearly demonstrate the influence of shear stress on the molecular kinetics of leukocyte rolling.

Effects of Shear Stress on Cell Deformation

Although shear stress plays an important role in leukocyte rolling through its effects on molecular interactions, shear stress can also influence leukocyte rolling by affecting cellular deformation. Previous studies have identified two scales for shear stress induced cell deformation: (I) local deformation through the extrusion of membrane tethers and (II) global deformation involving changes in cell morphology. Shao and Hochmuth first demonstrated the phenomenon of tether extrusion from leukocytes using a micropipette and antibody-coated microspheres.[223] They showed that when cells interacted with the beads and then were pulled away, occasionally thin cylinders of plasma membrane were extruded from the cell body. Because PSGL-1 is located on the tips of leukocyte microvilli, theoretical studies have suggested that microvillus extension can act as a mechanism for tether extrusion. Indeed, Pawar et al found through simulation that microvillus viscoelasticity influenced leukocyte rolling velocity at shear rates of 200 – 400 s^{-1} (P-selectin density = 150 sites/μm^2) but not under low shear and ligand density

conditions (10 – 100 s^{-1}; P-selectin density = 15 sites/μm^2).[186] The detachment of the plasma membrane from the cytoskeleton has also been suggested as an important step during membrane tether formation. Tether formation in red blood cells has been shown to involve the separation of the membrane from the membrane-associated cytoskeleton.[251] A recent study further observed that membrane tether formation in leukocytes appeared to coincide with the unbinding of the plasma membrane from the cytoskeleton.[56] This conclusion was strengthened by the significant decrease in force required to pull a membrane tether when neutrophils were treated with F-actin polymerization inhibitors.

Although these studies demonstrate that leukocytes form membrane tethers, they do not demonstrate a role for these tethers in leukocyte rolling. Chen and Springer suggested that membrane tethers might be responsible for balancing the fast dissociation rate of selectin-ligand bonds, thereby allowing leukocytes to roll even under high shear stress conditions.[35] Membrane tether formation was not observed during leukocyte rolling, however, until Schmidtke and Diamond published the first direct observations of this phenomenon.[219] They found that leukocytes interacting with selectin-coated surfaces or immobilized platelets under shear stress conditions could extrude thin membrane tethers (see Fig. 2). These tethers have since been shown to stabilize leukocyte rolling by reducing the angle of P-selectin/PSGL-1 bonds, thereby decreasing the torque applied to them.[182]

Additional investigation has shown that the formation of membrane tethers correlates to shear stress, as cells under high shear flow have been observed to pull multiple tethers at once.[197] Furthermore, Schmidtke and Diamond reported that

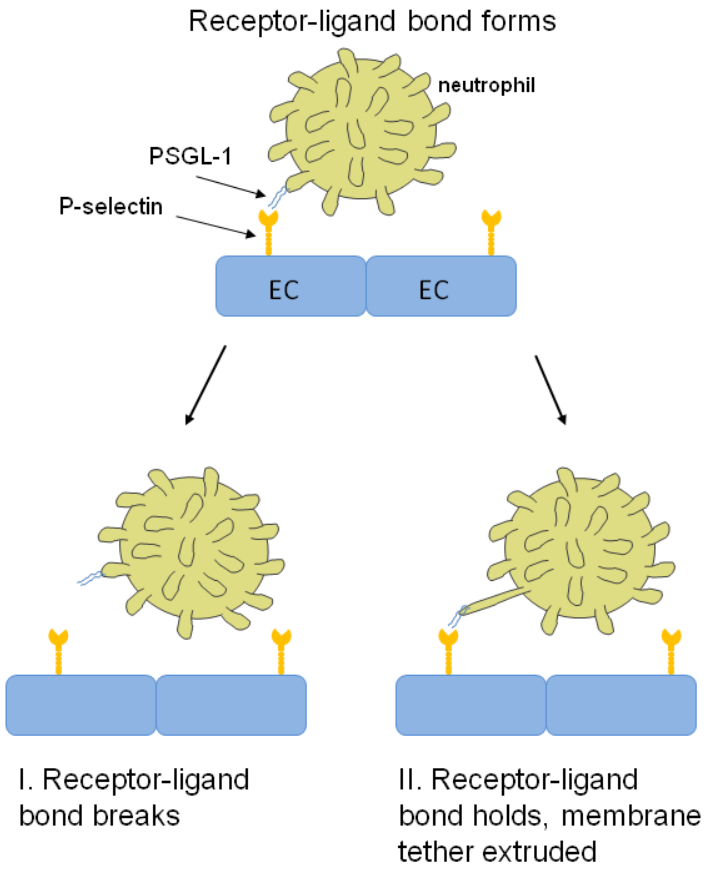


Figure 2: Schematic of membrane tether extrusion during P-selectin mediated rolling

these membrane tethers could potentially be multi-bonded to a selectin-coated surface.[219] This idea arose from observations that membrane tethers occasionally displayed branching structures rather than a simple straight line. The ability of membrane tethers to bond to a surface at multiple points suggested that rolling could be further stabilized as the tether length grew. These observations could also support the hypothesis that increased tether formation could be observed with increasing the number of sites available for selectin/PSGL-1 binding.

Shear stress has been shown to affect leukocyte rolling not only through local deformation effects, but also through global cell deformation. Firrell and Lipowsky reported that neutrophils rolling in rat mesenteric vessels elongated in the

direction of flow under increased shear stress.[63] Additional studies have also observed that adherent leukocytes in vivo deform from spherical shapes into ellipsoidal teardrop-like shapes when subjected to shear stress.[43, 49, 231] Theoretical simulations of leukocyte rolling have also posited that rolling leukocytes in flow can deform due to the viscoelastic nature of the cell membrane.[101, 112]

These studies suggested that cell deformation could influence leukocyte rolling through a significant increase in leukocyte-endothelial cell contact. This conclusion was supported by additional reports that leukocytes roll at near constant velocities under a wide range of shear stresses. As further evidence of the effects of cell deformation, Templeman et al observed that rigid ligand-coated microspheres, when rolled on the same surface with the same ligand density as deformable cells, exhibited higher rolling velocities than the cells.[239] Indeed, Yago et al observed that neutrophils could remain attached to P-selectin coated substrates even at relatively high shear stresses while ligand-coated microspheres could not sustain rolling interactions above a threshold shear stress.[259] While these studies demonstrate that shear stress influences leukocyte rolling through deformation, there is still much work to be done in determining the impact of these physical effects.

Influence of Selectin/Ligand Site Densities on Leukocyte Rolling

In addition to the effects of shear stress, it should be noted that the number of selectin and ligand molecules available for binding can also have a profound effect on leukocyte rolling. In fact, the dependence of leukocyte rolling on selectin site density has been well established. Lawrence and Springer reported a significant increase in the number of neutrophils bound to a lipid bilayer reconstituted with P-

selectin when site density was increased from 50 – 400 sites/μm^2[130]. Similarly, the same increase in site density resulted in a fourfold increase in rolling velocity at wall shear stresses ranging from 0.36 – 7.3 dynes/cm^2. Lawrence and Springer also reported the same trends were observed for neutrophils rolling on immobilized E-selectin, although rolling on E-selectin was noticeably slower compared to rolling on P-selectin[131]. Further studies also observed decreases in neutrophil adhesion when fewer P- or E-selectin sites were immobilized on plastic substrates or expressed by transfected CHO cells[129, 184]. P-selectin/ligand kinetics experiments performed by Alon et al have even suggested that neutrophils could interact with multiple selectin molecules at a site density of 15 sites/μm^2[5]. Computational simulations of neutrophil rolling on P-selectin have also suggested that decreased rolling velocity correlates with an increase in P-selectin site density[91]. Neutrophil rolling velocities have also been measured for L-selectin mediated rolling on PNAd[3] and cell surface ligand mediated rolling on L-selectin[2]. In both cases, decreases in rolling velocity correlated with an increase in the site density of the immobilized ligand.

In Vitro Models of Leukocyte Rolling

In vitro models have provided researchers with the opportunity to study physiologically-relevant events in a simplified system that requires control of only a small number of variables. Although these systems take a number of assumptions into account, they have provided valuable insight into the mechanisms behind many different physiological occurrences. One of the most common tools for modeling leukocyte rolling in vitro is the parallel-plate flow chamber (Figure 3A). These

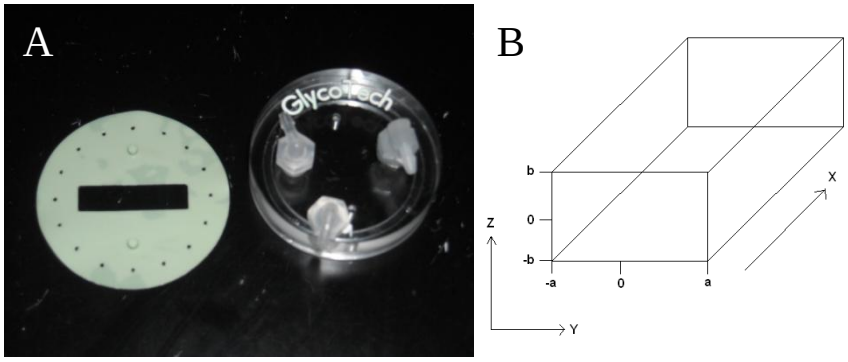


Figure 3: (A)A typical parallel-plate flow chamber (unassembled) (B)Schematic of a rectangular parallel-plate flow chamber

chambers typically consist of a rectangular channel bounded on the top and bottom by immobilized flat plates. The bottom wall is usually a glass cover slip or microscope slide which can be adhered to the rest of the chamber through vacuum. Often, the top wall will be comprised of a flow deck with the height and width of the channel provided by an attached gasket.

The flow velocity profile in a parallel-plate flow chamber can be modeled computationally by beginning with the conservation of momentum equation. If the x-axis is assumed to lie along the length of the channel and the y- and z-axes correspond to the width and height of the chamber respectively (Figure 3B), then the conservation of momentum equation for flow in the x-direction can be given as:

$$\rho\left(\frac{\partial v_x}{\partial t}+v_x\frac{\partial v_x}{\partial x}+v_y\frac{\partial v_x}{\partial y}+v_z\frac{\partial v_x}{\partial z}\right)=-\frac{dP}{dx}+\mu\left(\frac{\partial^2 v_x}{\partial x^2}+\frac{\partial^2 v_x}{\partial y^2}+\frac{\partial^2 v_x}{\partial z^2}\right)+\rho g_x \qquad (2)$$

Equation (2) can be simplified to the following differential equation:

$$0=-\frac{dP}{dx}+\mu\left(\frac{\partial^2 v_x}{\partial y^2}+\frac{\partial^2 v_x}{\partial z^2}\right) \qquad (3)$$

by negating terms according to well-accepted assumptions regarding fluid properties and experimental setup. Appendix A presents the full derivation for flow in a rectangular channel along with a discussion of the various assumptions.

Additionally, the second derivative of v_x with respect to y can be removed if the flow velocity is assumed to be independent of lateral position (chamber width). Previous studies have demonstrated this assumption holds if the ratio of channel width to height (W:H) is greater than 10:1[41, 214], which is the case for most parallel-plate flow chambers including the Glycotech chamber used in the following studies (W = 5000μm, H = 250μm).

The solution of equation (3) gives a parabolic velocity profile with respect to channel height with maximum velocity at the center. The velocity equation can be integrated over the height and width of the channel to determine the volumetric flow rate in terms of pressure drop, which can then be substituted back into the velocity equation. From there, taking the derivative of the velocity equation with respect to channel height yields the equation for shear rate (see Appendix A for full derivation). For adherent cells, the wall shear rate (shear rate at the vertical position equal to the bottom wall) is particularly important and is given in terms of channel dimensions and flow rate as:

$$\gamma_{z,wall} = 3Q/4b^2a \qquad (4)$$

where Q is the volumetric flow rate, b is half the channel height (H/2) and a is half the channel width (W/2).

Another important calculation in leukocyte rolling is the drag force applied to an adherent cell as a result of hemodynamic flow. Goldman, Cox and Brenner initially determined this force could be calculated as:

$$F_{GCB} = 6\pi kzR\tau_w \qquad (5)$$

Table 2: Flow Rate Comparison for Microfluidic vs. Glycotech Chamber

Wall Shear Rate (s-1)	Microfluidic Chamber Flow Rate (μL/min)	Microfluidic Chamber 5-Minute Perfusion (mL)	Glycotech Chamber Flow Rate (μL/min)	Glycotech Chamber 5-Minute Perfusion (mL)
25	2.5	12	80	400
50	5	25	160	800
100	10	50	320	1600
200	20	100	650	3300
400	40	200	1300	6500
800	80	400	2600	13000

where z is the distance between the wall and the center of the cell, k is a correction factor that takes wall effects into account, R is the radius of the sphere and τ_w is the wall shear stress[87]. Equation (5) assumes that the cell is a rigid sphere and that shear stress is constant across the height of the cell. The assumption of constant shear stress implies a linear velocity profile, which has been proven to be valid only when the ratio of cell diameter to chamber height (D_c/H) is less than 0.1.[194] Although this assumption works well for parallel-plate flow chambers, including the Glycotech chamber ($D_c/H = 0.03$ when $D_c \sim 8\mu m$), leukocyte rolling has most often been observed in post-capillary venules[7, 15, 63, 97, 106, 137, 174], which have diameters ranging from 30 – 100 μm. This means that the constant shear stress assumption made by Goldman, Cox and Brenner is not valid in these vessels, and large parallel-plate flow chambers will not properly model leukocyte rolling in the microvasculature. Therefore, in vitro modeling of leukocyte rolling in post-capillary venules requires flow chambers with similarly small dimensions. Custom microfluidic flow chambers can be fabricated to meet this criterion and can be practical alternatives to large parallel-plate flow chambers when limited sample

volumes are available (Table 2). Although custom microfluidic chambers have such great potential, their use in modeling leukocyte rolling has been limited.

Cell Size versus Channel Height in Microfluidic Chambers

Much effort has been devoted to investigating why leukocyte rolling is most often observed in the microvasculature and how this rolling differs from adhesion in larger vascular structures. Some studies have suggested that leukocytes entering post-capillary venules are pushed towards the vascular wall as a result of physical interactions with red blood cells[187, 235]. Indeed, previous observations have noted that red blood cells entering post-capillary expansions tend to flow faster than leukocytes, thereby displacing leukocytes toward the outer walls of the venules[218]. Additionally, physical interactions between red blood cells and leukocytes can potentially cause leukocytes to deform while adhering to the vessel wall, leading to increased surface area for adhesive interactions to take place[158].

Interactions between cells, however, are not the only factor involved in increased leukocyte adhesion in the microvasculature. In smaller vessels, a single adherent leukocyte will occlude a much larger percentage of the flow compared to larger veins. Theoretical studies have examined the effects of leukocyte adhesion on the flow in post-capillary venules and how these changes in flow in turn affect the forces acting on the leukocyte[31, 49]. These studies showed that as channel height decreases relative to cell size (increasing D_c/H), the greater flow occlusion leads to an increase in the drag force acting on the cell as a result of an increase in pressure drop across the cell surface. Simulations of leukocyte rolling in microfluidic chambers performed by Khismatullin and Truskey predicted this increased drag

force would result in increased cell contact time[111]. They explained that the increased drag force would result in a subsequent increase in torque on the cell, thereby bringing a greater portion of the front edge of the cell into contact with the chamber wall. Therefore, cells would be more likely to remain in contact with the wall instead of detaching.

Although numerous theoretical studies have examined the effect of cell size relative to channel height, little investigation has been done to determine how channel height actually affects leukocyte rolling behavior. While in vivo studies have been performed to examine leukocyte rolling in post-capillary venules, there are many factors in addition to the flow dynamics that must be accounted for. Microfluidic chambers provide a simplified system where the effects of flow on leukocyte adhesion in microvasculature-sized structures can be studied independent of other factors.

Microfluidic Studies Involving Channel Geometry

Microfluidic chambers can also serve as a novel technology for modeling leukocyte adhesion in studies involving channel geometry. Studies have shown that hemodynamic flow is dependent upon channel geometry and that geometric complexities can lead to regions of unsteady shear[119, 173, 205]. These unsteady shear regions have been observed to be target sites for atherosclerotic plaque formation[66, 170, 183]. One such particular geometric structure that is known to promote cellular adhesion due to unsteady shear is the bifurcation.

Bifurcations exist naturally throughout the vasculature and have been shown to be vulnerable sites for increased inflammation and atherogenesis. Studies

modeling the flow at bifurcation sites have been performed for some time, and the computational models built in these studies have become increasingly complex[16, 58, 70, 108]. More recently, researchers have used MRI or CT scan data to create models to overcome the problem of over-simplified geometries[124, 234]. These computational studies and others have shown that a stagnation point exists at the apex of a bifurcation[72, 188]. This low shear zone not only presents an area of unsteady shear which could potentially disrupt endothelial cell morphology and function, but could also serve as a site for leukocyte adhesion. Although these studies demonstrate that disturbed flow exists at bifurcations, they do not investigate the pattern of leukocyte adhesion in regions of disturbed flow.

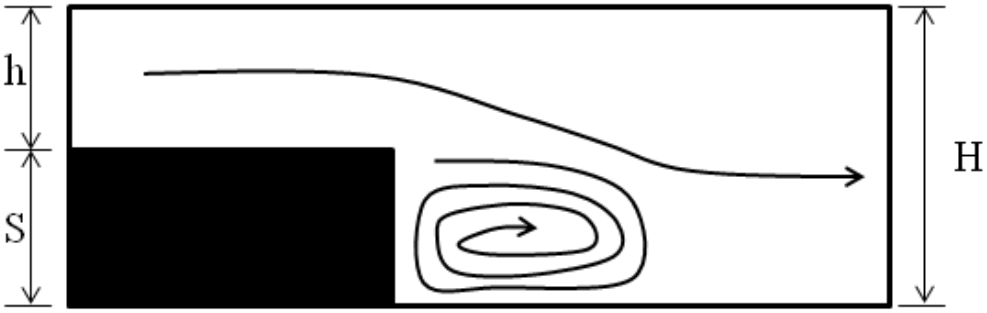


Figure 4: Side view schematic of a vertical step sudden expansion flow chamber with recirculation zone

Much of the work that has explored leukocyte adhesion under disturbed flow in vitro has been performed in sudden expansion flow chambers, where an additional gasket is used to create a vertical step function (Figure 4). Truskey et al demonstrated that this step function could induce the formation of recirculation zones just downstream of the step[240]. While these chambers have been used mostly to study the effects of recirculating flow on endothelial cells[38, 255-256],

Barber et al also reported that U-937 cells adhered to endothelial cells at certain points in the recirculation zone[9]. Further studies demonstrated that neutrophils could adhere to P-selectin in the recirculation zone even when the shear stress downstream of the step was too high to support selectin-mediated rolling[228]. Similarly, platelets immobilized on collagen were also able to capture free-flowing neutrophils in the recirculation zone even at high shear stress[229]. While these studies demonstrate leukocyte recruitment to areas of disturbed flow, they do not address the pattern of leukocyte adhesion specifically at bifurcated geometries.

Recent *in vivo* studies involving mice have reported patterns of atherogenesis at bifurcations similar to those found in humans[198, 254]. While these studies have demonstrated that bifurcations naturally promote cell adhesion and atherosclerotic plaque formation, there are many different factors that must be taken into account. In particular, it is extremely difficult to determine what role the vascular geometry plays in cell adhesion relative to other factors such as circulating proinflammatory signals and endothelial cell function and signaling. For this reason, microfluidic channels can be used to provide simplified systems in order to specifically study how channel geometry affects cell adhesion. Little work has been done, however, to investigate the effects of shear disturbance at bifurcations specifically on selectin-mediated leukocyte adhesion. As selectin-mediated rolling is known to be more prevalent at lower shear stresses, it is possible that regions of low shear such as those found at bifurcations could promote the initial PSGL-1/P-selectin interactions that mediate leukocyte rolling.

Overview and Significance

Leukocyte rolling on selectins has been shown to be an important first step in the inflammatory process and is also significant in the pathogenesis of a range of cardiovascular diseases. Shear stress influences selectin-mediated neutrophil adhesion and rolling by affecting both local and global cellular deformation. While the effects of global cell deformation on contact area have been investigated through measurements of the length of contact between the cell and underlying substrate, only a few studies have investigated methods for directly imaging the underlying footprints of rolling leukocytes. In chapter 2 we present reflective interference contrast microscopy (RICM) as a low-cost technique for visualizing the footprints of rolling neutrophils. A simple thresholding algorithm allowed us to isolate areas of low separation distance between the cell and substrate. RICM also visualized the formation of membrane tethers from these regions. This study also uses RICM to investigate the effects of shear stress and shear rate on tether formation and overall contact area or cell "footprint".

However, shear stress is only one of many factors that influence leukocyte rolling. Another significant factor is the number of selectin and ligand molecules available for binding. While the effects of selectin density have been well documented for leukocyte rolling, there have been no reports as to how it affects membrane tether formation. E-selectin has also been shown to mediate leukocyte rolling with reports of slower rolling velocities compared to P-selectin. Additionally, the ability of ligands distinct from PSGL-1 to mediate rolling on E-selectin is also under investigation. Chapter 3 uses differential interference contrast

(DIC) microscopy to investigate how ligand density and ligand type work in conjunction with shear stress to mediate membrane tether formation.

Chapter 4 presents an in-depth discussion of theoretical studies which have proposed that microfluidic chamber height plays a role in shear stress, which can in turn affect selectin-mediated leukocyte rolling. This discussion is accompanied by experimental work which investigates how varying microfluidic chamber height and the resulting changes in shear stress affect P-selectin-mediated neutrophil rolling. Chapter 5 extends the investigation of the effects of shear stress on neutrophil rolling to include channel geometry, specifically sites of bifurcation. This study examines how regions of low shear can promote neutrophil adhesion even when the overall perfusion rate is very high. Finally, chapter 6 discusses the overall conclusions of these studies and gives recommendations for future work.

The studies presented herein are significant in that they provide a better understanding of a vital physiological process. The studies in chapter 2 present a simple microscopy technique that gives insight into the dynamic nature of neutrophil footprints during selectin-mediated rolling. They also demonstrate that this technique can be used to gain a better understanding of the formation of membrane tethers, both in terms of the points in the cell footprint from which they originate and the observation that their formation is mediated by shear stress rather than shear rate.

Membrane tethers are important in that they stabilize leukocyte rolling velocities at a range of shear stresses. However, there has been little work to determine how other factors in conjunction with shear stress affect membrane tether

formation. The work discussed in chapter 3 demonstrates that increased tether formation correlates with increased ligand density as well as increased shear stress. This work also reports the direct observation of membrane tether formation on E-selectin and shows differences in membrane tether lifetime but not tether length on this ligand.

The studies in chapter 4 are novel in that they utilize microfluidic chambers with dimensions close to post-capillary venules (200 x 20 μm, W x H) that require 13 – 390 times less sample volume than previously reported microfluidic studies. The rolling velocities observed in these chambers experimentally confirm the predictions of previous theoretical studies that decreased leukocyte rolling velocity correlates with decreasing channel height, thereby demonstrating a need for new experimental methods to better model leukocyte rolling in the microvasculature. Additionally, understanding the effects of shear stress variations caused by channel geometry on leukocyte rolling may lead to a better understanding of the pathogenesis of atherosclerosis and myocardial infarction. Indeed, the work discussed in chapter 5 shows that adherent leukocytes can accumulate at the apex of a bifurcation even under very high shear stress. Furthermore, these studies demonstrate that this accumulation is dependent on cellular deformation, as well as specific molecular interactions and the geometric properties of the microfluidic chamber. Overall, the work detailed here provides additional insight into the physical influence of shear stress on P-selectin-mediated neutrophil rolling.

CHAPTER 2: Reflective Interference Contrast Imaging of Rolling Neutrophil Contact Areas and Membrane Tethers

Introduction

The recruitment of leukocytes to the blood vessel wall is a critical process in a number of acute and chronic physiological pathologies including thrombosis,[28, 179] inflammation,[135, 149-150] myocardial infarction,[68, 177] stroke,[204, 212] atherosclerosis,[54, 80, 198] and cancer metastasis[18, 100, 114]. Capture of leukocytes by the vessel wall leads to leukocyte rolling, which allows leukocytes to survey the endothelium for inflammatory signals that can activate them and cause firm adhesion and transendothelial migration. The initial capture and subsequent rolling of leukocytes on activated endothelial cells, activated platelets, or other leukocytes is mediated by a family of transmembrane glycoproteins called the selectins. P-selectin is expressed on activated platelets and endothelial cells, E-selectin is expressed on activated endothelium, and L-selectin is expressed on most leukocytes. Whether a leukocyte rolls on the vessel wall depends on the balance between the adhesive forces generated by selectin-ligand interactions at the cell membrane/substrate interface and the fluid shear forces leading to detachment.

Although prior experimental and computational work have shown that cell deformation is an important parameter in modulating leukocyte rolling, the relative importance of the different types of deformation: whole-cell deformation, changes in cell/substrate contact area, and membrane tether formation are still not fully understood. The relationship between whole-cell deformation and rolling velocity has been studied *in vivo* using intravital microscopy[63], in vitro using a novel side-view imaging system[132] or using fixed cells[182, 259]. Alternatively, the

importance in membrane tether formation in modulating leukocyte rolling velocities has been primarily assessed in vitro by differential interference contrast (DIC) microscopy[197]. Although estimates of cell contact areas have been made by measuring contact zone lengths and assuming circular contact zones[63, 132], direct measurement of leukocyte contact area measurements are desired.

Traditionally, imaging of the contact area between a rolling leukocyte and the underlying substrate has been difficult because of the dynamic nature of the interaction and the inability of the traditional microscopy techniques (i.e. phase contrast, DIC, epifluorescence, intravital) to image this region. Recently however, Sundd et al[236] have reported the direct imaging of the contact area between rolling leukocytes and selectin-coated substrates via quantitative dynamic footprinting which is an adaptation of total internal reflection fluorescence (TIRF) microscopy. In addition to providing direct measurements of the contact area or "footprint" of rolling neutrophils, this technique also allowed for direct imaging of the anchorage attachment points of membrane tethers.

Two requirements of the dynamic footprinting method that may limit its broad use are (i)it requires a specialized TIRF setup, which typically is expensive and (ii)it requires the use of fluorescent cells (e.g. DiI-labeled cell membranes, or green-fluorescent protein transfected cells). As a low-cost alternative to this technique we report the use of reflection interference contrast microscopy (RICM) to obtain dynamic measurements of the contact areas of rolling neutrophils and the adhesion points of membrane tethers. While this technique has previously been used to image the footprints of stationary[190], spreading[220] and settling[189]

leukocytes, it has not been used in conjunction with leukocyte rolling. Here, we demonstrate how RICM can be used to estimate neutrophil contact areas based on the cell/substrate separation distance. We also report the imaging of neutrophil membrane tethers from low separation distance adhesion points and the role of shear stress and shear rate on membrane tether formation and contact area.

Methods

Antibodies and Reagents

Human P-Selectin, anti-PSGL-1 mAb PL1, and anti-P-Selectin mAb G1 were kindly provided by Dr. Rodger McEver (Oklahoma Medical Research Foundation, Oklahoma City, OK). Anti-CD18 mAb IB-4 was purchased from Ancell and Human Serum Albumin (HSA), manufactured by ZLB Behring, was purchased from National Hospital Specialties.

Neutrophil Isolation

Venous human blood was obtained from healthy donors and anticoagulated with heparin. Neutrophils were isolated using the dextran sedimentation protocol set forth in Appendix B. Briefly, dextran sedimentation for 1 h yielded leukocyte-rich plasma, and sodium chloride solutions were used to lyse any remaining erythrocytes. Neutrophils were then isolated by centrifugation over Cellgro Lymphocyte Separation Medium (Mediatech). Following isolation, neutrophils were washed twice in Hank's balanced salt solution with Ca^{2+} and Mg^{2+} (HBSS; Gibco Laboratories) supplemented with 0.5% HSA. Neutrophils were then suspended in the same buffer at $5*10^5$ cells/mL. Cells counts were verified using a manual hemocytometer set (Hausser Scientific). The blood collection protocol was approved by the Institutional Review Board of the University of Oklahoma, and informed consent was obtained from all donors.

Substrates

Fisherbrand 45 mm x 50 mm glass cover slips were each incubated with a 25 μL drop of P-Selectin at a concentration of 1.5 μg/mL in humidified chambers at room temperature. After 3 h, the substrates were washed and then incubated with a 0.5% HSA in HBSS for 30 min to block non-specific binding. P-selectin Site density measurements were determined using ^{125}I-labeled mAb G1 as described.[162, 222]

Cell/Substrate Treatments

To block P-Selectin on the substrates they were incubated with mAb G1 for 30 min at 20 μg/ml prior to neutrophil perfusion. To block PSGL-1 on the surface of neutrophils the cells were incubated with mAb PL1 (anti-PSGL-1) at 20 μg/ml in 0.5% HSA/HBSS medium for 30 min and then perfused over normal P-Selectin substrates. Following perfusion of the PSGL-1-blocked cells, the substrates were washed by perfusing HBSS through the flow chamber. After this washing untreated neutrophils were perfused through the flow chamber to determine if rolling could occur.

Flow Assay and Metamorph Analysis

P-Selectin coated substrates were used as the lower wall in a Glycotech parallel flow chamber. Isolated neutrophils were initially allowed to accumulate for 60 s at a shear rate of 50 s^{-1}. The cell suspension was switched off and cell-free HBSS was perfused through the chamber at the desired shear rate. Cell rolling and adhesive interactions with the underlying substrate were imaged across the substrate using

reflective interference contrast microscopy (RICM) with a Zeiss 63X/NA 1.25 Plan-Neoflaur oil immersion antiflex objective on a Zeiss Axiovert 200 microscope. Observations were captured with a CCD camera (DAGE-MTI CCD-300) at 30 frames per second and recorded onto videotapes using a Sony S-VHS videocassette recorder. 15 s video segments of rolling cells were digitized from videotapes using the software program Metamorph (Molecular Devices, version 7.5) loaded onto a Pentium-based workstation. Instantaneous rolling velocities were measured by frame-by-frame analysis using the Track Objects function in the Metamorph software.

Image Analysis

Instantaneous cell footprint areas were measured by frame-by-frame analysis of rolling neutrophils over 30 frames to determine the average footprint area for 1 second of rolling. A thresholding algorithm previously used by Pierres et al[189] was used to correlate pixel intensity (I) to separation distance between the cell and substrate (z) with the following equation:

$$z = (\lambda/4\pi)*\arccos((2I - I_m - I_M)/(I_m - I_M)) \quad (6)$$

where λ is the wavelength of light (546 nm) and I_m and I_M are the minimum and maximum pixel intensities which correspond to separation distances of $z = 0$ and $z = \lambda/4$ (137 nm), respectively. We chose separation distances of $z < 137$, 100, 75 and 50 nm to perform thresholding analysis.

Further analysis of digitized video segments produced three distinct membrane tether events. The first type of cells rolled without pulling any

observable membrane tethers. Rolling cells that produced membrane tethers were further classified according to tether fate: tethers that retracted back to the cell body and tethers that broke away from the cell body resulting in the deposition of a piece of cellular membrane. The lengths of the membrane pieces left behind were measured using the linescan function of the Metamorph software. Membrane pieces were separated into two categories: microparticles (length < 1 μm) and microfragments (length > 1 μm).

Ficoll Experiments

To determine the effect of shear stress on microparticle formation, isolated human neutrophils were resuspended in HBSS supplemented with 0, 3, and 6% (wt/vol) of Ficoll (M = 400,000, Sigma) in order to increase the viscosity. The respective viscosities of the media were measured at 1.0, 1.8, and 2.6 cP at room temperature using a u-tube viscometer. Wall shear stress was calculated from the equation $\tau_w = (6Q\mu)/(B^2W)$, which is the solution of the Navier-Stokes equation for laminar flow of a Newtonian liquid between parallel plates, where Q is the flow rate, μ is the viscosity, B is the total plate separation and W is the width. Wall shear rate was calculated as $\gamma_w = (6Q)/(B^2W)$.

Results

Neutrophil contact area during rolling is dependent on cell/substrate separation distance and shear stress. Neutrophil rolling on P-selectin is mediated by PSGL-1 expressed on the tips of neutrophil microvilli. When sufficient force is applied to these selectin bonds, membrane tethers are extruded[197, 219]. To characterize the transient, discrete, adhesive interactions between the cell membrane and the underlying surface, we imaged unlabeled neutrophils during rolling on P-selectin by reflective interference contrast microscopy (RICM). As shown in Figure 5a, RICM visualized the region of the cell body in close contact with the underlying substrate. This cellular "footprint" translocated downstream in real time as the neutrophil rolled. By processing the image to remove the background, we were able to isolate and measure the cell footprint area. Based on RICM theory, this area corresponded to the surface of the cell within a separation distance (z) of 137 nm. Similarly, we used a threshold algorithm based on pixel intensity as previously described by Pierres et al[189] to isolate areas of the cell with separation distances at $z < 50$, 75 and 100 nm. We observed that these areas decreased with decreasing separation distance to the point that at $z < 50$ nm the cell surface area visualized was contained in a handful of small distinct points (Fig. 5a). Conversely, we observed little difference between the contact areas when thresholding for a separation distance of $z < 100$ nm compared to the overall cell footprint. These data demonstrate that RICM can be used to image the contact areas of rolling neutrophils and that these contact areas are dependent on the separation distance between cell and substrate.

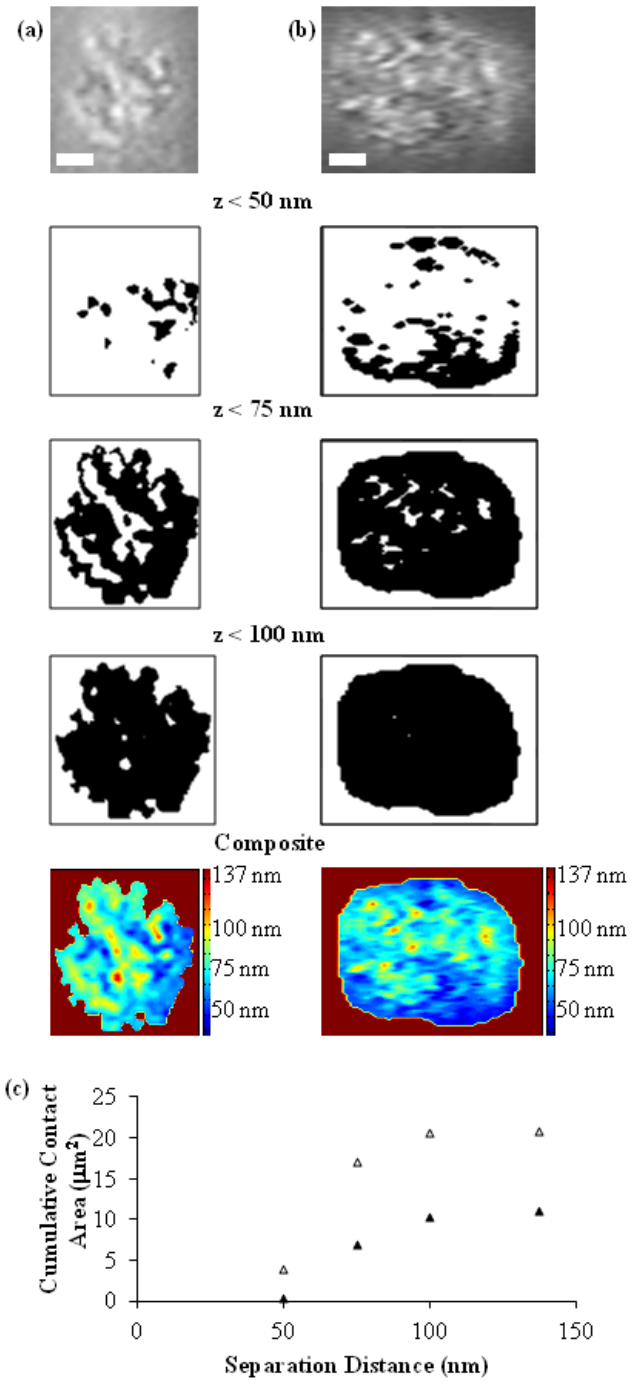


Figure 5: RICM allows for the visualization of the cellular "footprint" or contact area, which we isolated through a thresholding algorithm at separation distances of z < 50, 75 and 100 nm. Also presented are color composites of the overall cell footprints. These cells were visualized during rolling at (a)1 dyne/cm^2 and (b)8 dynes/cm^2. (c)The cumulative contact area increased with increasing separation distance for cells rolling at 1 dyne/cm^2 (dark symbols) and 8 dynes/cm^2 (open symbols).

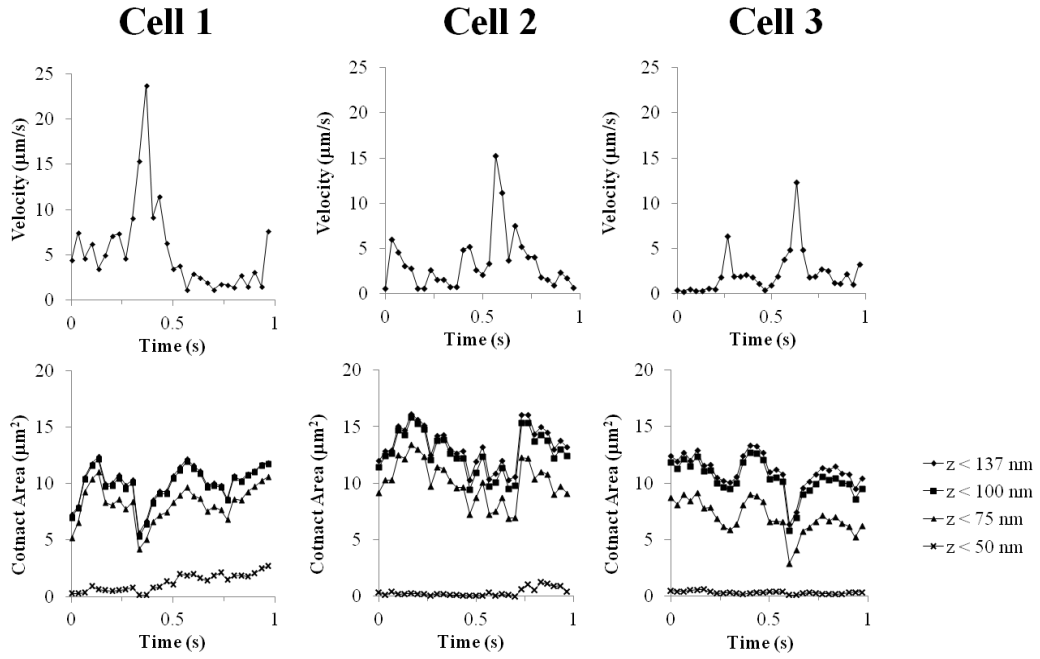


Figure 6: We used frame-by-frame analysis of RICM images to measure the instantaneous velocities and of neutrophils rolling at 1 dyne/cm^2 over a 1 second period. We also measured instantaneous contact areas over a 1 second period by thresholding images based on separation distances of z < 50, 75, 100 and 137 nm. This analysis was performed for three cells to ensure reproducibility.

To investigate the role of shear stress on neutrophil contact area, we observed neutrophil rolling with RICM on substrates coated with a constant P-selectin concentration (1.5 μg/mL) at wall shear stresses of 1 and 8 dynes/cm^2. Figure 5b shows that at separation distances of z < 50, 75 and 100 nm, a greater portion of the cell surface was visible at 8 dynes/cm^2 compared to 1 dyne/cm^2. Similarly, the overall cell footprints of cells rolling at 8 dynes/cm^2 were also significantly larger. Figure 5c illustrates the increase in contact area between cells rolling at 1 dyne/cm^2 (dark symbols) and 8 dynes/cm^2 (open symbols), as well as the increase in cumulative contact area we observed with increasing separation distance.

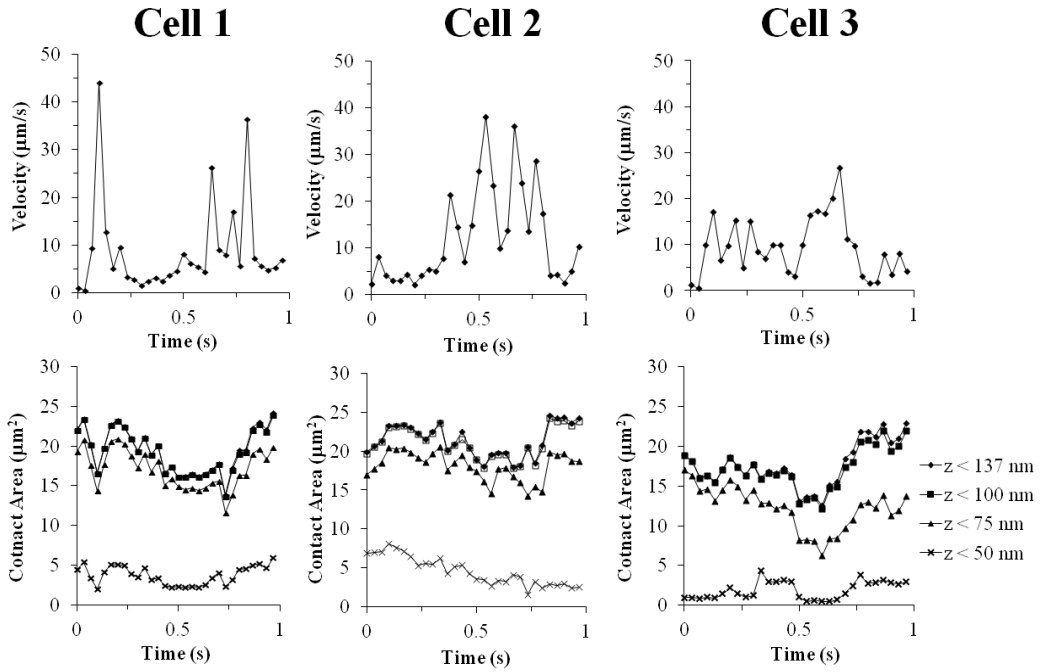


Figure 7: A similar frame-by-frame analysis was performed for neutrophils rolling at 8 dynes/cm^2 over a 1 second period. We also measured the instantaneous contact areas over a 1 second period at separation distances of z < 50, 75, 100 and 137 nm and found them to be significantly greater than cells rolling at 1 dyne/cm^2. This analysis was performed for three cells to ensure reproducibility.

We also measured a plateau in cumulative contact area at z > 100 nm at both shear stresses.

Neutrophil contact area is dynamic and relates to instantaneous rolling velocity.

Using frame by frame analysis, we measured the instantaneous velocities and contact areas of rolling neutrophils at 1 and 8 dynes/cm^2 over a period of 1 second. At a wall shear stress of 1 dyne/cm^2, rolling was characterized mostly by low velocities with the occasional spike (Fig. 6) while at 8 dynes/cm^2 velocity spikes were larger and fewer pauses or periods of low velocity were observed (Fig. 7). When contact areas were plotted over time based on the different separation distances, we observed that lower separation distance always corresponded to a

smaller contact area at both 1 and 8 dynes/cm^2 (Fig. 6-7). At a separation distance of $z < 50$ nm, contact areas were typically less than 1 μm^2 at 1 dyne/cm^2 while areas at 8 dynes/cm^2 ranged from approximately 2 – 7 μm^2. As separation distance was increased, however, we observed significant differences in contact area between the two shear stresses. Figure 6 shows that at 1 dyne/cm^2, the greatest contact areas ($z <$ 137 nm) ranged from approximately 8 – 12 μm^2 while at 8 dynes/cm^2 the overall area ranged from approximately 15 – 25 μm^2 (Fig. 7). We also observed that fluctuations in contact area at higher separation distances appeared to correlate with spikes in rolling velocity.

To better illustrate this trend, we plotted instantaneous velocity against contact area at the four previously mentioned separation distances for three cells at 1 dyne/cm^2 (Fig. 8). We also observed a general trend that higher rolling velocities appeared to correspond with lower contact areas. This same trend also appeared for cells that rolled at 8 dynes/cm^2 (Fig. 9). Although we were unable to determine a specific correlation between the two factors, the trend that appeared was similar to a model presented recently in a master's thesis at the Massachusetts Institute of Technology[19]. This model suggested that decreasing the microvillus tip area resulted in an increase in rolling velocity. By assuming a hemispherical microvillus tip area of 0.06 μm^2 (surface area of a hemisphere = $2\pi R_{mv}^2$, R_{mv} = 0.1 μm[11, 111]), we used our contact area measurements at $z < 50$ nm to calculate the number of microvilli interacting with the substrate (Fig. 10). At 1 dyne/cm^2, we found that typically less than 10 microvilli were in contact with the substrate, though some cells could have upwards of 30 microvilli at this distance. Conversely,

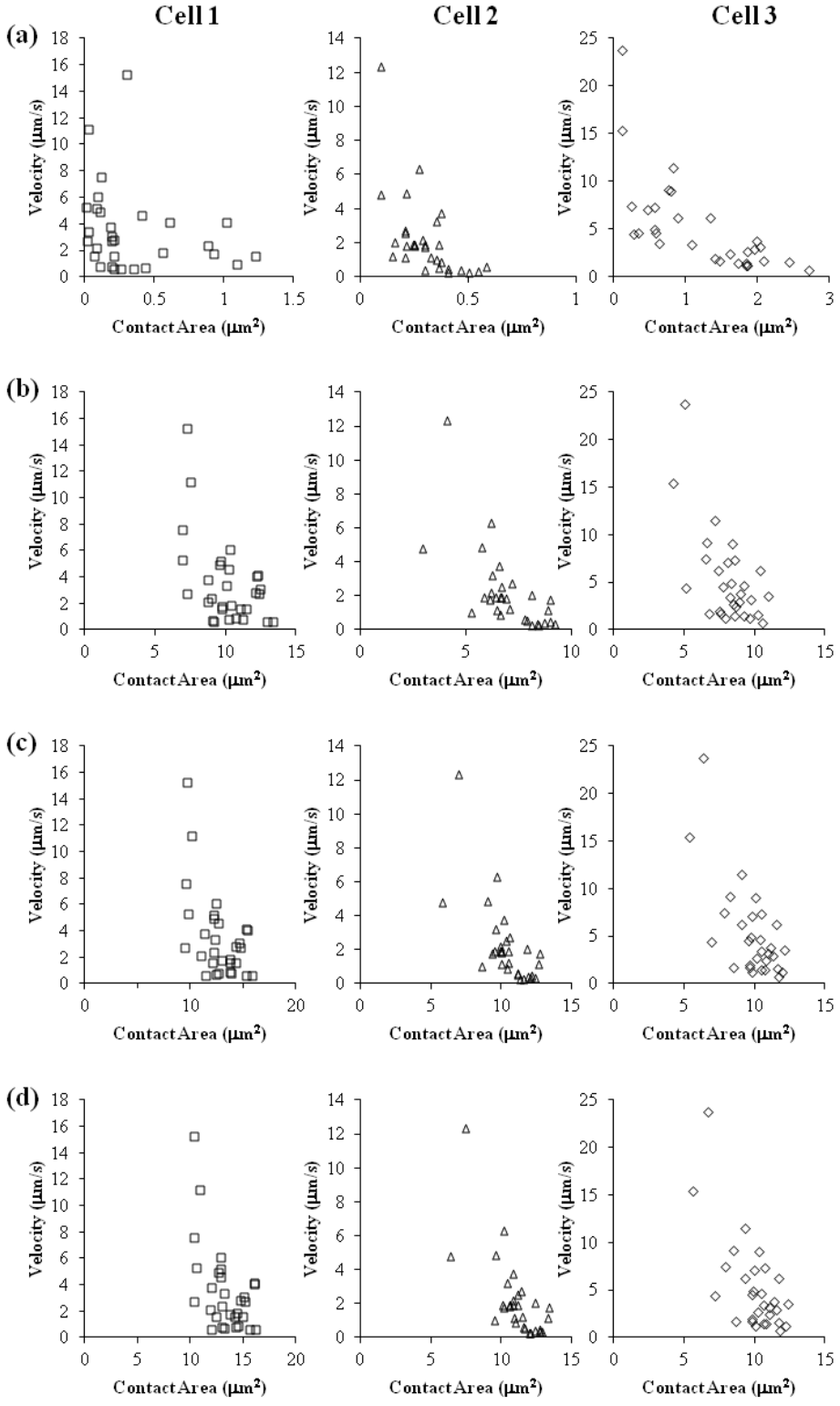


Figure 8: Instantaneous velocities were plotted against their corresponding contact areas for 3 cells rolling at 1 dyne/cm^2. Thresholding was applied for separation distances of z < (a)50, (b)75, (c)100 and (d)137 nm.

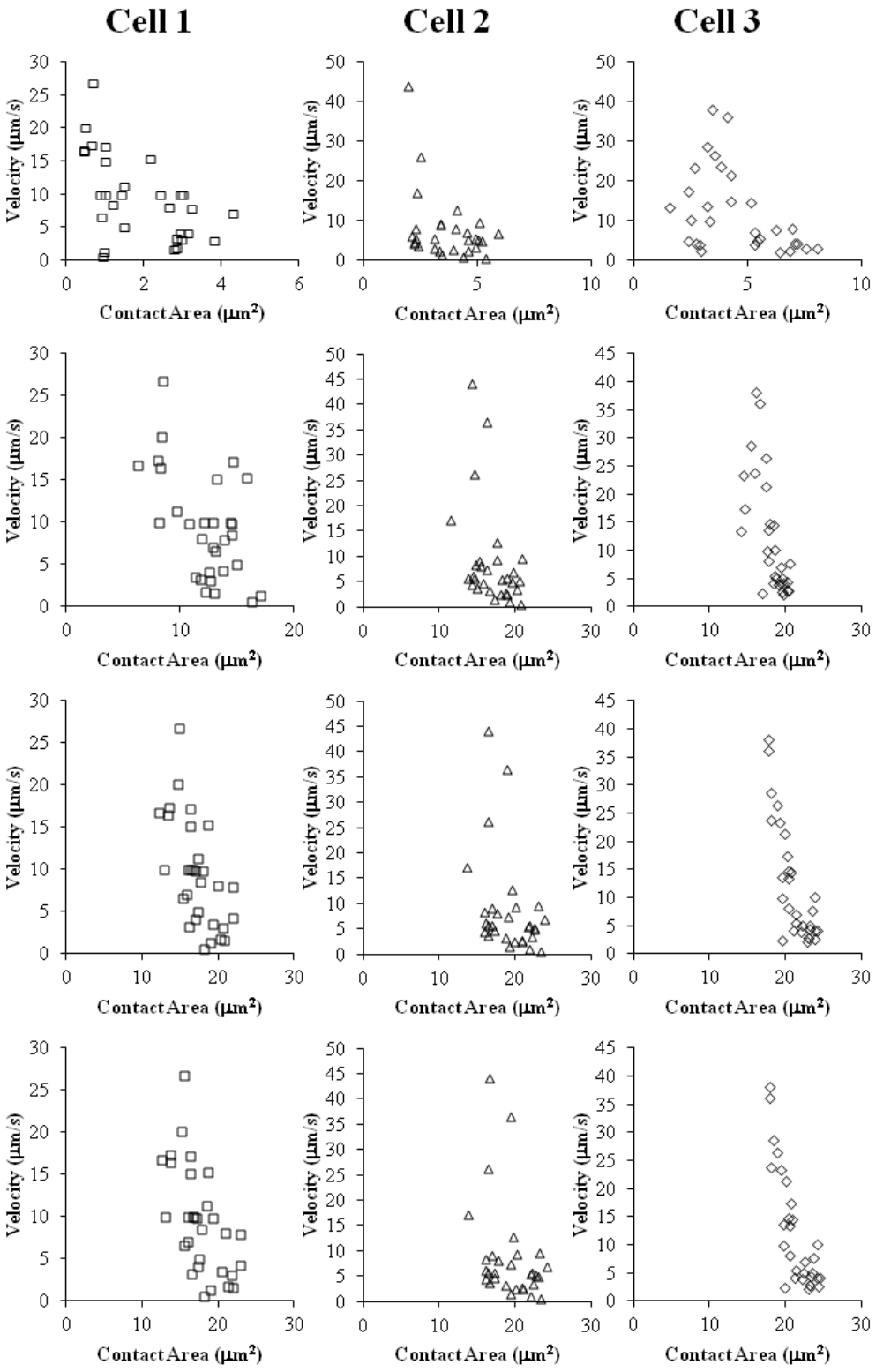


Figure 9: Instantaneous velocities were plotted against their corresponding contact areas for 3 cells rolling at 8 dynes/cm^2. Thresholding was applied for separation distances of z < (a)50, (b)75, (c)100 and (d)137 nm.

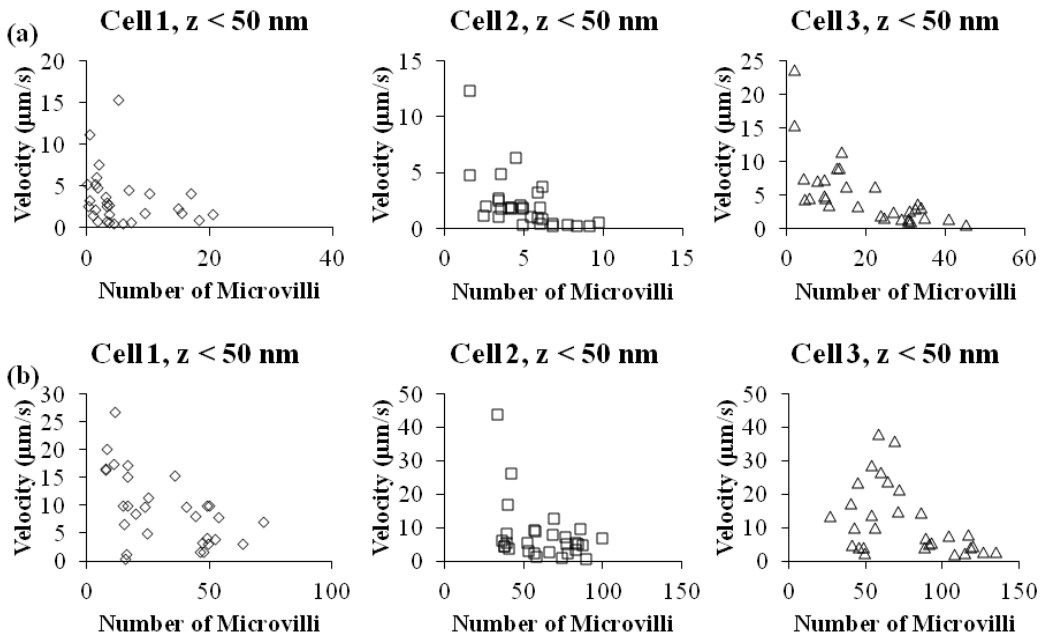


Figure 10: We calculated the number of microvilli interacting with the substrate at z < 50 nm by assuming a microvillus tip area of 0.06 μm^2 for 3 cells rolling at (a)1 dyne/cm^2 and (b)8 dynes/cm^2.

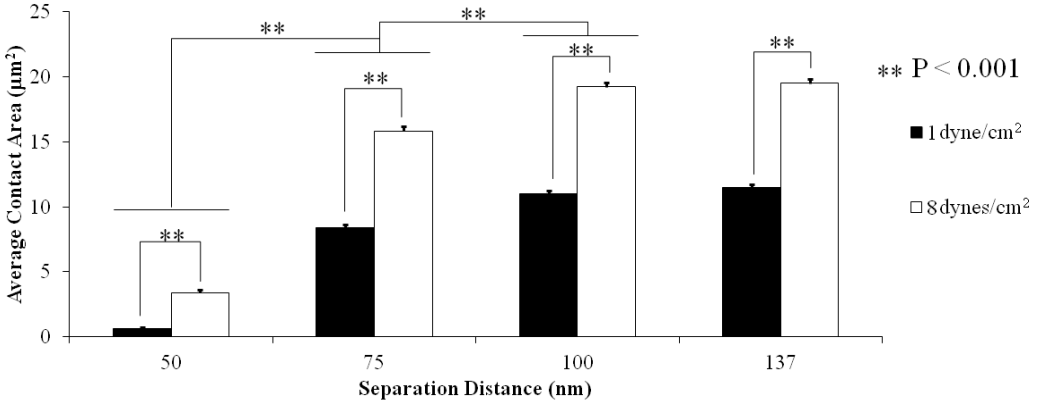


Figure 11: Average contact area was calculated based on separation distance for 3 cells rolling at 1 and 8 dynes/cm^2. Significant differences were observed at all separation distances between the two shear stresses. Contact areas were also significantly higher at z < 75 and z < 100 nm but did not significantly change between z < 100 and 137 nm.

at 8 dynes/cm^2 we calculated a significantly greater number of interacting microvilli (25 – 75 with > 100 microvilli in extreme cases).

In addition, we continued to observe that contact area depended on separation distance. This could be seen in the shift in contact area points toward higher values with increasing separation distance. We also noted that contact areas were nearly similar for separation distances greater than 75 nm. We quantified the influence of separation distance on contact area by calculating the average contact area for each separation distance. Figure 11 shows that contact areas at 8 dynes/cm^2 were always significantly greater than at 1 dyne/cm^2. Furthermore, there was a significant increase in average contact area between $z < 50$ – $z < 75$ nm and $z < 75$ nm – $z < 100$ nm. However, there was no significant change when separation distance was increased beyond 100 nm.

RICM images the formation and breakage of membrane tethers during rolling.

While observing neutrophil rolling with RICM, we noted that the dark regions corresponding to areas of low separation distance between the cell and substrate did not always disappear, but remained stationary after the cell had translocated downstream and resulted in the formation of membrane tethers (Fig. 12a). In general, membrane tether structures grew to be ~ 3-5 μm in length before releasing, but in some cases they grew significantly longer (> 20 μm). For the elongated tethers, we also observed branching of the tethers and distinct contact points confirming our previous reports[219] of tethers being multi-bonded to the surface (see Fig. 12b, white arrows).

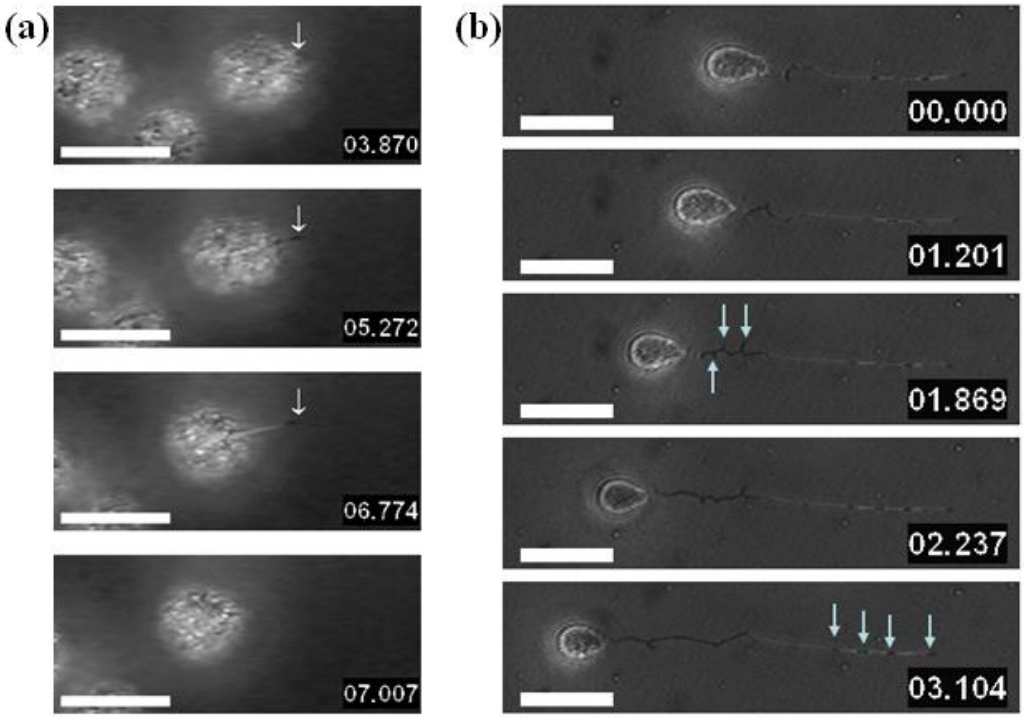


Figure 12: (a)During rolling, neutrophils contacted the underlying substrate directly through distinct points of low separation distance. These points could remain in place as the cell translocated downstream resulting in the formation of a membrane tether (white arrows). Often, membrane tethers released from the substrate and retracted back to the cell body. Scale bar = 10 μm. (b)Occasionally, we observed very long tethers with several branches and contact points (white arrows). Scale bar = 10 μm.

During the course of the experiments tethers generally released from the substrate and retracted to the cell body. On rare occasions, however, a tether would separate from the cell somewhere along its length before releasing from the substrate. These tether breakage events resulted in the deposition of membrane pieces, which would remain on the substrate while the cell continued to translocate downstream. We measured the lengths of these deposited pieces and classified them into two categories: microparticles (MP) which had lengths less than 1 μm (see Figure 13a), and microfragments (MF), which were greater than 1 μm in length (see Figure 13b).

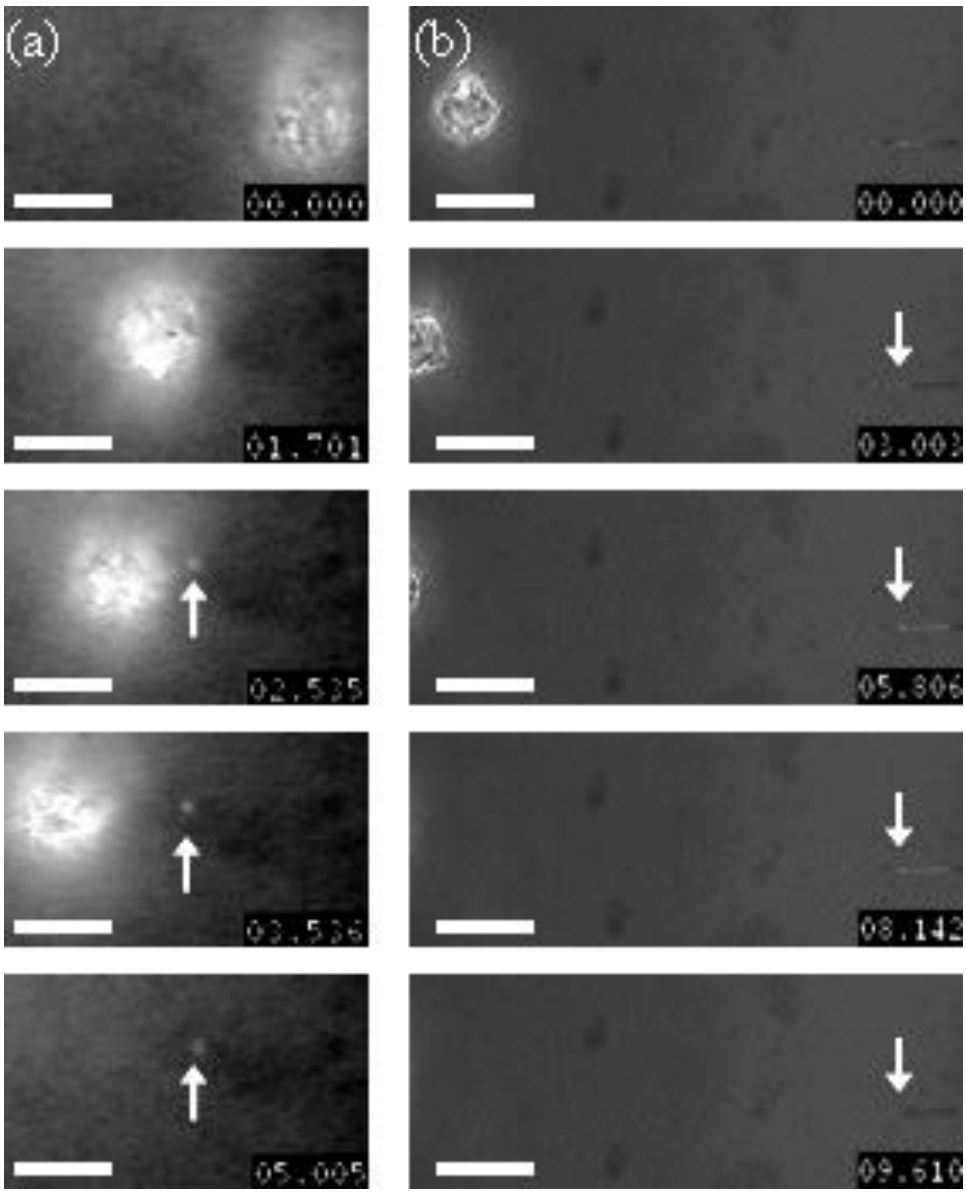


Figure 13: On rare occasions, we observed the deposition of pieces of cell membrane following the separation of membrane tethers from the cell body. We classified these pieces into two categories according to their length: (a)microparticles, length < 1 μm and (b)microfragments, length > 1 μm.

Membrane tether formation and breakage correlate with elevated wall shear stress levels. To determine the effects of shear stress on the frequency of membrane tether formation and breakage, we observed 50 neutrophils rolling on 1.5 μg/mL P-selectin at wall shear stresses ranging from 1 – 8 dynes/cm^2. Neutrophils were categorized

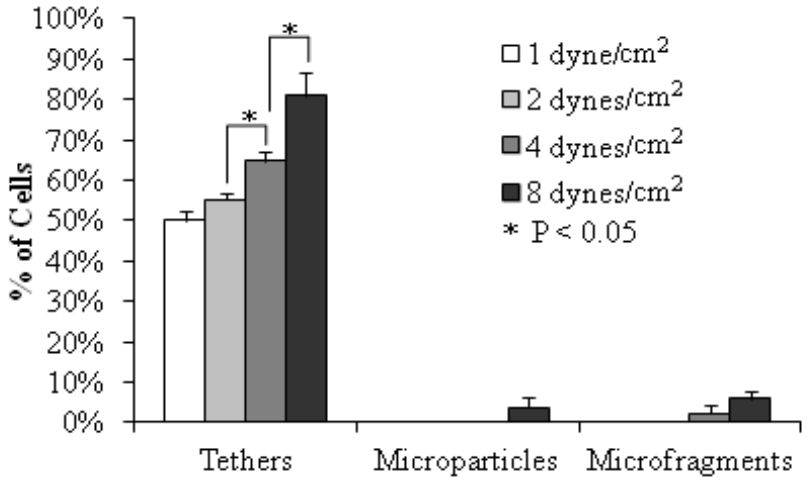


Figure 14: Isolated neutrophils were perfused at various shear stresses (1 – 8 dyn/cm^2) over substrates coated with P-Selectin at a density of 490 sites/μm^2. An increase in tether formation is seen with increasing shear stress. Microparticle and microfragment deposition were rare but did occur under elevated shear stress conditions (> 4 dyn/cm^2).

based on the presence or absence of membrane tethers. Cells that formed membrane tethers were further divided according to membrane tether fates (retraction or breakage) and broken tethers were divided according to the breakage result (MP/MF deposition). Figure 14 shows that an increase in the frequency of membrane tether formation significantly correlated with increased shear stress. We observed approximately 50% of cells pulling at least one tether at a wall shear stress of 1 dyne/cm^2, which increased to nearly 80% of cells at a wall shear stress of 8 dynes/cm^2. In contrast, tether breakage events appeared to be rare occurrences that were only observed under high shear stress conditions (> 4 dynes/cm^2). However, at a wall shear stress of 8 dynes/cm^2 we did observe approximately 4% and 6% of cells depositing a microparticle or microfragment, respectively (Fig. 14). These data demonstrate that tether formation and tether breakage correlate with elevated wall shear stress conditions.

Overall contact area and membrane tether formation correlate with shear stress rather than shear rate. The above data (Fig. 14) suggests that the frequency of membrane tether formation is directly related to shear stress applied to the PSGL-1/P-selectin bond(s). Shear stress applies both a force and a torque on the rolling cell. Thus one mechanism is that as the shear stress increases the force on the cell and the PSGL-1/P-selectin bonds, the probability that the cell membrane will separate from the cell cytoskeleton and form a membrane tether also increases. However, since shear stress is the product of shear rate and viscosity, it is possible that an increased shear rate increases the formation of new PSGL-1/P-selectin bonds before previous bonds dissociate[29, 35, 62]. The formation of these additional bonds may stabilize the adhesive interaction between the cell and the surface and promote tether formation. To differentiate the relative roles of shear stress and shear rate on membrane tether formation we independently varied these two parameters by perfusing cells in media of different viscosities over substrates coated with a P-selectin concentration of 1.5 μg/mL. The viscosity of the media was varied by adding Ficoll at 3% or 6% w/v as previously described in the literature[36, 260-261]. With no Ficoll added, shear rates of 100, 200, 400 and 800 s^{-1} corresponded to shear stresses of 1, 2, 4 and 8 dyn/cm^2, respectively. Buffer supplemented with 3% w/v Ficoll gave shear stresses of 1.8, 3.6, 7.2 and 14.4 dyn/cm^2, and buffer supplemented with 6% w/v Ficoll gave shear stresses of 2.6, 5.2, 10.4 and 20.8 dyn/cm^2.

Figures 15a and 15b show tether formation plotted as a function of shear rate and shear stress respectively. When plotted as a function of shear rate, the curves

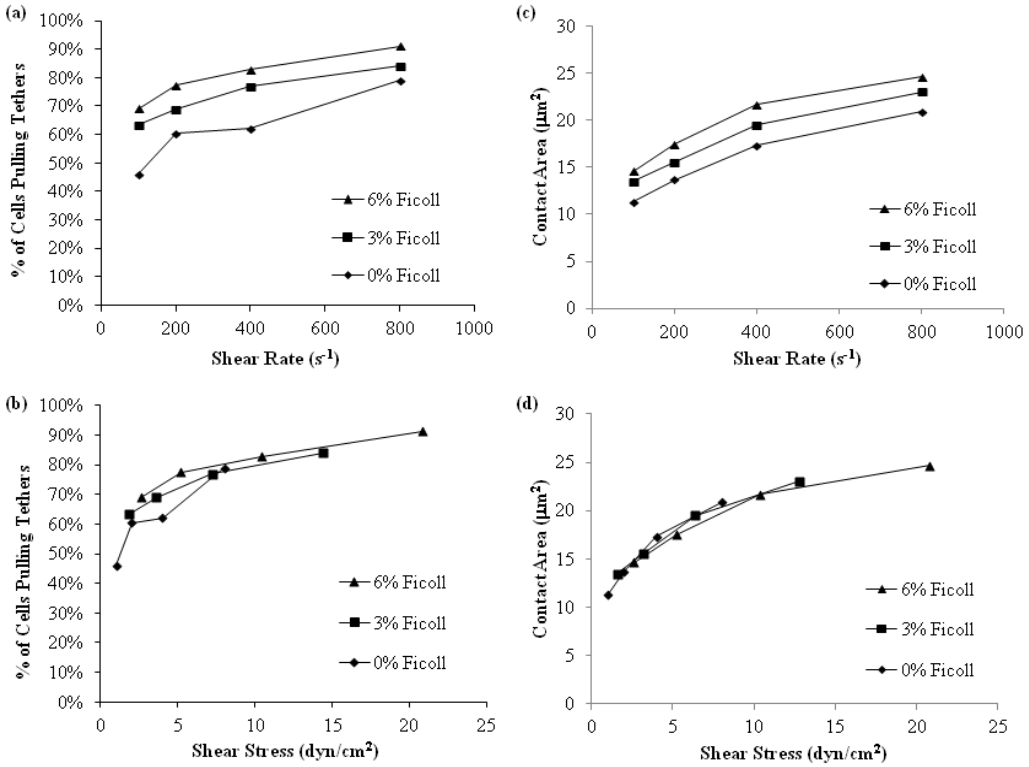


Figure 15: Isolated neutrophils were suspended in HBSS supplemented with Ficoll 400 at 0% w/v, 3% w/v and 6% w/v. These suspensions were perfused over substrates coated with P-Selectin (490 sites/μm^2) at various shear rates (100-800s^{-1}). The variation of the Ficoll concentration allowed for the manipulation of shear stress independently of the shear rate. (a)Neutrophils show increasing tether formation with increasing shear rate, but that increase is independent with respect to Ficoll concentration. (b)The increase in tether formation with increasing shear stress, however, is not independent of Ficoll concentration. (c-d) The same is true for overall cell footprint area measurements (z < 137 nm).

for the three different viscosities were parallel to each other and show that for a given shear rate the frequency of membrane tether formation could be increased by increasing the viscosity or shear stress (i.e. force). In contrast, when the membrane tether formation frequency was plotted as a function of shear stress, the data curves for the different viscosities aligned over the overlapping range of shear stresses. Alignment of these curves suggests that the frequency of membrane tether formation was primarily controlled by shear stress rather than shear rate.

Similarly, we plotted the overall neutrophil footprint area as a function of shear rate (Fig. 15c) and shear stress (Fig. 15d). Like membrane tether frequency, we observed three distinct parallel curves corresponding to the three different viscosities when contact area was plotted as a function of shear rate. Conversely, plotting the contact area against shear stress revealed overlapping curves which aligned to illustrate a single trend of increasing contact area with increasing shear stress. In this case, contact area increased from approximately 11 – 24 μm^2 when shear stress increased from 1 – 20 dynes/cm^2. These data demonstrate that contact area is also controlled by shear stress rather than shear rate.

Discussion

In these studies, we used reflective interference contrast microscopy (RICM) to directly observe the underlying footprints of neutrophils rolling on P-selectin substrates. Our observations revealed that, while a portion of the rolling cell's surface is very close to the substrate, there are subtle variations in the separation distance between the cell and the substrate across the cell surface. We applied a thresholding algorithm similar to that used by Pierres et al[189] to isolate specific areas of the footprint at $z < 50$ nm revealed distinct points of adhesion between the cell and substrate. While these adhesions points appeared and subsequently disappeared as a rolling cell translocated downstream, we also observed the extraction of membrane tethers when adhesion points remained in place after the cell had moved downstream. Using Ficoll to vary the viscosities of cell suspensions, and consequently the shear stress independent of shear rate, we also demonstrate that membrane tether formation and changes in contact area are dependent on shear stress. These studies are novel in that (i) they utilize RICM to visualize the footprints of rolling neutrophils in real time, (ii) they demonstrate that neutrophil contact area is a dynamic quantity dependent on shear stress, (iii) we report the direct observation of membrane tethers forming from distinct points of adhesion and (iv) we show that the frequency of membrane tether formation and neutrophil contact area are dependent on shear stress rather than shear rate.

The measurement of leukocyte contact areas during rolling adhesion has been a significant topic of investigation in previous theoretical and experimental studies. However, leukocyte rolling has typically been visualized by phase contrast

microscopy, direct interference contrast microscopy, epifluorescence or intravital microscopy, all of which do not allow for the visualization of cell footprints. Previous studies overcame this difficulty by experimentally measuring the contact lengths of adherent cells and assuming a circular contact area[49, 63]. The assumed contact areas calculated from these contact length measurements ranged from 20 – 40 μm^2. Theoretical models of rolling cells as two dimensional elastic rings also predicted contact lengths on the same order of magnitude as experimental measurements. More recently, three dimensional models of rolling leukocytes have predicted a wide range of contact areas. Pospiezsalska et al[192] reported contact area measurements of approximately 3 μm^2 for neutrophils rolling at a shear stress of 0.5 dynes/cm^2 using their event-tracking model of adhesion. On the other hand, Jadhav et al[101] predicted contact areas between 15 – 30 μm^2 at shear rates ranging from 100 – 400 s^{-1} using the immersed boundary method. However, these studies did not offer corresponding experimental measurements.

Recently, Sundd et al[236] reported using quantitative dynamic footprinting (qDF) to image the footprints of rolling neutrophils labeled with DiI or neutrophils from knock-in mice in which green fluorescent protein was expressed as a soluble cytosolic protein. This study demonstrated that contact area measurements are dependent on the separation distance between points on the cell surface and the underlying substrate. At a separation distance of $z < 100$ nm, they reported significantly greater contact area measurements (~12 μm^2) for neutrophils rolling at higher shear stresses (6 – 8 dynes/cm^2). It should be noted, however, that this technique requires fluorescent labeling of cells as well as a microscope set up to

perform total internal reflective fluorescence microscopy. In addition, the neutrophils used in this study all came from mice. They did not report similar measurements for human neutrophils.

As a simple alternative to qDF, we employed RICM to observe in real time the footprints of rolling human neutrophils and P-selectin coated glass substrates. This has been previously employed by Reininger et al to visualize discrete adhesion points (DAPs) between platelets and vWF coated substrates and the deposition of platelet membrane microparticles[201]. Previous studies have also used this technique to visualize the footprints of stationary, spreading or settling leukocytes. As illustrated in Figure 5, RICM imaged the neutrophil footprint as a contrast pattern where pixel intensity was based on the separation distance between the point on the cell surface and the substrate. By thresholding the RICM images according to specific z values, we observed that neutrophils rolling under low shear stress (1 dyne/cm^2) adhered to the substrate in distinct points at $z < 50$ nm. Conversely, contact areas at multiple separation distances were significantly increased at elevated shear stress (8 dynes/cm^2, see Fig. 7). For example, at a separation distance of $z < 100$ nm, we report contact areas ranging from 8 – 12 μm^2 at 1 dyne/cm^2 and 15 – 25 μm^2 at 8 dynes/cm^2. Although these values are slightly higher than the average value reported by Sundd et al (~12 μm^2 at 6 dynes/cm^2, $z < 100$ nm), this difference may be related to differences in P-selectin site density (490 vs. 20 sites/μm^2).

The qDF technique has been used to measure cell footprints at 6 and 8 dynes/cm^2 [236], but it was not tested at lower shear stresses even though

simulations by Pospiezsalska and Ley[192] predicted lower contact areas for cells rolling at 0.5 dynes/cm^2 (~ 3 μm^2). Interestingly, our measurements are also similar to the calculated values reported by Firrell and Lipowsky (20 – 40 μm^2)[63] even though neutrophil footprints at high shear stress do not appear circular as they assumed. This study and others have also reported increased contact lengths at elevated shear stress[63, 132], which agrees with our results. Three-dimensional simulations of rolling leukocytes have also predicted that increased shear stress results in increased global cell shape deformation[101, 112], which may relate to increased contact area.

We also demonstrate that contact area measurements are dependent on the separation distance chosen (Fig. 5c). Similarly, we show that the cumulative contact area averaged over time increases with increasing separation distance (Fig. 11). Additionally, we observed that a significant portion of the cell footprints were within 75 – 100 nm of the substrate, which agrees with the report by Sundd et al[236] that microvilli are typically at a distance of approximately 70 nm. Our plots of velocity against contact area also showed that increased rolling velocity corresponded to a decrease in footprint area (Figs. 8-9). Our calculations of the number of microvilli interacting with the substrate further elucidated a trend that appeared to agree with model data presented in a recent master's thesis[19]. We also predicted an increase in the number of microvilli with increasing shear stress, which is in agreement with published models of leukocyte rolling[111, 193]. However, our microvilli numbers are significantly greater than those suggested by these models and the results reported by Sundd et al using qDF[236]. This may be explained by

our significantly greater P-selectin site density or our assumption that the entire contact area is populated by microvilli. In other words, it is possible that a large contact area cluster may contain fewer microvilli than what we calculate or that contact area spots smaller than the area of a single microvillus tip may not correspond to actual microvilli.

In addition to neutrophil contact areas, RICM allowed for the visualization of membrane tether extrusion, which occurred through distinct adhesion points (see Fig. 12). As the neutrophil translocated downstream and the membrane tether elongated, the location and number of DAPs was dynamic. An additional advantage of the RICM technique was that it demonstrated that membrane tethers often have multiple contact points with the underlying surface confirming earlier reports by other imaging methods[219] and the recent report of Sundd et al[236]. While most membrane tethers released from the substrate and retracted back to the cell body, we observed the breakage of membrane tethers on rare occasions under high shear stress (> 4 dynes/cm^2) which resulted in the deposition of microparticles (length < 1 μm) and microfragments (length > 1 μm). Although less than 10% of cells were observed depositing a microparticle or microfragment, further study could clarify whether this tether breakage could be a physiologically relevant mechanism for the deposition of cellular membrane pieces which have been previously visualized during in vitro and in vivo rolling.

The frequencies of membrane tether formation that we report here (Fig. 14) are lower than those reported by previous observations. Imaging membrane tether formation and subsequent microparticle/microfragment deposition under dynamic

conditions is difficult due to the fact that the radius of membrane tethers (40 – 200 nm)[45, 223, 250] is at or below the resolution limit of optical microscopes. Furthermore during tether formation by a rolling cell, the angle between the tether attachment point with the underlying surface and the cell body is constantly changing, and makes simultaneous imaging of both attachment points challenging even with high resolution imaging techniques (e.g. DIC microscopy). This imaging challenge is even more difficult in vivo, where intravital microscopy is typically performed with lower power objectives.

Recent studies have reported that leukocyte deformation[231], PSGL-1/P-selectin dissociation kinetics[36], and PSGL-1/L-selectin dissociation kinetics[260] were a function of wall shear stress or the force applied to the bond or cell. In contrast PSGL-1/P-selectin bond formation[36] was shown to be dependent on shear rate or the time available for receptor-ligand bonding. To distinguish whether contact area and membrane tether formation were shear-rate or shear-stress dependent, we performed experiments in which wall shear rate was varied independently of wall shear rate by suspending neutrophils in media of different viscosities. As shown in Figure 15, contact area and membrane tether formation were dependent on the force or shear stress applied. The observation that the frequency of neutrophil membrane tether formation increases with shear stress agrees with our previous results[197] obtained by a different microscopic imaging technique and extends the range of shear stresses (1-20 dynes/cm^2) over which neutrophil membrane tethers are formed during rolling. Additionally, our contact area measurements reveal a plateau in the overall footprint area for neutrophils

rolling at 10 – 20 dynes/cm^2. This agrees with previous theoretical predictions[132] as well as calculations made from contact length measurements combined with the circular contact area assumption[63].

In summary, we have demonstrated that RICM can be used as a low cost alternative to quantitative dynamic footprinting to visualize the underlying footprints of neutrophils during rolling on P-selectin coated substrates. These footprints reveal that contact area measurements depend on setting a separation distance between the cell and substrate similar to quantitative dynamic footprinting. We also report the imaging of membrane tether formation from distinct points of adhesion as well as the occasional breakage of these tether structures, resulting in microparticle or microfragment deposition. Additionally, we show the effects of shear stress and shear rate on contact area and membrane tether formation. Further studies using RICM to observe neutrophil rolling will continue to elucidate the roles of neutrophil contacts, cell deformation and membrane tethers.

CHAPTER 3: The Effect of Ligand Density and Ligand Type on Neutrophil Membrane Tether Formation during Rolling

Introduction

Leukocytes adhere to activated endothelial cells and platelets during inflammation and thrombosis through molecular interactions between selectins and their respective ligands [136, 151]. The selectins are P-selectin expressed on platelets [153] and endothelial cells [152], E-selectin expressed on endothelial cells [14] and L-selectin expressed on leukocyte microvilli [238]. Leukocytes also express P-selectin glycoprotein ligand-1 (PSGL-1) on their microvilli, which is the primary ligand for the selectins [162]. Typically these selectin-ligand interactions dissociate rapidly as a result of shear force applied from hemodynamic flow [5, 36].

Leukocytes employ various mechanisms for countering force-induced cell detachment, which relate to cell deformation [63, 132, 230, 239, 259], the viscoelasticity of the plasma membrane [61, 74, 175, 202] and the pliable nature of microvilli [182, 219, 223-224]. Yago et al demonstrated that cell deformability allows neutrophils to roll on selectin coated surfaces at shear stresses as high as 30 dynes/cm^2 [259]. Shao and Hochmuth also showed that microvilli are deformable and can stretch to form cylindrical structures called membrane tethers [223]. Although they suggested that membrane tethers could play a role in neutrophil rolling adhesion, Schmidtke and Diamond reported the first direct observation of membrane tethers which were extracted from neutrophils during adhesive interactions with immobilized platelets or rolling on P-selectin coated surfaces under physiological shear conditions [219]. The phenomenon of membrane tether formation has also been observed during leukocyte rolling *in vivo* [232].

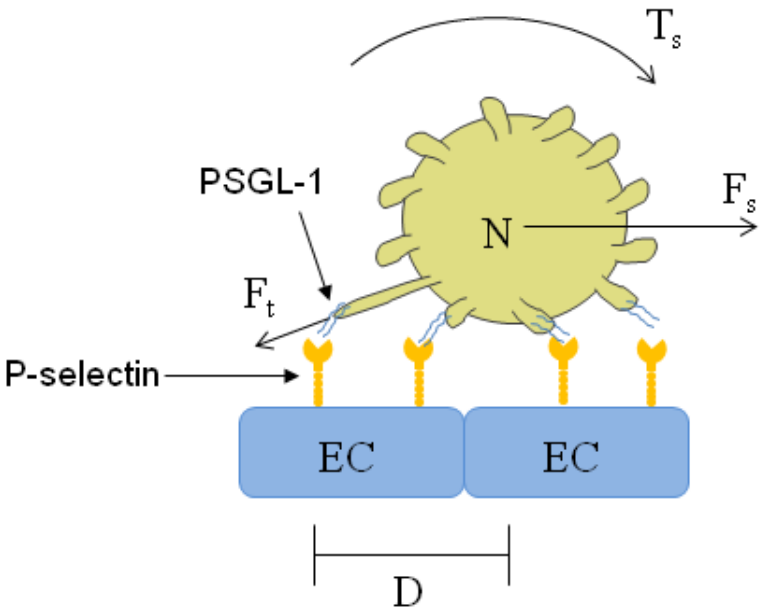


Figure 16: Schematic of the forces involved in membrane tether formation

Membrane tether structures appear to play an important role in leukocyte rolling, in that they help to stabilize rolling velocity over a wide range of shear stresses [182, 197]. Membrane tethers decrease the point force applied to selectin-ligand bonds by increasing the lever arm which relates the tether force to the hydrodynamic drag force (Fig. 16)[35]. Several groups have estimated the critical force required to form a membrane tether to be approximately 45 pN [147, 223], suggesting that the extraction of a membrane tether occurs when the plasma membrane separates from the cytoskeleton when a point force is applied [147]. Recently, a series of articles examined the unbinding of the membrane from the cytoskeleton and demonstrated the force required for this event varies with the pulling rate [56, 95, 115]. Numerical simulations presented by King et al suggested that membrane tether extraction during rolling occurs when this unbinding force is exceeded by the selectin-ligand binding force [115].

A significant parameter in determining whether this unbinding force will be exceeded is the number of selectin sites available for binding. The dependence of neutrophil rolling velocity on selectin site density has been well established with inverse correlations between ligand density and rolling velocity having been reported for all three selectins [2, 129-131, 184]. P-selectin/ligand kinetics experiments performed by Alon et al have even suggested that neutrophils could interact with multiple selectin molecules at a site density of 15 P-selectin molecules/μm^2 [5]. Computational studies of neutrophil rolling on P-selectin have also suggested that decreased rolling velocity correlates with an increase in ligand density [25, 91, 186]. The influence of ligand density on neutrophil rolling velocity suggests that it may also play a role in membrane tether formation.

In addition to ligand density, another factor that may affect membrane tether formation is the type of ligand presented. Table 3 shows that previous studies have investigated tether extraction through interactions between PSGL-1 and P-selectin, antibodies to various neutrophil ligands and neutrophil interactions with immobilized platelets or neutrophils. Girdhar and Shao also reported simultaneous tether extraction from neutrophils and endothelial cells using the micropipette aspiration technique with a neutrophil as the force transducer[84]. While it is possible that interactions between neutrophil PSGL-1 and endothelial cell E-selectin were involved in this tether extraction, little is known about neutrophil membrane tether formation during rolling on E-selectin coated surfaces. E-selectin is significant to neutrophil rolling on endothelial layers in that stimulated endothelial cells express E-selectin at a significantly higher site density than P-selectin [221].

Furthermore, previous studies have demonstrated that leukocytes can roll on E-selectin in the absence of PSGL-1[258, 262], which suggests that other neutrophil ligands may be able to mediate rolling on E-selectin.

In this study, we use in vitro parallel-plate flow chamber assays to investigate the effects of ligand density on neutrophil membrane tether formation and lifetimes. We demonstrate that increasing the density of selectin molecules available for binding affects neutrophil rolling by increasing membrane tether lifetimes. Additionally, we report the direct observation and characterization of membrane tether formation on E-selectin coated surfaces and show through the use of a blocking mAb to PSGL-1 that other cell surface ligands to E-selectin can mediate membrane tether extraction. These studies are significant in that they provide a better understanding of the roles that ligand density and ligand type play in membrane tether formation and ultimately how they affect selectin-mediated neutrophil rolling.

Table 3: Published studies on membrane tether extraction from neutrophils

Reference	**Experimental Method***	**Ligand**	**Ligand Coating**
Evans 2005	BFP	P-selectin	constant
Heinrich 2005	BFP	P-selectin	constant
Marcus 2002	micropipette	anti-CD18	constant
Shao 1996	micropipette	anti-PSGL-1/anti-L-selectin/ anti-CD45/anti-CD18	constant
Shao 1998	micropipette	anti-PSGL-1/anti-L-selectin/ anti-CD45/anti-CD18	constant
Edmondson 2005	bead collision	P-selectin	constant
Furlow 2011	bead collision/PPFC	P-selectin/ICAM-1	constant
Oh 2008	bead collision/PPFC	P-selectin/Endothelial Cells	constant
Diamond 2000	neutrophil collision	L-selectin	N/A
Kadash 2004	neutrophil collision	L-selectin	N/A
Sundd 2010	PPFC	P-selectin	constant
Schmidtke 2000	platelet collision/PPFC	P-selectin	constant
Park 2002	PPFC	P-selectin	constant
Ramachandran 2004	PPFC	P-selectin	constant
Williams 2003	PPFC	E-selectin	constant
this work	PPFC	P-selectin/**E-selectin**	**varied**

*BFP = biomembrane force probe
PPFC = parallel plate flow chamber (immobilized protein/cell surfaces)

Methods

Antibodies and Reagents

Human P-selectin isolated from platelet membranes (mP-selectin) and anti-PSGL-1 mAb PL1 were kindly provided by Dr. Rodger McEver (Oklahoma Medical Research Foundation, Oklahoma City, OK). Recombinant human (rh) P- and E-selectin were purchased from R&D Systems. These constructs consist of the extracellular domain of the selectin linked to the Fc region of human IgG_1 (Fig. 17) and exist as disulfide linked homodimers while mP-selectin can form multimers[246]. Human serum albumin (HSA) was purchased from Gemini Bio-Products.

Human P-selectin from Platelet Membranes (McEver Lab)

Extracellular Domain (Trp42 – Ala771)	Transmembrane Domain (Leu772 – Leu795)	Cytoplasmic Domain (Arg796 – Pro830)

Recombinant Human P-selectin Fc Chimera (R&D Systems)

Human P-selectin (Trp42 – Ala771)	Linker Peptide (IEGRMD)	Human IgG_1 (Pro100 – Lys330)

Recombinant Human E-selectin Fc Chimera (R&D Systems)

Human E-selectin (Trp22 – Pro556)	Linker Peptide (IEGRMD)	Human IgG_1 (Pro100 – Lys330)

Figure 17: Schematic of mP-selectin and rhP- and E-selectin Fc chimeras

Human Neutrophil Isolation

Venous human blood was obtained by venipuncture from healthy donors after informed consent was given and anti-coagulated with sodium heparin. Neutrophils

were isolated according to the lympholyte protocol in Appendix B. Briefly, whole blood was layered on top of a cell separation medium (Lympholyte-poly, Cedar Lane Laboratories) and spun at 400g for 30 minutes. The resulting granulocyte layer was removed and washed in Hank's balanced salt solution (HBSS; Lonza) with Ca^{2+} and Mg^{2+}. RBCs that were removed with the neutrophils were lysed with 0.2% and 1.6% sodium chloride solutions. Remaining neutrophils were washed three times in HBSS supplemented with 0.5% HSA. Cells were suspended in this same buffer at a final concentration of $5*10^5$ cells/mL which was verified by a manual hemocytometer set (Hausser Scientific). For PSGL-1 blocking experiments, isolated neutrophils were incubated with 20 μg/mL anti-PSGL-1 mAb PL1 in 0.5% HSA/HBSS for 30 minutes prior to use.

Substrates

P- and E-selectin were diluted with HBSS to the desired concentrations. Fisherbrand 45 x 50 mm glass cover slips were cleaned with 20% nitric acid and incubated with a solution of 1% Aquasil (Thermo Scientific) to provide a uniform hydrophobic surface. Aquasil treated cover slips were incubated with a 25 μL drop of protein solution for 3 h and then washed and incubated with 0.5% HSA/HBSS for 30 minutes to block non-specific binding.

Parallel Plate Flow Assay

Parallel plate flow chambers were assembled by adhering a Glycotech flow deck with a single channel gasket (5000 x 250 μm, W x H) to P- and E-selectin coated

substrates. Wall shear rate was calculated using the analytical solution of the Navier-Stokes equation for flow in a rectangular channel: $\gamma_w = 6Q/H^2W$, where Q is the flow rate in μL/min and H and W are the height and width of the channel, respectively. Isolated human neutrophil suspensions were introduced at a high flow rate and then stopped for 1 minute to allow cells time to settle. Flow was then restarted at 50 s^{-1} for 30 s to allow cells to accumulate before increasing to the desired shear rate. Rolling interactions of individual cells were observed using a Zeiss 200A inverted microscope with a 63X (NA 1.40) Plan-Apochromat oil immersion objective. Observations were recorded to VHS tapes using a CCD camera (DAGE-MTI CCD-300) at 30 frames/second and a Sony S-VHS videocassette recorder.

Tether Analysis

Video segments of rolling cells observed with DIC microscopy were digitized using Metamorph 7.5 (Molecular Devices). Instantaneous rolling velocities of cells were measured using frame-by-frame analysis with the Track Objects function in the Metamorph program. Membrane tether lengths were measured from DIC microscopy observations using the Linescan function in Metamorph.

Results

Elevated P-selectin concentration increases tether lifetime but not tether length.

Neutrophils form membrane tethers during rolling on P-selectin when the selectin/ligand bond force overcomes the attachment strength between the plasma membrane and the cytoskeleton. To determine whether an increase in P-selectin concentration would influence membrane tether formation, we observed at least 50 rolling neutrophils with DIC microscopy on substrates coated with P-selectin concentrations ranging from 0.5 – 3.0 μg/mL. Figure 18A shows a significant decrease in average rolling velocity with increasing P-selectin concentration at multiple shear stresses (τ = 1 and 2 dynes/cm^2). To determine whether this decrease in rolling velocity correlated with increased tether formation we measured the percentage of cells observed forming at least one membrane tether for each P-selectin concentration (Fig. 18B). At a wall shear stress of 1 dyne/cm^2, 50% of cells formed at least one membrane tether on 0.5 μg/mL P-selectin compared to 63% of cells on 3.0 μg/mL P-selectin. When the shear stress was increased to 2 dynes/cm^2, however, 85 – 100% of the cells observed pulled membrane tethers on P-selectin concentrations from 0.5 – 3.0 μg/mL.

To further characterize the effects of P-selectin concentration on the membrane tethers formed, we measured the lengths and lifetimes of membrane tethers on each P-selectin concentration. Figure 18C shows that average tether length was unaffected by differences in P-selectin concentration with no clear trends observed. Indeed, average tether length varied from 2.2 μm (1.5 μg/mL P-selectin) to 2.8 μm (0.75 μg/mL P-selectin) at 1 dyne/cm^2. Increasing tether length correlated

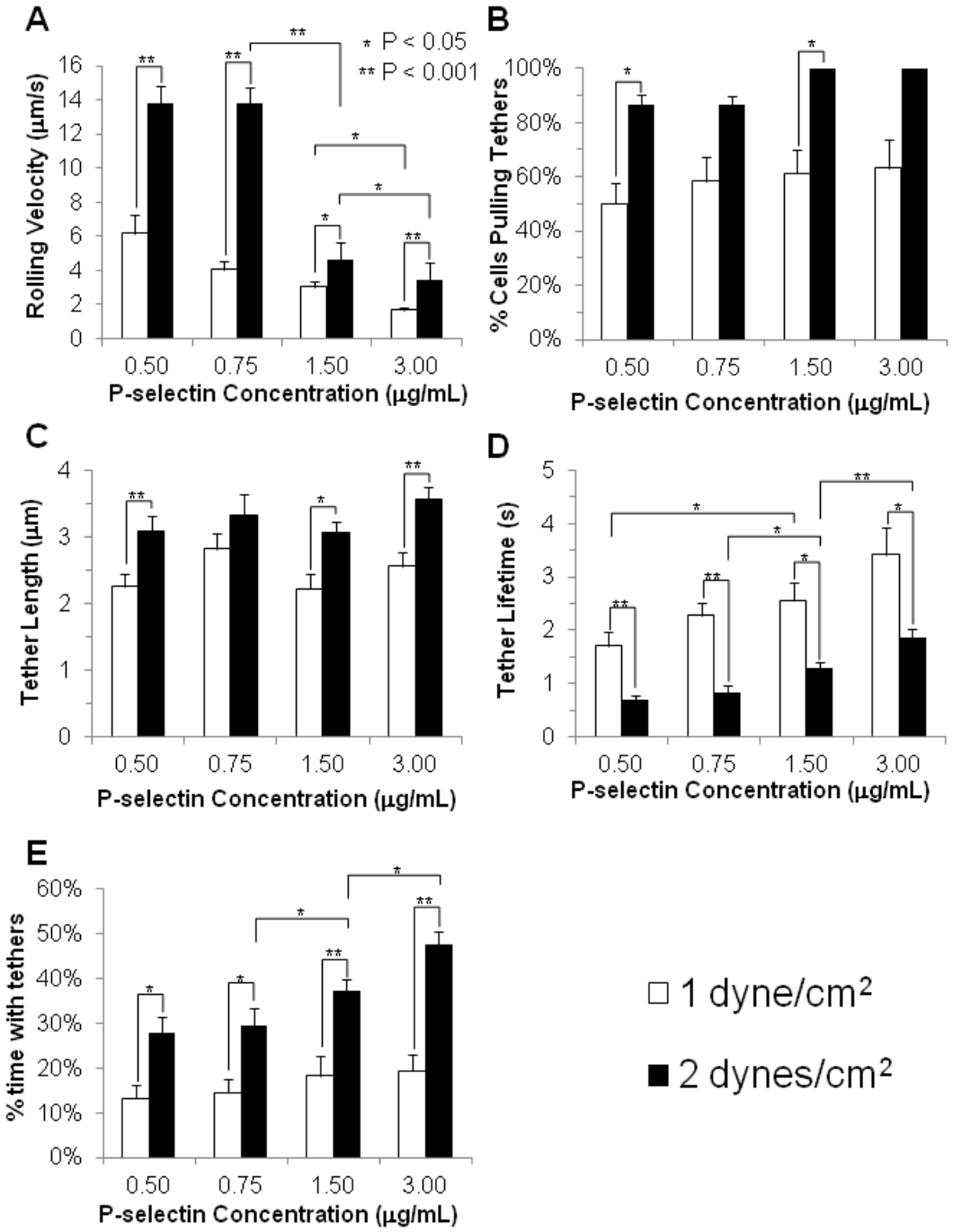


Figure 18: Human neutrophils were perfused over glass substrates incubated with various concentrations of P-selectin at wall shear stresses of 1 and 2 dynes/cm^2. Rolling velocity(A) and the percentage of cells that pulled at least one membrane tether(B) varied with both P-selectin concentration and wall shear stress. For those cells that exhibited membrane tether formation, tether length was only affected by wall shear stress(C) while tether lifetime(D) and the percent time with tethers(E) were affected by wall shear stress and P-selectin concentration.

with increased wall shear stress, ranging from 3.1 μm (1.5 μg/mL P-selectin) to 3.6 μm (3.0 μg/mL P-selectin) when shear stress was increased to 2 dynes/cm^2. Varying P-selectin concentration did significantly impact the average lifetime of membrane tethers (Fig. 18D). Membrane tethers formed during rolling on 0.5 μg/mL P-selectin lasted for an average of 2.9 seconds at 1 dyne/cm^2. Increasing the P-selectin concentration to 3.0 μg/mL resulted in a 38% increase in tether lifetime to 4.0 seconds. As expected, increasing wall shear stress resulted in an overall decrease in the average tether lifetime, however a similar increase in tether lifetime was observed with increasing P-selectin concentration. At 2 dynes/cm^2, the average tether lifetime more than doubled from 0.7 seconds (0.5 μg/mL) to 1.9 seconds (3.0 μg/mL).

We also measured the percentage of time during rolling that at least one membrane tether was present (Fig. 18E). At 1 dyne/cm^2, there was a slight increase in the percentage of time with tethers from 0.5 to 0.75 μg/mL P-selectin. However, there was no significant change at concentrations greater than 0.75 μg/mL. When shear stress was increased to 2 dynes/cm^2, the percent time with tethers increased from 28% at 0.5 μg/mL to 48% at 3.0 μg/mL. These data demonstrate that an increase in P-selectin concentration results in an increase in tether lifetime but not tether length.

Membrane tethers stabilize rolling on high P-selectin concentrations but grow at slower rates. Previously, Ramachandran et al demonstrated that membrane tethers help stabilize neutrophil rolling velocities, even under high shear stress

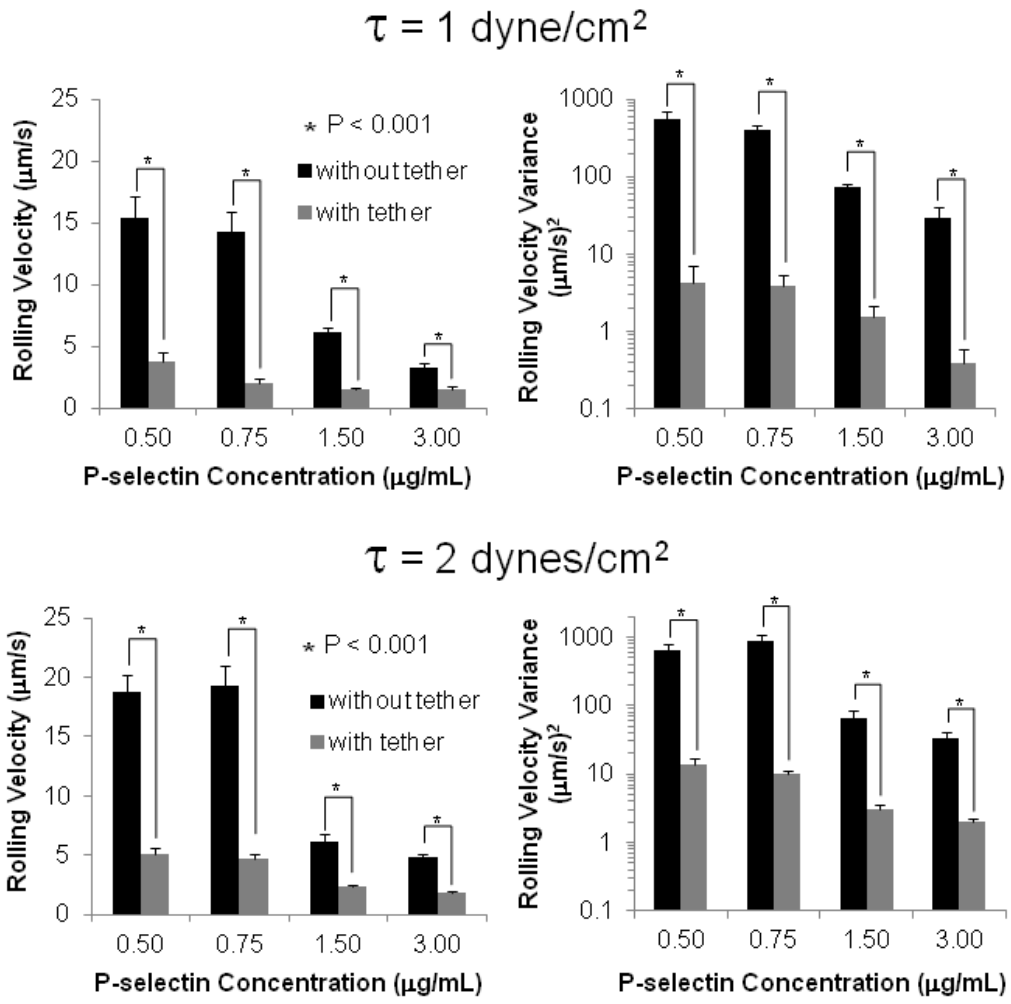


Figure 19: The correlation between the presence of membrane tethers and slower rolling was quantified by measuring the average rolling velocity and velocity variance of neutrophils in the presence and absence of tethers. Cells were perfused at wall shear stresses of 1 dyne/cm^2 and 2 dynes/cm^2.

conditions[197]. Increasing P-selectin concentration also stabilizes rolling velocities. To determine whether an increase in P-selectin concentration correlates with velocity stabilization by membrane tethers, we calculated average rolling velocities of fifty neutrophils on each P-selectin concentration in the presence and absence of membrane tethers at wall shear stresses of 1 and 2 dyn/cm^2 (Fig. 19). On all P-selectin concentrations, the average rolling velocity in the presence of at least

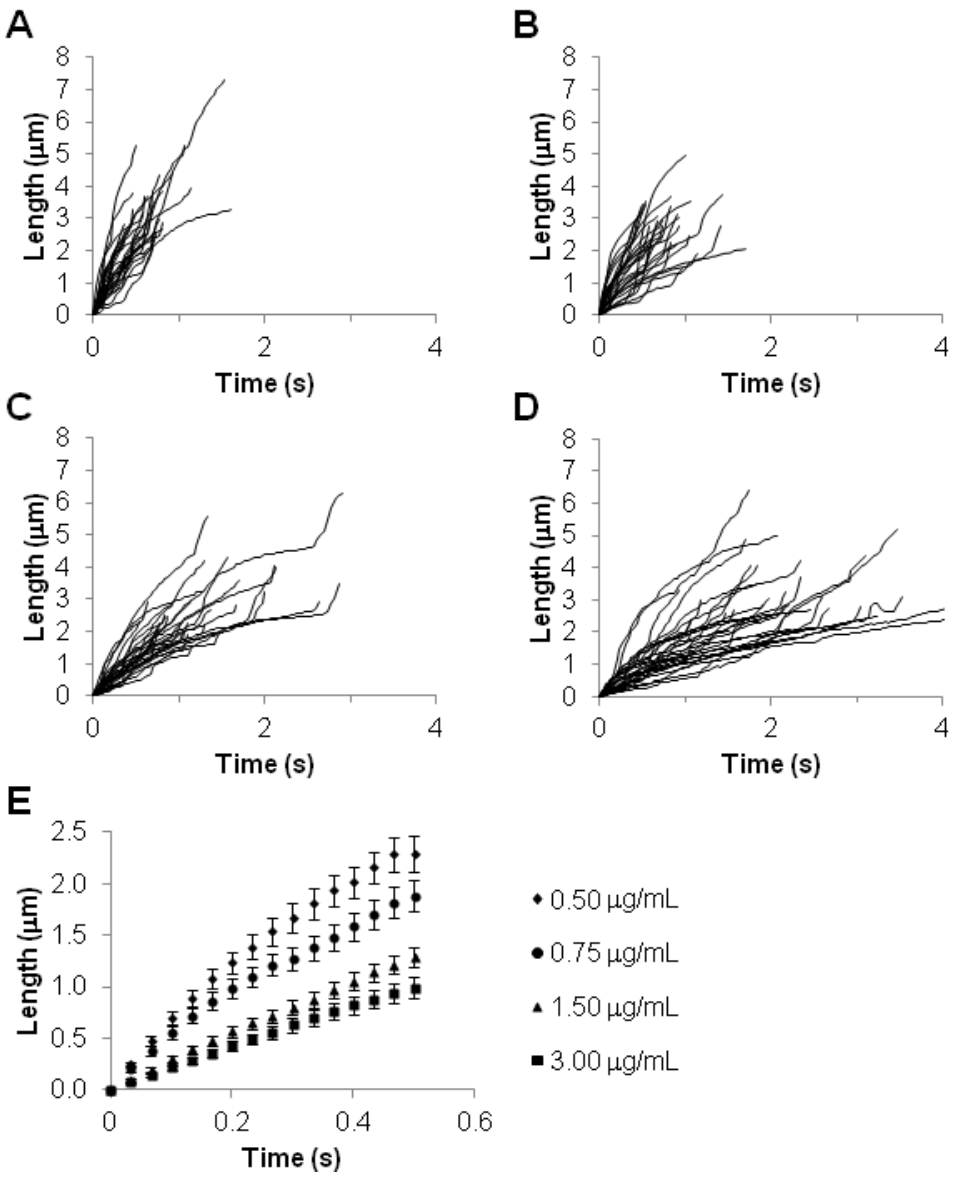


Figure 20: Frame-by-frame analysis was used to measure the instantaneous lengths of 30 tethers formed during rolling on P-selectin concentrations of (A)0.50, (B)0.75, (C)1.50 and (D)3.00 mg/mL. The instantaneous lengths were plotted as a function of time to illustrate tether growth rate, which decreases with increasing P-selectin concentration(E).

one membrane tether was significantly lower than the average velocity in the absence of membrane tethers. Although an overall trend was observed where decreasing velocity correlated with increasing P-selectin concentration, the presence of membrane tethers always resulted in a significant velocity decrease. Indeed,

neutrophils rolling on 0.5 μg/mL P-selectin saw an average velocity decrease of 73% in the presence of membrane tethers, while the average rolling velocity of neutrophils on 3.0 μg/mL P-selectin was decreased by 62%. Furthermore, we calculated the average variance of rolling velocity in the presence and absence of tethers (Fig. 19). Again, an overall decrease in variance was observed with increasing P-selectin concentration. However, on all concentrations a significant drop in variance correlated with the presence of membrane tethers.

We observed a slight decrease in neutrophil rolling velocity in the presence of membrane tethers when P-selectin concentration was increased. To better quantify the decreasing velocity even in the presence of membrane tethers, we measured the instantaneous lengths of membrane tethers formed on each of the P-selectin concentrations at a wall shear stress of 2 dyn/cm^2. These instantaneous lengths were plotted against time to illustrate the relationship between tether growth rate and P-selectin concentration (Fig. 20A-D). Although we observed a wide range of tether growth rates for each P-selectin concentration, there appeared to be a general trend where tethers grew more slowly on higher P-selectin coating concentrations. A plot of the average tether length for time points from 0 – 0.5 s for each of the P-selectin concentrations (Fig. 20E) showed that increasing P-selectin coating concentration led to a decrease in tether growth rates. These data demonstrate that membrane tethers can further stabilize rolling velocities on high P-selectin concentrations, even though they elongate slower than tethers formed on low P-selectin concentrations.

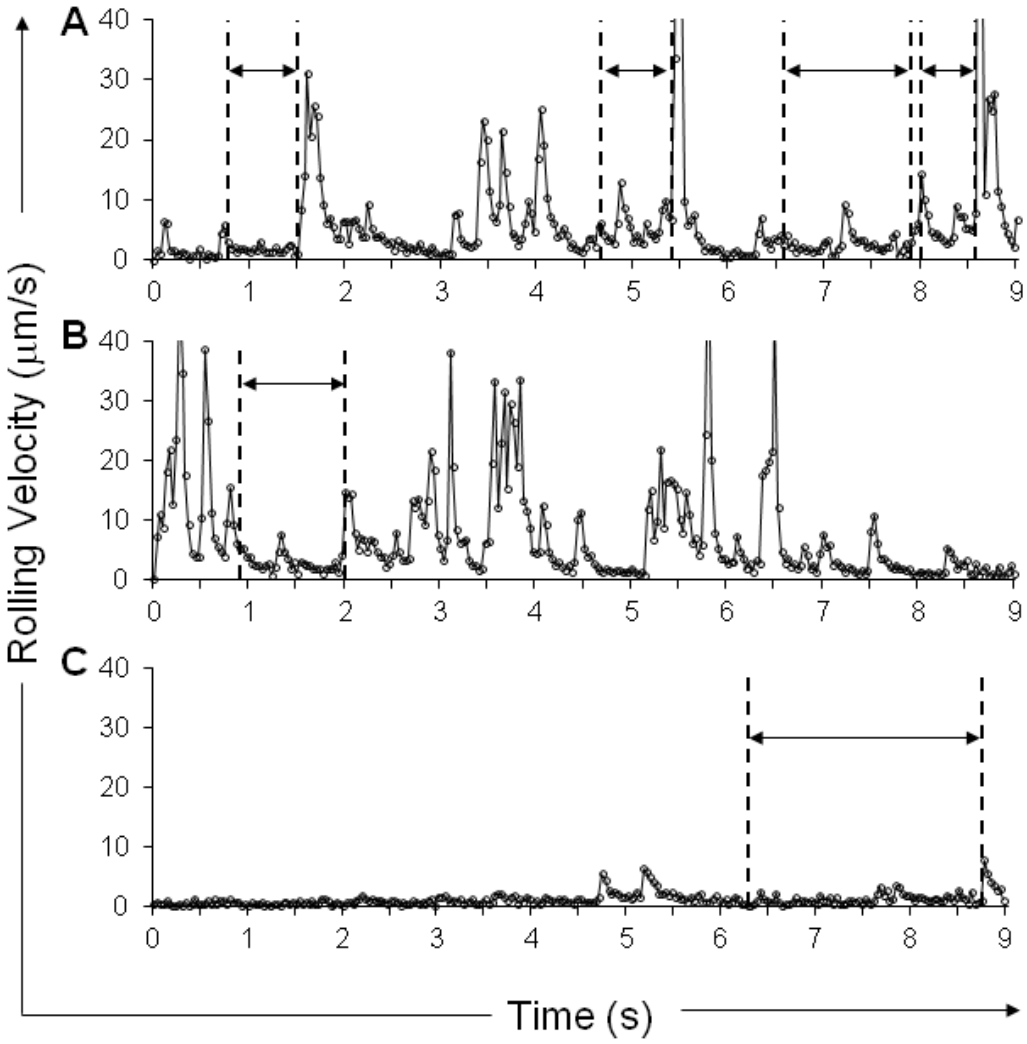


Figure 21: Instantaneous rolling velocities were measured for individual neutrophils rolling on glass substrates incubated with 0.5 μg/mL of (A) P-selectin, (B) rhP-selectin and (C) rhE-selectin. Cells were perfused at a wall shear stress of 2 dynes/cm^2. The highlighted portions of each plot indicate the presence of a membrane tether.

Membrane tether lengths and lifetimes are unchanged on a P-selectin-Fc chimera.

To investigate the effects of ligand type on tether formation and retraction, we perfused isolated neutrophils over surfaces coated with P-selectin isolated from platelet membranes (mP-selectin) and a recombinant human P-selectin-Fc chimera (rhP-selectin) (see Fig. 17). Figure 21 shows the instantaneous velocity profiles of individual neutrophils rolling on mP- and rhP-selectin (0.5 μg/mL). When perfused

at a shear stress of 2 dynes/cm^2, we observed similar neutrophil rolling velocity profiles on both types of P-selectin. Interestingly, neutrophils rolling on rhP-selectin appeared to extrude fewer membrane tethers than neutrophils on mP-selectin even though tether lifetimes appeared to be unchanged.

We performed a further investigation on neutrophil rolling and tether formation on mP- and rhP-selectin by calculating the average rolling velocities and tether properties of fifty neutrophils (Fig. 22). For P-selectin concentrations of 0.50 and 0.75 μg/mL, we found slightly higher rolling velocities on mP-selectin compared to rhP-selectin. At concentrations greater than 1.5 μg/mL, however, the average velocity on rhP-selectin was significantly greater than mP-selectin (Fig. 22A). Membrane tethers formed during rolling grew to lengths between 3 – 3.5 μm on both types of P-selectin (Fig. 22B). Tether lifetimes on rhP-selectin were also similar to mP-selectin, ranging from 0.9 – 1.6 s for the P-selectin concentrations tested (Fig. 22C). Interestingly, we observed a significant change in the percentage of time that tethers were present. Compared to mP-selectin (28 – 48%), membrane tethers were present only 12 – 21% of the time during rolling on rhP-selectin (Fig. 22D). To better understand this change, we calculated the frequency of tether formation as the number of membrane tethers that formed in a 9 second period. For mP-selectin, neutrophils formed 0.49 tethers/second on 0.50 μg/mL which decreased to 0.29 tethers/second on 3.00 mg/mL (Fig. 22E). On rhP-selectin, the tether formation frequency increased from 0.13 to 0.22 tethers/second when concentration increased from 0.50 to 0.75 μg/mL. From there, tether formation frequency decreased to 0.16 tethers/second on 3.00 μg/mL. These data suggest that

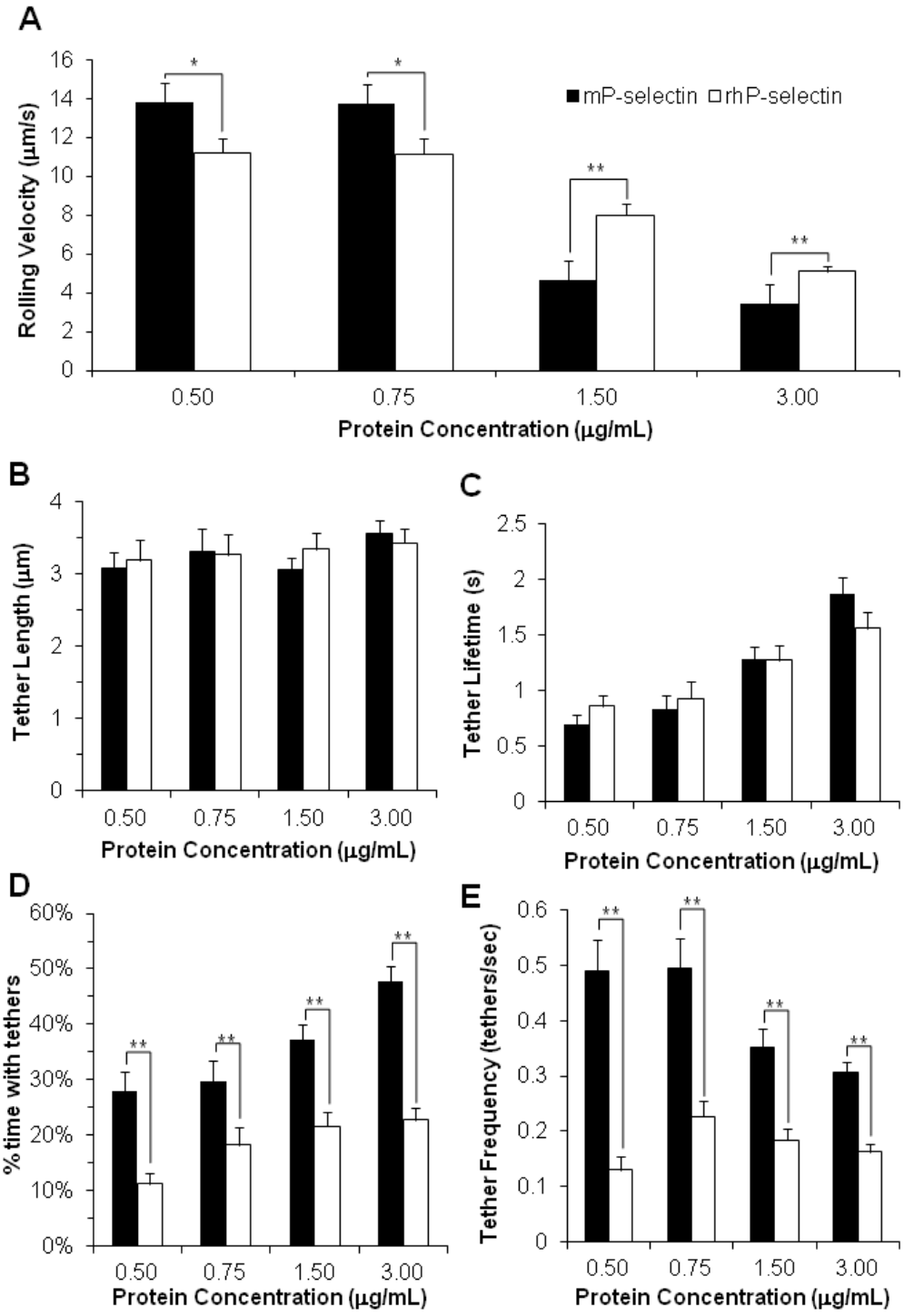


Figure 22: (A)Average rolling velocities were higher on mP-selectin at low concentrations. However, at higher concentrations rolling was slower on mP-selecitn. These differences in rolling velocity were not the result of any significant change in membrane tether length(B) or lifetime(C). The percentage of time that tethers were present and tether formation frequency were significantly lower on rhP-selectin.

the main difference between P-selectin isolated from platelets and recombinant P-selectin chimera is the frequency of tether formation.

Membrane tether lengths are unchanged on rhE-selectin but lifetimes are significantly longer compared to rhP-selectin. We observed that neutrophils exhibited significantly lower rolling velocities and fewer, less intense velocity spikes on rhE-selectin compared to rhP-selectin (Fig. 21). Simultaneously we observed that membrane tethers formed during rolling on rhE-selectin lasted significantly longer than tethers formed on either type of P-selectin. To quantify the differences between rolling on rhP- and rhE-selectin, we calculated the average velocities and tether properties of 50 neutrophils on each ligand. Figure 23A shows that neutrophils rolled significantly lower on rhE-selectin coated surfaces (2.1 – 1.3 μm/s) compared to rhP-selectin (13.7 – 6.0 μm/s) at low and high concentration levels (0.5 – 3.0 μg/mL). Similar to varying concentrations of rhP-selectin, mean tether length did not change significantly with rhE-selectin concentration (Fig. 23B).

Mean tether lifetime on rhE-selectin coated surfaces increased by 38% (2.9 – 4.0 seconds) with increasing concentration (Fig. 23C). These lifetime values were significantly greater than the tether lifetimes measured on rhP-selectin (0.7 – 1.7 seconds) and correlated with the significant decrease in rolling velocity. The longer tether lifetimes on rhE-selectin coated surfaces paralleled with an increase in the percent time that membrane tethers were present (Fig. 23D). Interestingly, the percent time with tethers on rhP-selectin surfaces increased with increasing concentration (11 – 25%) while the percent time with tethers on rhE-selectin

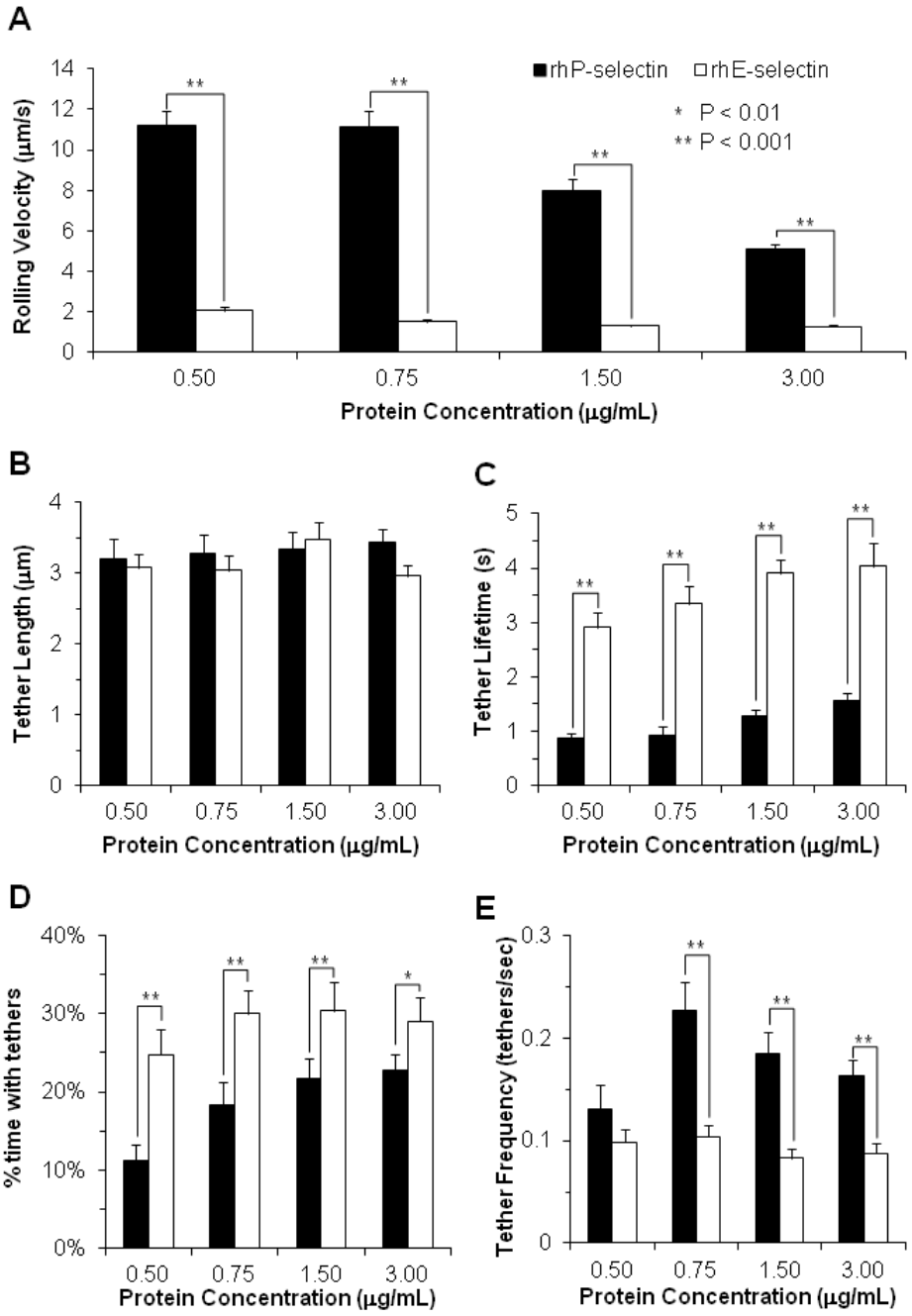


Figure 23: Human neutrophils were perfused over glass substrates incubated with various concentrations of Fc-conjugated recombinant P-selectin (rhP-selectin) and Fc-conjugated recombinant E-selectin (rhE-selectin). Rolling velocity was significantly decreased on rhE-selectin(A), which correlated with a significant increase in tether lifetime(C). Tether length remained relatively unchanged regardless of ligand type or coating concentration(B). Cells rolling on E-selectin exhibited lower tether frequencies than on P-selectin(D), however percent time with tethers present was increased(E) which can likely be attributed to the significant increase in tether lifetime.

surfaces did not vary much with concentration (25 – 30%). Similarly, Fig. 23E shows that membrane tether formation frequencies were relatively unchanged with regard to rhE-selectin concentration (0.08 – 0.10 tethers/second). These values were significantly lower than the frequencies on rhP-selectin for all ligand concentrations except 0.50 μg/mL. These data provide evidence that there are significant differences in tether lifetime but not length for similar concentrations of rhP- and rhE-selectin.

Membrane Tethers Formed During Rolling on rhE-selectin Last Longer Compared to rhP-selectin at Equivalent Rolling Velocities. To further investigate whether the significant increases in membrane tether lifetime on rhE-selectin were related solely to the decrease in rolling velocity, we decreased the coating concentration of rhE-selectin until the average neutrophil rolling velocity was equivalent to values obtained for 3.00 mg/mL rhP-selectin. At a coating concentration of 0.10 mg/mL rhE-selectin, we measured the average rolling velocity of 30 neutrophils at 3.2 mm/s compared to 3.7 mm/s on 3.00 mg/mL rhP-selectin (Fig. 24). Although the average rolling velocity on rhP-selectin was slightly higher, statistical analysis showed this difference was not significant. Measurements of tether length revealed that membrane tethers on average grew to lengths of 3.5 and 3.7 mm on rhP- and rhE-selectin, respectively (Fig. 24). However, membrane tethers continued to remain attached to the substrate for significantly longer periods of time on rhE-selectin. Indeed, membrane tethers lasted an average of 2.6 s on 0.10 mg/mL rhE-selectin compared to 1.5 s on 3.00 mg/mL rhP-selectin (Fig. 24). These data suggest

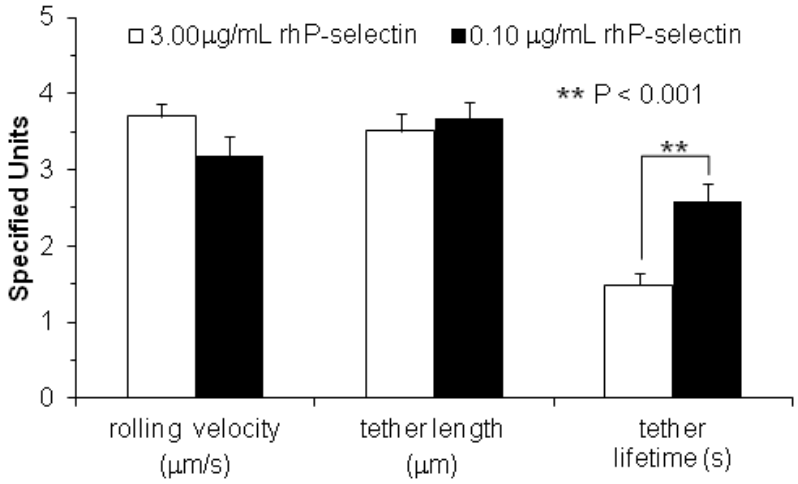


Figure 24: Neutrophils rolled with equivalent velocities on separate substrates coated with 3.00 μg/mL rhP-selectin and 0.10 μg/mL rhE-selectin. While tether lengths continued to be unaffected by protein coating concentration, tether lifetimes remained significantly longer on rhE-selectin.

that increased membrane tether lifetimes on rhE-selectin are not solely the result of decreased rolling velocity.

Multiple leukocyte ligands mediate membrane tether formation on E-selectin.

Although PSGL-1 appears to be the only physiologically relevant ligand to influence neutrophil rolling on P-selectin, recent studies have suggested that multiple ligands may be involved in rolling on E-selectin[258, 262]. However, no studies have investigated whether these additional ligands can mediate membrane tether formation during rolling. To investigate whether ligands distinct from PSGL-1 could mediate tether formation we incubated neutrophils with PL1, a blocking mAb to PSGL-1. We investigated PL1-treated and untreated neutrophil rolling on 0.5 μg/mL rhP- and rhE-selectin coated substrates. As expected, neutrophil rolling was entirely abolished on rhP-selectin after incubation with PL1. To verify that the

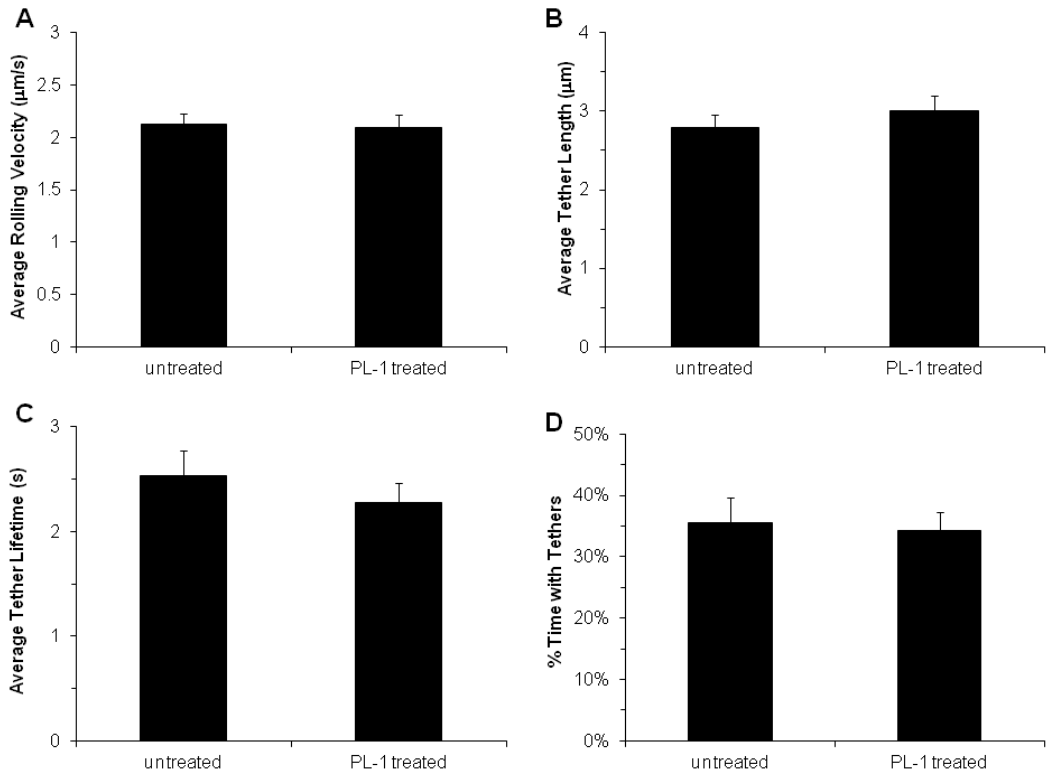


Figure 25: Human neutrophils were incubated with anti-PSGL-1 mAb PL1, a blocking antibody to PSGL-1. PL1-treated and untreated neutrophils were perfused over substrates coated with 0.5 μg/mL rhE-selectin. At a wall shear stress of 2 dynes/cm^2 there was no significant change in (A)rolling velocity, (B)tether length or (C)tether lifetime. As a result, the percentage of time that tethers were present was also relatively unaffected by PL1 treatment(D).

P-selectin was functional, untreated neutrophils were perfused over the same substrate with no change in rolling velocity or tether properties.

However, Figure 25A shows that neutrophil rolling velocities on rhE-selectin were relatively unchanged following PL1 incubation. Figure 25B shows that membrane tethers pulled by PL1-treated cells grew to approximately 3 μm, which was only slightly longer than tethers formed by untreated cells (2.7 μm). PL1-treatment of neutrophils did lead to a slight decrease in tether lifetimes from 2.6 – 2.3 seconds (Fig. 25C). Further analysis showed that this decrease was not

statistically significant. Similarly, there was only a slight decrease in the percentage of time that tethers were present (Fig. 25D). These data suggest that leukocyte ligands to E-selectin distinct from PSGL-1 can mediate membrane tether formation.

Discussion

In this study, we demonstrate that increasing the concentration of P-selectin used to coat glass substrates for in vitro neutrophil rolling experiments increases the lifetimes of membrane tethers but does not affect membrane tether length. A comparison of membrane tethers formed on P-selectin isolated from platelet membranes and a recombinant human P-selectin-Fc chimera revealed no significant differences in tether length or lifetime for similar coating concentrations. We also report the direct observation of neutrophil membrane tether formation during rolling on E-selectin coated surfaces and show that slower rolling on E-selectin corresponds to an increase in membrane tether lifetimes. These results are significant for four reasons: (i)we demonstrate that ligand density, in addition to shear stress, plays a role in membrane tether formation, (ii)we compare membrane tether formation on P-selectin isolated from different sources, (iii) we report the characterization of membrane tether formation on E-selectin coated surfaces and (iv)our PSGL-1 blocking experiments support previous studies which suggested that multiple ligands mediate rolling on E-selectin[258, 262] and demonstrate that ligands other than PSGL-1 can mediate membrane tether formation.

Previously, human neutrophils rolling on P-selectin coated surfaces have been shown to stabilize their rolling velocities through the extrusion of membrane tethers[197]. The formation of membrane tethers reduces the hydrodynamic force imposed on selectin-ligand bonds by lengthening the lever arm, thereby resulting in an increase in bond lifetimes[35]. However, leukocytes have also been shown to roll slower when a higher concentration of selectin ligand is available for binding[130-

131, 184]. Several groups have also demonstrated that membrane tether formation occurs at a critical force[56, 147, 223], which during rolling is supplied by selectin-ligand interactions. We investigated the influence of selectin concentration on membrane tethers by observing neutrophil rolling on substrates coated with varying P-selectin concentrations (0.5 – 3.0 μg/mL). Our rolling velocity measurements decreased significantly with increasing P-selectin concentration, which agreed with a previous report by Lawrence and Springer. These results suggested that an increase in P-selectin coating concentration increased the number of P-selectin sites available for binding. Of the rolling cells we observed at 2 dynes/cm^2, nearly all cells formed at least one membrane tether during 15 seconds of observation. Similarly, Ramachandran et al reported that 100% of cells formed at least one membrane tether after 15 seconds of rolling at 2 dynes/cm^2[197].

In observing membrane tether formation, we found that P-selectin coating concentration had a profound impact on membrane tether lifetimes. While there was no significant difference between tether lifetimes on 0.50 and 0.75 μg/mL P-selectin, increasing P-selectin concentration beyond 0.75 μg/mL resulted in significant increases in tether lifetime. Schmidtke and Diamond reported the observation of membrane tethers with branches along their lengths and suggested that this phenomenon may be indicative of tethers being multi-bonded to the surface[219]. Our tether lifetime measurements suggest that at higher P-selectin concentrations, a single membrane tether may interact with multiple P-selectin molecules along its length. Multiple selectin-ligand interactions points would mean that the hydrodynamic force applied to the tether is shared, thereby reducing the

force on a single bond pair and allowing the membrane tether to remain attached to the substrate for a longer period of time. The increase in tether lifetime was also confirmed by an increase in the percentage of time that membrane tethers were present.

Interestingly, membrane tether length did not significantly change with P-selectin concentration. Although tethers lasted longer on substrates with higher P-selectin concentrations, the average tether length never exceeded approximately 3.5 μm. The extrusion of a membrane tether has been shown to depend on the adhesion energy between the plasma membrane and the cytoskeleton[56, 147]. Once this crossover point is reached, excess plasma membrane feeds out from the cell body onto the tether. Raucher and Sheetz reported that membrane tethers pulled from fibroblasts could not be extended beyond a certain length unless the actin cytoskeleton was disrupted with cytochalasin[200]. Our tether length measurements also showed that normally only a finite amount of membrane was available to feed out onto the tether. This suggests that membrane tether length is an inherent property of the membrane/cytoskeleton attachment energy and not the pulling force applied by selectin-ligand interactions.

We also compared the average rolling velocities and velocity variances of cells in the presence and absence of membrane tethers. While Ramachandran et al reported that membrane tethers stabilize rolling velocities over a range of shear stresses[197], this study did not test multiple P-selectin coating concentrations. Our results indicate that membrane tethers stabilize rolling velocity on a wide range of P-selectin concentrations. On substrates coated with a low concentration of P-

selectin (0.5 μg/mL) we found that rolling velocities and velocity variances were significantly lower when a membrane tether was present. Similarly, there was also a statistically significant difference in average velocity and velocity variance when P-selectin concentration was high (3 μg/mL). This indicates that even when a high number of sites are available for binding, the reduction of force on selectin-ligand bonds by a membrane tether can still significantly impact rolling behavior.

When comparing rolling velocities in the presence of a membrane tether on different P-selectin concentrations, we noted that there was a slight decrease in these velocities with increasing selectin concentration. This suggested that P-selectin concentration played a role in the growth rates of membrane tethers. In reporting the first direct observation of membrane tethers under flow, Schmidtke and Diamond observed tether growth rates between 1 – 6 μm/s for leukocytes rolling on P-selectin coated surfaces at a wall shear rate of 150 s^{-1} [219]. Higher growth rates of 5 – 15 μm/s have been reported in studies involving collisions between leukocytes and P-selectin coated microspheres[74, 175]. The growth rates we measured at 2 dynes/cm^2 (1.5 – 4.5 μm/s) were in the same range as those reported by Schmidtke and Diamond. We also observed that tether lengths tended to be smaller at a particular time point on high P-selectin concentration while tethers grew to a longer length in a shorter period of time on low concentration. This suggests that P-selectin concentration influences tether growth through a force sharing mechanism. In other words, when there are more bonds formed during rolling the hydrodynamic force will be shared among a larger number of bonds resulting in less force applied to the membrane tether which results in a slower growth rate. Conversely, tethers formed

during rolling on low concentrations of P-selectin grow faster, thereby shielding bonds at the trailing edge of the cell and stabilizing rolling velocity.

Although membrane tether formation from neutrophils alone plays a role in P-selectin mediated rolling, Girdhar and Shao demonstrated that tethers can be simultaneously extracted from leukocytes and endothelial cells[84]. Also, membrane tethers have been observed during neutrophil rolling on endothelial cell layers in vivo[232]. While previous reports have suggested that P-selectin is expressed on activated endothelial cells at a density of 25 - 50 molecules/μm^2[94], Setiadi and McEver reported that E-selectin was expressed on cytokine-activated HUVECs at a density of approximately 350 molecules/μm^2[221]. However, little is known about tether formation on E-selectin coated surfaces. The only known reference of tether formation on E-selectin coated surfaces was by a previous master's student in Dr. Schmidtke's group[257], however these results were not published. This study also did not look at ligand density and used a soluble E-selectin instead of an E-selectin-Fc chimera. To determine whether membrane tether formation can be affected by the type of ligand present, we performed similar experiments with neutrophils on surfaces coated with recombinant human (rh) P- and E-selectin-Fc chimeras. Membrane tether lengths and lifetimes were relatively unchanged regardless of the type of P-selectin used (Fig. 22). Using DIC microscopy, we were able to directly observe the formation of membrane tethers during neutrophil rolling on E-selectin. Neutrophil rolling velocities were significantly lower on E-selectin compared to P-selectin for identical coating concentrations, which agreed with a previous report by Lawrence and

Springer[131]. The decreased rolling velocities on E-selectin correlated with a significant increase in membrane tether lifetime, however the percentage of time that tethers were present as well as the frequency of tether formation were lower than on P-selectin.

Although the decreased rolling velocities and increased tether lifetimes we observed on E-selectin could partially owe to differences in ligand density following substrate incubation, it may also be explained by differences in E-selectin bond kinetics or the presence of other ligands to E-selectin on the neutrophil surface. Lawrence and Springer demonstrated that neutrophils roll slower on E-selectin compared to P-selectin at equal site densities[131]. More recently, Wayman et al observed that E-selectin/ligand bonds display a triphasic force dependence, transitioning from slip bond to catch bond kinetics at a shear stress of 0.3 dyn/cm^2 and then back to slip bond kinetics at a shear stress of 0.5 dyn/cm^2[252]. In regard to the existence of multiple ligands to E-selectin, previous studies have shown that in the absence of PSGL-1 leukocytes are still able to adhere to and roll on E-selectin [258, 262]. Xia et al observed that leukocytes from PSGL-1 knockout mice were still able to roll on E-selectin coated surfaces, but they reported an 80% reduction in rolling on E-selectin in TNF-α-activated venules when P-selectin was blocked[258].

Using decreased concentrations of rhE-selectin such that neutrophils rolled at velocities similar to those measured on rhP-selectin, we measured membrane tether lifetime on rhP- and rhE-selectin independent of rolling velocity. Even at equivalent rolling velocities, we noted that membrane tethers continued to last significantly longer on rhE-selectin (Fig. 24), suggesting a difference in bond

kinetics or the presence of additional cell surface ligands. In our investigation of E-selectin ligands other than PSGL-1, we observed that incubating neutrophils with PL1, a blocking mAb to PSLG-1, did not significantly reduce rolling velocities or membrane tether length or lifetimes on E-selectin (Fig. 25). Xia et al also reported little difference in the rolling velocities of wild-type and PSGL-1 knockout leukocytes on E-selectin[258]. Conversely, PL1-incubated cells did not roll on substrates coated with the same concentration of P-selectin (0.5 μg/mL). While this may be partially the result of a difference in site densities, the markedly contrasting behaviors of PL1-incubated cells on E- and P-selectin coated substrates suggests that leukocyte ligands to E-selectin aside from PSGL-1 are able to mediate membrane tether formation on E-selectin. The exact nature of these additional ligands and whether they mediate tether formation alone or in conjunction with PSGL-1 is still under investigation.

In summary, our results demonstrate the important role of selectin-ligand interactions in membrane tether formation during neutrophil rolling. We have shown that increased selectin density significantly increases membrane tether lifetime while tether length is a property inherent to the cell membrane. We also report the characterization of membrane tether formation on E-selectin and demonstrate that there may be other ligands aside from PSGL-1 that mediate this phenomenon. These results are significant in that they: (i)demonstrate that factors other than shear stress can affect membrane tether properties, (ii)provide support to studies that have suggested that leukocytes express multiple ligands to E-selectin

and (iii)demonstrate the importance of attachments between the plasma membrane and the cytoskeleton to neutrophil rolling adhesion.

CHAPTER 4: Effects of Microfluidic Channel Geometry on Leukocyte Rolling Assays

Leukocyte adhesion and rolling are important in many physiological processes and adverse cardiovascular events. These adhesive interactions are mediated by P- and E-selectin expressed on platelets and endothelial cells[14, 107] and their corresponding ligands (e.g. PSGL-1, L-selectin) expressed on leukocyte microvilli.[162, 238] Leukocyte rolling arises from a balance between the adhesive forces of these receptor-ligand interactions and the hydrodynamic fluid forces that cause cells to translocate downstream.[36, 130]

Parallel plate flow assays have provided significant insight into the molecular and biophysical mechanisms of leukocyte rolling. By using flow chambers with specific geometric ratios (e.g. chamber width:chamber height), the shear stress and torque acting on a rolling cell can be easily calculated. Previous theoretical and experimental studies have demonstrated the effects of this ratio on the flow regime for macroscale dimensions.[41, 86, 241] Specifically, in chambers with a width:height ratio of 10:1, the flow can be approximated as unidirectional and independent of lateral position across a large percentage of the chamber width.[41] Chambers with this ratio, however, may require large volumes for even short perfusion times making them a drawback in assays where sample volume is severely limited.

Microfluidic flow chambers have become increasingly popular over the last decade in cell adhesion assays due to the reduced amount of sample required.[22, 39, 89-90, 118, 142, 172, 215, 227]. These devices have been used with many different cell types including endothelial cells[118], platelets[118, 172, 214],

fibroblasts[142], bacteria[122], and cancer cells.[213] As Table 4 demonstrates, microfluidic studies with leukocytes have emerged focusing on rolling behavior[40, 52, 215-216], cell adhesion strength[89], migration during chemotaxis[103, 139] and cell sorting applications.[166, 208] It should be noted that there also have been recent reports of leukocyte rolling velocities utilizing glass microcapillary tubes.[123, 264] While some of these studies investigated leukemic cell rolling on various ligands[40, 52], only a few have reported neutrophil rolling velocity measurements on E-selectin[123, 215] or P-selectin.[123] Furthermore, the microfluidic devices used in these leukocyte studies encompassed a wide variety of dimensions. When designing microfluidic chambers for adhesion assays, a balance arises between the geometric effects on reduced sample volume and wall shear stress. For example we have previously demonstrated that in microfluidic devices with a width:height ratio of 4:1 the volume of blood needed is minimized, but that this aspect ratio results in sidewall effects and a non-uniform shear profile across the width of the channel.[214] In contrast, an aspect ratio of 10:1 has a uniform shear profile but may require larger volumes of blood to achieve physiological levels of wall shear rate.

A parameter that needs to be considered in microfluidic assays is the ratio of cell diameter (D_c) to chamber height (H). Previously Goldman, Cox and Brenner presented calculations for the drag force and torque acting on a rigid sphere in simple shear flow[87] when the chamber height is much greater than the cell diameter. In addition, Pozrikidis demonstrated theoretically that the simple shear assumption is

Table 4: Comparison of recent leukocyte studies using microfluidic devices

Ref.	H (μm)	Cell Type	Dc/H	Ligand	Shear (dyn/cm^2)	Volume* (μL)	Velocity (μm/s)
215	100	neutrophil	0.08	E-selectin**	2.0	20	3.7 - 4.5
216	100	neutrophil	0.08	E-selectin**	2.0	60	0.0 - 8.0
this work	20	neutrophil	0.40	P-selectin	0.5 - 8.0	0.8	1.0 - 2.5
	30		0.27			2.7	1.5 - 4.5
	75		0.11			42	3.0 - 9.0
	100		0.08			100	3.7 - 9.0
	150		0.05			340	3.5 - 8.0
	250		0.03			3125	3.0 - 7.5
40	145	KG-1a	0.10	hyaluronan	0.0 - 5.0	315	2.0 -15.0
52	30	HL60	0.40	P-selectin	0.3 - 2.2	10.8	N/A
166	57	Raji/Molt-3	0.26	anti-CD5/ - CD19	5.0 – 15.0	N/A	N/A
89	35	neutrophil	0.23	fibrinogen	0.7 - 5.0	N/A	N/A
103	45	neutrophil	N/A	E-selectin/ ICAM-1	< 0.1	N/A	N/A
139	50	neutrophil	N/A	IL-8	< 0.1	N/A	N/A
208	13	neutrophil/HL60/ ALL/AML***	N/A	none	>100	N/A	N/A

*Volume = amount of sample required based on 5 min perfusion at 2 dynes/cm^2
**Expressed by transfected L-cells (mouse fibroblast) cultured in device
***ALL = acute lymphoid leukemic cells, AML = acute myeloid leukemic cells

only valid for adherent cells when the ratio of cell diameter to chamber height (D_c/H) is less than 0.1.[194] Typical parallel-plate flow chambers have heights anywhere between 100 and 250μm, and thus for adhesion studies involving leukocytes (D = 8 - 10 μm) a D_c/H ratio of 0.1 or less is normally present. Previous microfluidic studies that have studied the rolling behavior of neutrophils[215] or leukemic cells[40] have employed D_c/H ratios of 0.1 (Table 4). However, the diameter of a postcapillary venule, where leukocyte rolling typically occurs, may be only about three to four times the diameter of a leukocyte[88] and thus the D_c/H ratio is greater than 0.1. Furthermore, in these vessels, a minimal number of adherent leukocytes can significantly increase flow resistance.[53, 97] Theoretical

studies modeling cells as rigid spheres[21, 30-32], hemispherical bulges on microchannel walls[77, 194] and viscoelastic or elastic spheres[49, 111, 181] have demonstrated numerically that the drag coefficient increases with increasing flow occlusion or decreasing chamber height, which can be attributed to an increase in pressure drop across the cell surface.

Recently, Khismatullin and Truskey computationally investigated the effect of channel height on leukocyte adhesion by three dimensional numerical simulations of rolling monocytes (D_c = 13 μm).[111] In simulations at constant wall shear stress, it was observed that both the monocyte's contact area with the underlying substrate as well as the contact time increased as the channel height was decreased from 80 μm to 20 μm which corresponds to changes in D_c/H from 0.16 to 0.65. They attributed these changes in contact time and area to changes in cell deformation. They did not, however, report the impact of channel height on leukocyte rolling velocities.

We designed and fabricated microfluidic chambers that required perfusion rates as low as 40 nL/min. In comparison to previous reports with microfluidic devices or micron-sized glass capillary tubes [40, 52, 215], our smallest chambers require 13 – 390 times less perfusion volume (Table 4). Rolling velocity measurements in P-selectin coated microdevices revealed that neutrophils exhibit more stable rolling behavior in chambers with heights close to the diameter of postcapillary venules when compared to rolling in flow chambers with conventional heights. Numerical simulations of leukocyte rolling velocities show a similar trend with channel height. Rolling assays with fixed cells and PSGL-1 coated beads in the

devices suggest that the observed changes in rolling velocity are related to the ability of the neutrophils to deform. These results are important in the design of low-volume flow adhesion assays that maybe used as point-of care devices in developing countries, for basic biology studies with blood from knockout-mice, or in analysis of blood from newborns.

Methods

Proteins and Reagents

P-selectin purified from human platelet membranes was kindly provided by Dr. Rodger McEver (Oklahoma Medical Research Foundation, Oklahoma City, OK). Fc-conjugated human PSGL-1 was purchased from R&D Systems. Human serum albumin (HSA) solution was purchased from Gemini Bio-Products.

Fabrication of Microfluidic Chambers

Master templates for microfluidic chambers were fabricated through a standard negative photolithography process similar to that previously described.[171, 214] Glass microscope slides were cleaned with 20% HCl for 10 minutes, rinsed with distilled water and dried at 200^{o}C for 10 minutes. Different photoresists were used to achieve the thickness necessary for each of the different chamber heights. The exact parameters for each photoresist layer thickness are given in Appendix C. KMPR resists were spun directly onto the slide surface, while SU-8 resists were preceded by a primer (Omnicoat; Microchem Corporation) which was spun for 30 s at 3000 rpm. Slides were exposed through chrome masks designed in AutoCAD and fabricated by Advance Reproductions. Unexposed photoresist was removed by sonication in SU-8 developer for 60 s.

PDMS stamps were fabricated using Sylgard 184 Silicone Elastomer kits. The base and curing agent were mixed together in a 10:1 ratio and poured over the channel templates. An elbow outlet port (Small Parts) was placed at one end of the template and the mixture was cured at 100^{o}C for 30 minutes. After curing, the hardened

PDMS was removed from the oven and cut out of the Petri dish. A reservoir was cut out at the end of the channel opposite the outlet port, and PDMS that had entered the outlet port and cured was bored out with a needle. Stamps were cleaned in 20% HCl and 70% ethanol, dried in an oven and sealed to clean glass cover slips pattern side down by treating both stamp and cover slip with a high voltage gun.[171]

Flow Characterization in Microfluidic Chambers

Experimental determination of the velocity profiles in the channels of different heights was accomplished by measuring the velocity of latex beads at several flow rates. Microfluidic chambers were incubated with a solution of 0.5% HSA in HBSS for 30 min to block non-specific interactions with the glass and PDMS surfaces. Polystyrene microspheres (D = 6 μm; Polysciences) were washed three times with HBSS to remove surfactant and incubated for 30 minutes in the same HSA/HBSS solution. Microspheres were then perfused through the chambers at wall shear rates of 25, 50, 100 and 200 s^{-1} calculated at the bottom wall of the channel. Perfusion was observed with a Zeiss Axiovert 200 inverted microscope at 10X magnification and recorded to VHS tapes at 30 frames per second using a Daige MTI camera and a Sony S-VHS videocassette recorder. 15 s video segments of microsphere perfusion were digitized and the velocities of free-flowing microspheres in the same focal plane as the bottom wall of the chamber were determined using Metamorph version 7.5 software (Molecular Devices).

PSGL-1 Coated Beads

Polystyrene microspheres were washed as described above to remove surfactant. Microspheres were then incubated with Fc-conjugated Human P-selectin-glycoprotein-ligand-1 (PSGL-1; R&D Systems) at a concentration of 200 μg/mL in HBSS without HSA for 45 minutes with gentle agitation. Following protein incubation, microspheres were washed three times with a 0.5% HSA/HBSS solution to prevent non-specific binding. Microspheres were then diluted in HSA/HBSS to a concentration of $2.5*10^5$ microspheres/mL for rolling experiments. The presence of PSGL-1 adsorbed onto the microspheres was confirmed by flow cytometry with mouse-anti-PSGL-1 mAb PL1 and a FITC-conjugated goat-anti-mouse secondary antibody (data not shown).

Neutrophil Isolation

Human blood was obtained from healthy donors by venipuncture and anticoagulated with sodium heparin. Whole blood was layered on top of a cell separation medium (Lympholyte-poly, Cedarlane Laboratories) and spun at 400 g for 30 minutes. The resulting neutrophil layer was removed and washed with Hanks Balanced Salt Solution with Ca^{2+} and Mg^{2+} (HBSS, GIBCO Laboratories) supplemented with 0.5% HSA. Remaining erythrocytes were lysed with sodium chloride solutions, and neutrophils were washed two more times with the HSA/HBSS solution. Neutrophils were suspended in the same solution at $2.5*10^5$ cells/mL. Cell counts were verified using a manual hemocytometer set (Hausser Scientific). For experiments with fixed, non-deformable cells, isolated neutrophils were incubated in a solution of 1%

paraformaldehyde for 20 minutes and then washed five times to remove any remaining paraformaldehyde. The blood collection protocol was approved by the Institutional Review Board of the University of Oklahoma, and informed consent was obtained from all donors.

Rolling Velocity and Contact Area Experiments

Fully assembled microfluidic chambers were incubated with a solution of 1% Aquasil (Thermo Scientific) for 10s, rinsed three times with ultra-pure water and dried under vacuum at 80^{o}C for 30 minutes. Following Aquasil treatment, chambers were then incubated with 1.5 μg/mL P-selectin for 3 h, and then washed and incubated for 30 minutes with a solution of 0.5% HSA in HBSS to prevent non-specific binding. Isolated human neutrophils were perfused through the flow chambers at wall shear stresses of 0.5, 2, and 8 dynes/cm^2. Cells were observed rolling on the bottom walls of the chambers using a Zeiss 200A inverted microscope with a 63X (NA 1.40) Plan-Apochromat oil immersion objective. Adhesive and rolling interactions were recorded to VHS tapes using a Daige-MTI camera and a Sony S-VHS videocassette recorder. To determine the effects of cell deformation on rolling velocity, neutrophils fixed with paraformaldehyde and polystyrene beads coated with Fc-conjugated human PSGL-1 were also perfused through P-selectin coated chambers at a wall shear stress of 2 dynes/cm^2.

Video segments (t = 15 seconds) of untreated cell, fixed cell or polystyrene bead rolling were digitized, and instantaneous rolling velocities, average velocity, and velocity variance were measured using frame-by-frame analysis over 2 second

intervals. For a single shear stress, average velocities and velocity variances were compared statistically using an analysis of variance across the range of D_c/H values (0.032 – 0.4), followed by a Student's t-test on specific D_c/H pairs.

Similarly, the footprints of rolling neutrophils were observed using interference reflection microscopy (IRM) with 63x (NA 1.25) Plan-Neoflaur oil immersion antiflex objective. IRM was used in conjunction with frame-by-frame analysis to measure the instantaneous cell footprints of rolling neutrophils. These instantaneous values were averaged over 30 frames to determine the average footprint area for 1 second of rolling. The average footprints of 30 neutrophils were then averaged for wall shear stresses of 0.5, 2 and 8 dynes/cm^2 and chamber heights between 20 – 100 μm (D_c/H values from 0.4 – 0.08). Average footprint areas were compared statistically with an analysis of variance across the ranges of channel heights and shear stresses, followed by a Student's t-test on specific height and shear stress pairs.

Numerical Model

The P-selectin mediated rolling of a single leukocyte in a rectangular microchannel was simulated by a custom incompressible computational fluid dynamics (CFD) solver, referred to as VECAM (ViscoElastic Cell Adhesion Model). VECAM has the following features: 1) fully three-dimensional model; 2) two viscoelastic fluid compartments of the cell (the nucleus and the cytoplasm); 3) cortical tension takes into account elasticity of the plasma membrane and an underlying cortex; 4) the cell shape is tracked by the Volume-of-Fluid (VOF) / Piecewise-Linear Interface

Calculation (PLIC) method and the force exerted on the cell membrane is determined by the Continuous Surface Force (CSF) method; 5) quasi-uniform distribution and viscoelasticity of cell microvilli; 6) tether pulling from a microvillus at a supercritical force; 7) stochastic receptor-ligand binding kinetics with receptor (P-selectin) and ligand (PSGL-1) distributed uniformly over lower surface of a channel and a microvillus tip, respectively; 8) the spring/peeling model for the forward and reverse reaction rates [46]; 9) dimeric receptor-ligand bonds; and 10) realistic flow field based on a series solution for the laminar flow velocity in a rectangular flow channel. More details about VECAM are available in [112-113]. The values for model parameters used in the simulation can be found in Table 5[11, 23, 71, 113, 144, 163, 174, 192, 203, 217, 224, 242, 244, 267]. These simulations were performed by Dr. Damir Khismatullin from Tulane University.

Table 5: VECAM model parameters

Parameter	Value	Ref
Leukocyte diameter	8 μm	
Nucleus volume fraction	21%	217
Leukocyte cortical tension	30 μN/m	242, 267
Cytoplasmic viscosity	10 Pa * s	217
Cytoplasmic relaxation time	0.176 s	217
Nucleus viscosity	25 Pa * s	244
Number of microvilli	729	23
Unstressed microvillus length	0.5 μm	144
Microvillus radius	50 nm	144
Density of dimeric PSGL-1 molecules	12393 molec/cell	163
P-selectin surface density	150 molec/μm^2	
Microvillus spring constant	43 pN/μm	224
Microvillus viscosity	30.1 (pN * s)/μm	224
Tether viscosity	11.0 (pN * s)/μm	192
Critical force for tether formation	47.5 pN	192
Equilibrium length of PSGL-1/P-selectin bonds	70 μm	192
Forward reaction rate coefficient	1.70 μm^2/(s * molec)	203
Reverse reaction rate coefficient	1 s^{-1}	5
Bond bound state spring constant	5.3 pN/μm	71
Bond force amplification factor	8	117
Bond transition state spring constant	0.106 pN/μm	11
Wall shear stress	0.5 dyn/cm2	

Results

Microfluidic Channel Fabrication and Characterization. We fabricated microfluidic devices with varying dimensions that required very low sample volume for perfusion at physiologically relevant shear stresses (0.5 – 8 dynes/cm^2). Microfluidic chambers were fabricated by affixing PDMS molds of photolithography templates to glass cover slips for *in vitro* observation and characterization of neutrophil and microsphere rolling. The microfluidic channels that resulted from the assembly of the PDMS molds to glass cover slips resembled rectangular ducts with side walls at y = -a and y = a and top and bottom walls at z = b and z = -b, respectively. For a rectangular channel bounded on all four sides, the conservation of momentum equation reduces to:

$$\frac{1}{\mu}\frac{dP}{dx} = \left(\frac{\partial^2 v_x}{\partial y^2} + \frac{\partial^2 v_x}{\partial z^2}\right) \tag{7}$$

A solution to this second-order, nonlinear partial differential equation was published by Batchelor[10], with the flow velocity for an element of fluid being:

$$v_x = \frac{1}{2}\frac{\Delta P}{\mu L}\left(z^2 - b^2\right) + \sum_{n=0}^{\infty} A_n \cos\frac{(2n+1)\pi z}{2b} \cosh\frac{(2n+1)\pi y}{2b} \tag{8}$$

where,

$$A_n = \frac{16b^2\left(\frac{\Delta P}{\mu L}\right)(-1)^n}{\left[(2n+1)\pi^3\right]\cosh\left(\frac{(2n+1)\pi a}{2b}\right)}$$

Volumetric flow rate (Q) can be calculated in terms of the pressure gradient (ΔP) by integrating equation 8 with respect to the height and width of the channel:

$$Q = \int_{-a}^{a} \int_{-b}^{b} v_x \, dz \, dy \tag{9}$$

From there, the solution of this integral is rearranged to give ΔP in terms of Q and then substituted for ΔP in equation 8. Once v_x is in terms of Q, one can determine the wall shear rate at the bottom wall of the channel simply by evaluating the derivative of v_x with respect to the height of the channel at z = b:

$$\gamma_{z,wall} = \left. \frac{\partial v_x}{\partial z} \right|_{z=b} \tag{10}$$

Equation 8 shows that the flow velocity for a fluid element is dependent on both its position in relation to the channel's height and width. In both cases the velocity profile is parabolic, which means there will be non-uniform flow across both the height and width of the channel. A previous study, however, demonstrated that increasing the width:height ratio of a rectangular channel resulted in more uniform flow across the width of the channel.[214] It was observed that free flowing velocities were near constant over approximately 90% of the channel width when the width:height ratio was 10:1. Therefore, the microfluidic channels in this study were fabricated with this ratio so that observations and/or measurements were not restricted to the middle of the chamber width.

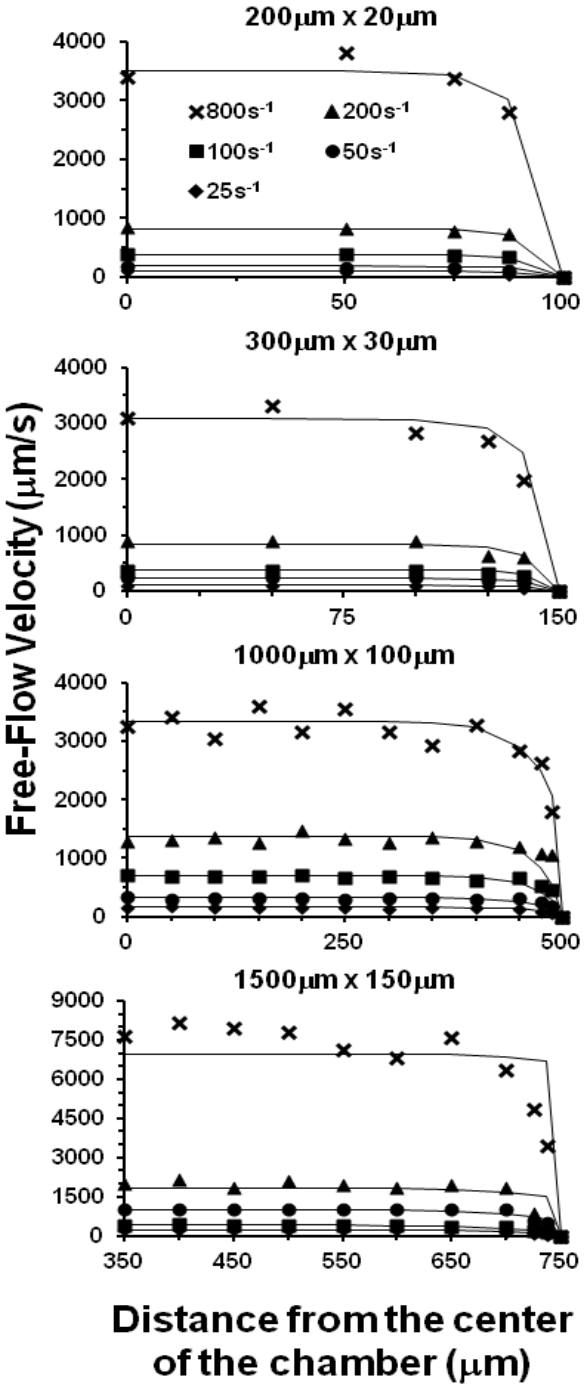


Figure 26: Microspheres were perfused through microfluidic devices at various shear rates in order to systematically characterize the flow with respect to the channel width. The velocities of free flowing microspheres were measured at varying distances from one of the lateral walls (individual points) and compared to an analytical solution (solid lines) through a least-squares analysis.

Prior to rolling experiments, the flow in these microfluidic channels was systematically characterized. Polystyrene microspheres blocked with HSA (0.5% in HBSS) were perfused through channels that had also been blocked with albumin. Coating the microspheres and the channel walls with albumin prevented non-specific adhesion of the microspheres to the walls or bottom of the microfluidic devices. The velocities of microspheres in free flow near the bottom channel wall were measured and compared to those determined from the analytical solution. Because it is not easy to measure the z-position of a microsphere, a least-squares analysis based on the average separation distance of the microspheres was used to compare the experimental and analytical results. Figure 26 shows the comparison of experimental and analytical data for the various channel sizes. These comparisons showed that uniform flow across a large portion of the width in all channel sizes was achieved.

Shear stress was calculated as the shear rate with respect to the channel height, multiplied by viscosity:

$$\tau_z = \mu \frac{dv_x}{dz} = \frac{3Q\mu z}{4b^3 a} \tag{11}$$

Using a channel width:height ratio of 10:1 allows one to assume nearly uniform flow across the width of the channel and drop the sum term from equation 8 before taking the derivative. Wall shear stress was determined by evaluating equation 11 at z = -b. As the size of the channel was decreased, wall shear stress was held constant simply by changing the rate of perfusion.

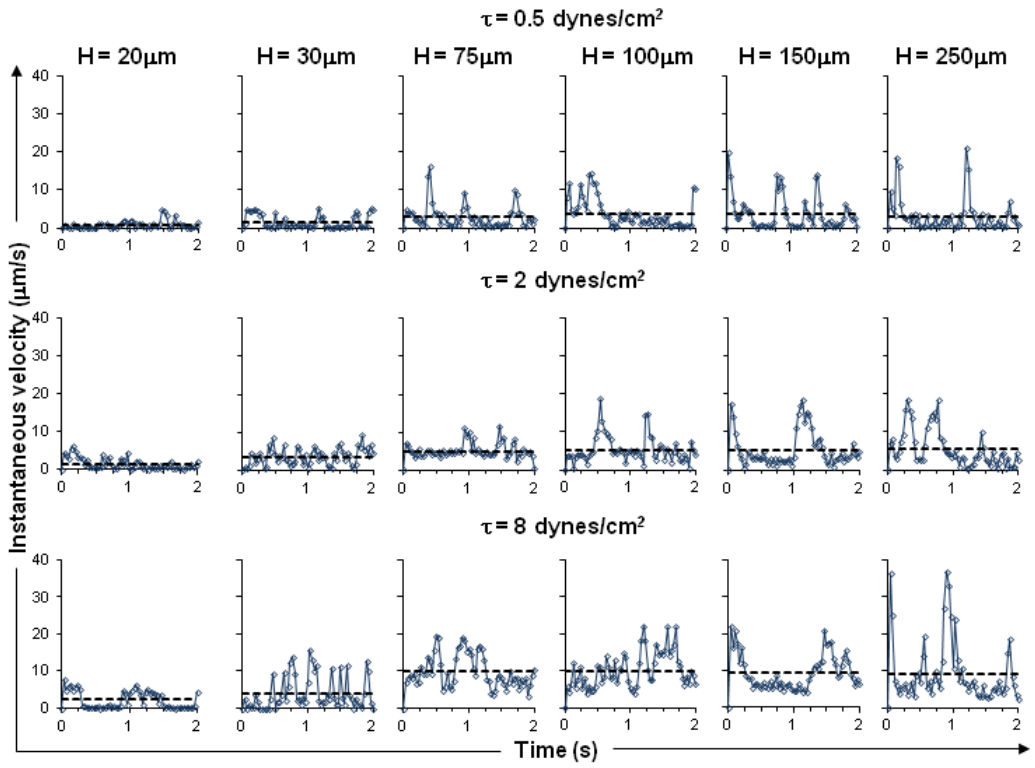


Figure 27: Instantaneous velocities of neutrophils rolling on P-selectin were measured over a two second period in microfluidic chambers of varying height (20 - 150 μm) and in a standard a Glycotech flow chamber (H = 250 μm). The P-selectin coating concentration in both the microfluidic and Glycotech chamber was 1.5 μg/mL and cell suspensions were perfused at wall shear stresses of 0.5, 2 and 8 dynes/cm^2. The data were recorded at 30 fps.

Effects of D_c/H on neutrophil rolling behavior. To investigate the behavior of neutrophils rolling in these chambers, isolated neutrophil suspensions were perfused at wall shear stresses of 0.5, 2 and 8 dynes/cm^2 through chambers coated with 1.5 μg/mL P-selectin. We observed neutrophils rolling in each of the six chamber sizes and noted significant differences in rolling behavior that appeared to be dependent on the ratio of cell diameter to chamber height (D_c/H). Figure 27 shows the instantaneous velocities of individual neutrophils rolling on P-selectin in microfluidic channels of varying heights (20-150 μm) and D_c/H values (0.053 - 0.4).

An additional data series at $D_c/H = 0.032$ represents a Glycotech parallel plate flow chamber (H = 250 μm) typically used for *in vitro* cell adhesion experiments.

At a wall shear stress of 0.5 dynes/cm^2, neutrophils rolling in microfluidic channels with channel heights similar in size of the cell (i.e. 20 μm and 30 μm), exhibited relatively stable rolling velocities, which frequently approached zero, and had limited spikes in the rolling velocity (Figure 27). As the chamber height increased to 100 μm, both the average rolling velocity (dashed lines) as well as the frequency of spikes in the rolling velocity increased. Furthermore, fewer pauses were observed during rolling in the larger chambers, which also contributed to an increase in the average velocity over the two second period. For channel heights greater than 100 μm, the average rolling velocities slightly decreased. Similar trends of uniform slow rolling at small channel heights, and faster and more variable rolling at taller channel heights were observed at higher shear stresses (2 and 8 dynes/cm^2). It should be noted that at a wall shear stress of 8 dynes/cm^2 very few pauses, if any, were observed for channel heights 75 μm or greater, and the magnitude of the velocity spikes was significantly increased.

To further quantify the qualitative changes observed in the instantaneous rolling velocity profiles presented in Figure 27, the average velocities of 50 neutrophils rolling in each of the six chamber heights were calculated from the instantaneous velocities measured with frame-by-frame analysis (Fig. 28A). As previously observed with the instantaneous velocity profiles, neutrophils that rolled in the taller microfluidic chambers (lower values of D_c/H) exhibited significantly

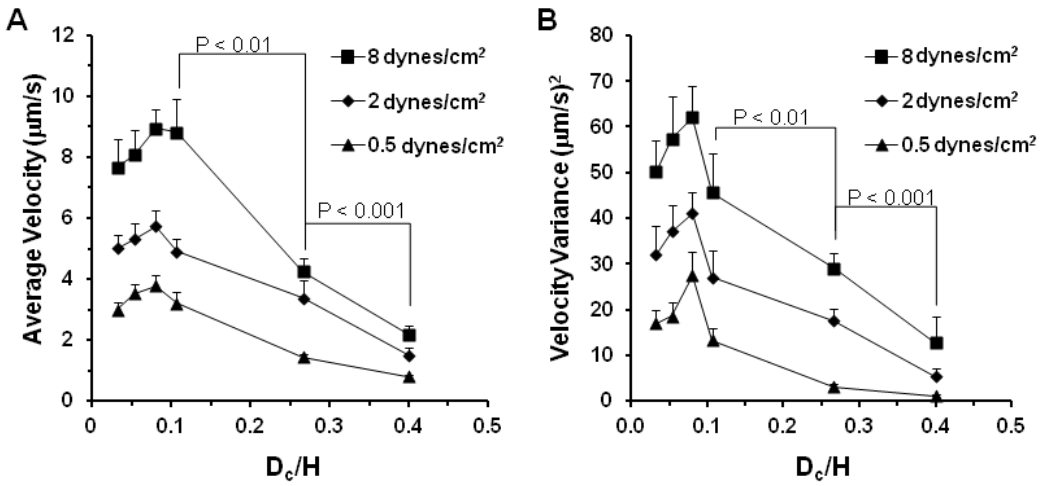


Figure 28: Each data point represents the (A) average rolling velocities or (B) average velocity variance of 50 neutrophils in each of the six chamber sizes. Cell suspensions were perfused at wall shear stresses of 0.5, 2 and 8 dynes/cm^2 and the coating concentration of P-selectin was 1.5 μg/mL. Significant differences in the velocity and variance trends were confirmed using an analysis of variance for each shear stress level ($P < 0.001$). Further analysis showed significant differences between specific D_c/H ratios of 0.11 (H = 75 μm), 0.27 (H = 30 μm) and 0.4 (H = 20 μm).

faster average rolling velocities compared to rolling velocities when D_c/H was increased at constant shear stress levels of 0.5, 2 and 8 dynes/cm^2 (ANOVA, $P < 0.001$). Further analysis using the Student's t-test on specific D_c/H pairs showed significant differences in average velocity between D_c/H values of 0.08 – 0.27 and 0.27 – 0.4. Indeed, increasing the ratio of D_c/H from 0.08 (H = 100 μm) to 0.27 (H = 30 μm) resulted in average rolling velocity decreases of 62%, 41% and 52% at wall shear stresses of 0.5, 2 and 8 dynes/cm^2, respectively. A further increase of D_c/H from 0.27 to 0.4 (H = 20 μm) decreased average rolling velocities by 44%, 55% and 48% at wall shear stresses of 0.5, 2 and 8 dynes/cm^2, respectively. Similarly the variance in the average rolling velocity also depended on the channel height (Fig. 28B). Neutrophil rolling behavior was significantly more erratic in taller chambers (H > 100 μm) at each of the three shear stresses (ANOVA, $P < 0.001$). Statistical

analysis demonstrated significant differences in velocity variance again between D_c/H ratios of 0.08, 0.27 and 0.4.

Numerical Simulation of the Effects of D_c/H on neutrophil rolling behavior. In a previous numerical study by Khismatullin and Truskey[111], it was demonstrated that an adherent leukocyte experiences less drag than a rigid sphere due to its deformation, and that the contact area of the leukocyte membrane with a selectin-coated substrate increases as the cell diameter-to-channel height ratio D_c/H increases. Here, we use VECAM to test whether an increase in channel height increases the mean rolling velocity, which would indicate that an increased contact area would lead to reduced rolling velocities.

Figure 29 shows the numerical data on instantaneous rolling velocities of neutrophils in channels with heights ranging from 20 - 250 μm (D_c/H values of 0.400 – 0.032). In agreement with our experimental results, the simulation predicted more stable rolling behavior as channel height approached cell diameter. Furthermore, the average rolling velocity decreased from 5.07 μm/s to 3.97 μm/s (22% difference) between $D_c/H = 0.4$ and 0.08 (Fig. 30). As in experiments (Fig. 28), the numerical model predicted a peak at $D_c/H = 0.08$, with a slight drop in the mean velocity to 4.22 μm/s at $D_c/H = 0.032$ (Fig. 30). The mean velocity values were also in the range of the experimental data. Thus, our numerical analysis demonstrated that a decrease in the channel height below 100 μm, or alternatively, an increase in the cell diameter-to-channel height ratio above 0.08 led to reduced rolling velocities provided the wall shear stress was kept constant.

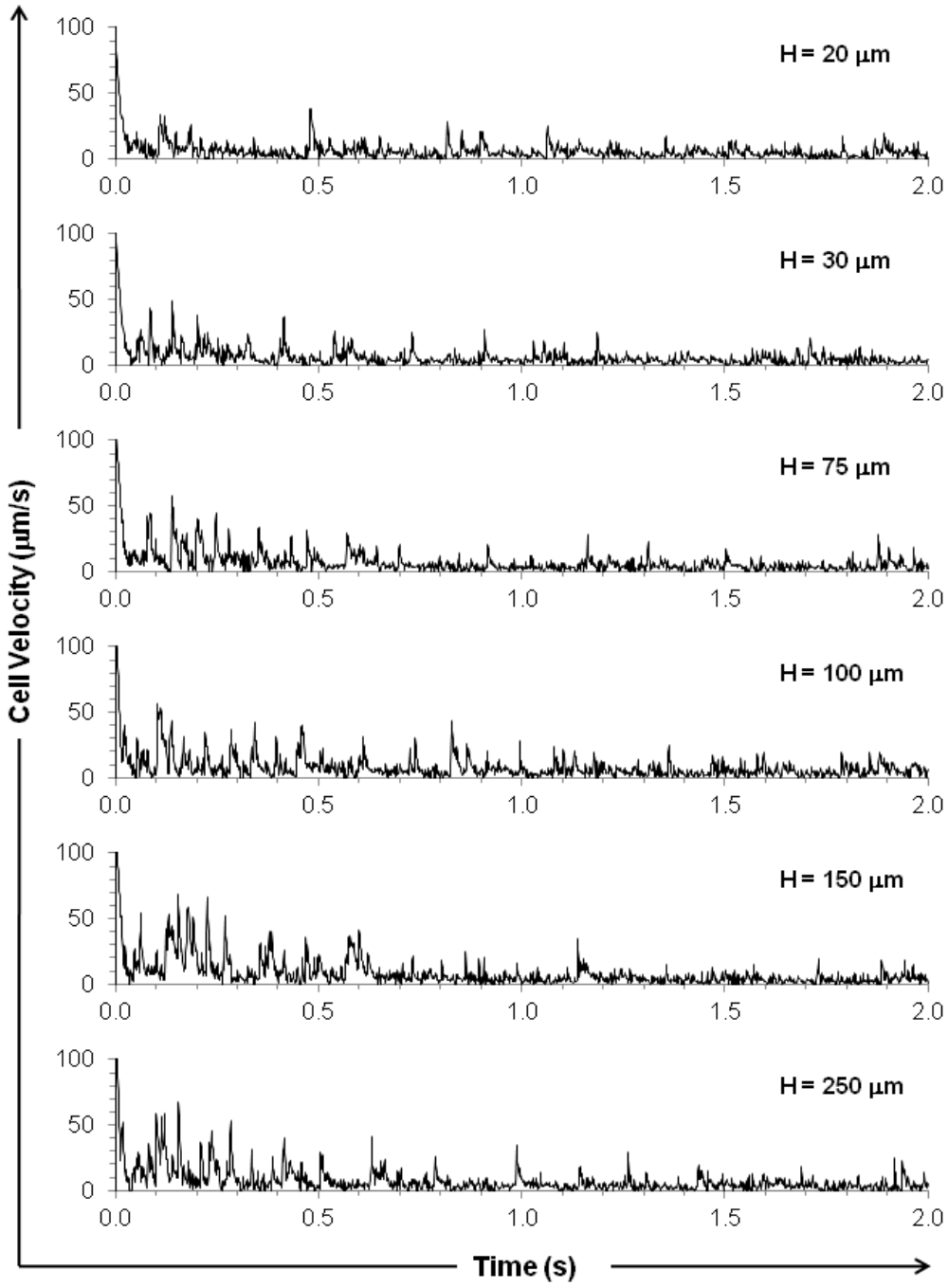


Figure 29: Instantaneous velocities were given by the numerical simulation of neutrophil rolling in 20, 30, 75, 100, 150 and 250 μm tall channels. Wall shear stress was held constant at 0.5 dynes/cm^2.

Rolling Differences are Correlated to Cell Rigidity. To determine whether differences in rolling velocity were the result of cell deformation, neutrophils fixed with paraformaldehyde were perfused through channels of varying heights at a wall

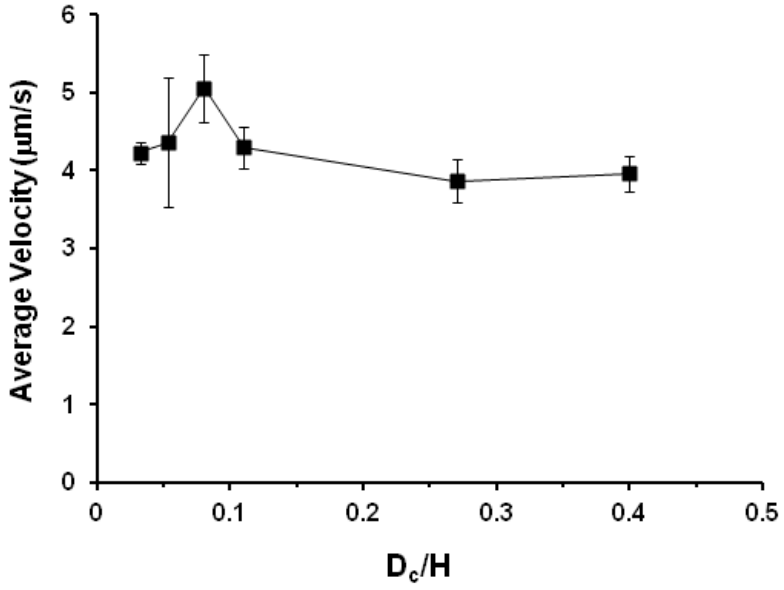


Figure 30: Average rolling velocities were calculated from instantaneous rolling velocities given by the numerical simulation of neutrophil rolling in channels with heights ranging from 20 – 250 μm (D_c/H = 0.4 – 0.032).

shear stress of 2 dynes/cm^2. Paraformaldehyde fixed neutrophils rolled significantly faster than untreated cells (Figure 31), and as the chamber height was decreased from 150μm to 20μm, fixed neutrophils showed only a 22% decrease in rolling velocities as compared to untreated neutrophils (72%). Similar to control cells, paraformaldehyde fixed cells also exhibited a slight decrease in rolling velocity when channel height was increased from 100μm to 150μm, however it should be noted this drop in rolling velocity at larger heights was not statistically significant.

To further test whether cellular deformation was a factor in the changes in rolling velocities, 6μm-diameter polystyrene microspheres were coated with a human PSGL-1/Fc chimera and perfused through P-selectin coated microfluidic channels at a wall shear stress of 2 dynes/cm^2. The rolling velocities for PSGL-1 coated microspheres were significant higher than those observed for either fixed or

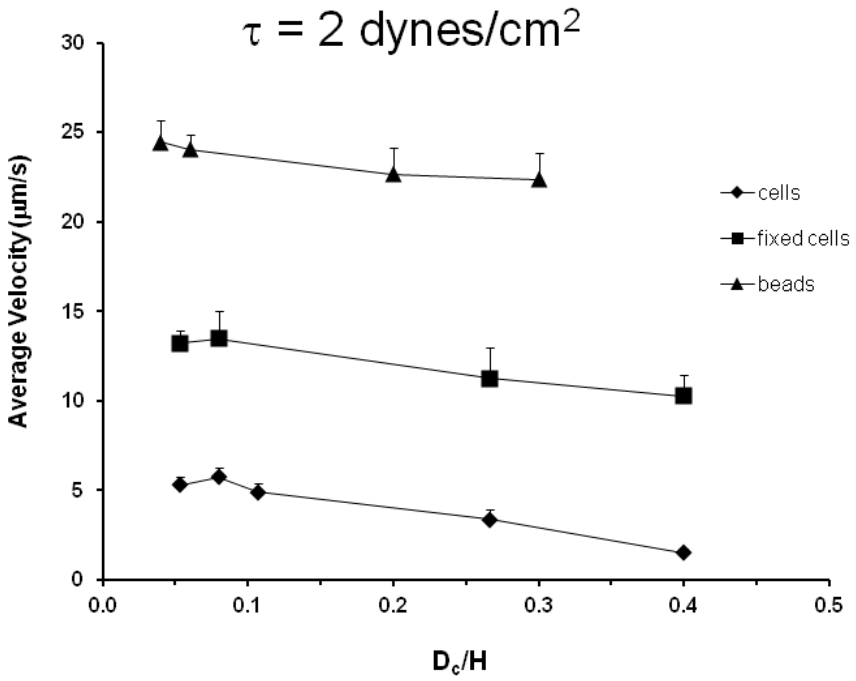


Figure 31: Average rolling velocities for neutrophils, paraformaldehyde-treated neutrophils and PSGL-1-coated microspheres rolling in microfluidic chambers of various sizes incubated with P-selectin (1.5 μg/mL). Suspensions were perfused at a wall shear stress of 2 dynes/cm^2.

untreated neutrophils (Figure 31). Because the diameter of the microspheres was slightly smaller than the average neutrophil diameter, chamber heights of 20, 30, 100 and 150μm corresponded to D_c/H values of 0.3, 0.2, 0.06 and 0.04, respectively. The same trend of decreasing rolling velocity with increasing D_c/H was observed for PSGL-1-coated microspheres, however, rolling velocity decreased only by 9% between D_c/H values of 0.04 and 0.3.

Effects of D_c/H on Neutrophil Contact Area during Rolling. Numerical simulations of two dimensional rolling leukocytes have suggested that cell deformability should correlate with the rolling velocity through changes in contact length.[91, 132] This parameter has been experimentally measured in vivo using a side-view intravital

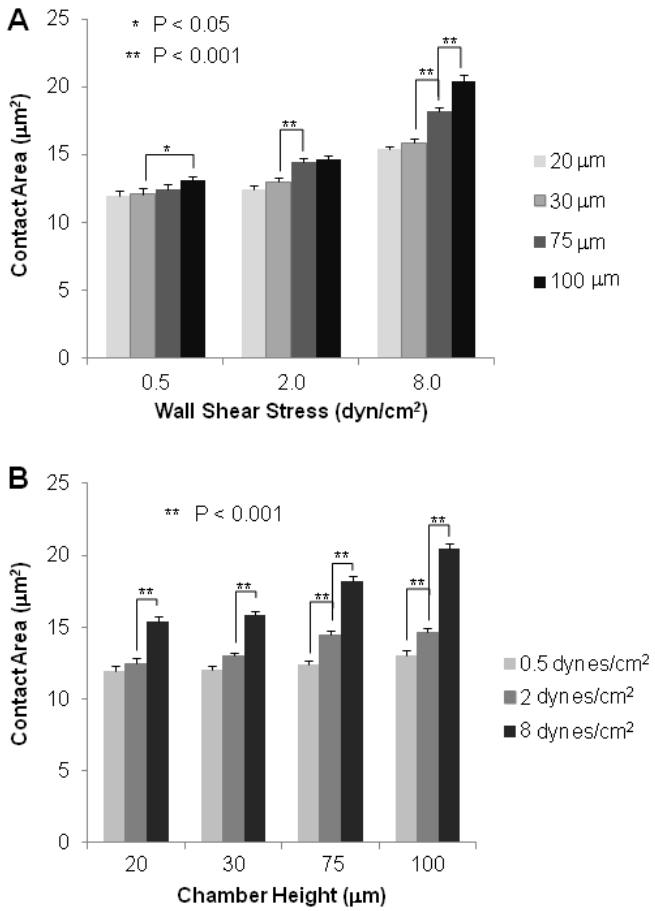


Figure 32: Average contact areas of isolated neutrophils rolling in P-selectin coated microfluidic chambers were calculated from instantaneous measurements using interference reflection microscopy in combination with frame-by-frame analysis. The results were compared for two cases: (A)increasing channel height with constant wall shear stress and (B)increasing wall shear stress with constant channel height.

microscopy technique[49]. More recent theoretical studies have simulated three dimensional rolling leukocyte and have calculated changes in the cell's contact area.[101, 111] Techniques to characterize or directly visualize the contact area between a cell and a ligand-decorated surface include: variable angle total internal reflective fluorescence (VA-TIRF) microscopy[236] and reflective interference contrast microscopy (RICM).[83, 190] Specifically, the RICM technique visualizes the cell-surface interface as a contrast pattern created from the destructive and

constructive interference patterns generated from reflections at the substrate-buffer and the buffer-cell interfaces. Areas where a cell is in close contact with the substrate will appear dark while more distant regions will appear dark grey or white.

Using RICM, we were able to visualize the dynamic adhesive interactions and contact area (i.e. "footprints") of rolling neutrophils with the P-selectin coated glass surface. At a constant wall shear stress of 0.5 dynes/cm^2 (Figure 32A) increasing the microfluidic chamber height from 20 to 100 μm (decreasing D_c/H) resulted in a slight overall increase in contact area of 9%. A Student's t-test revealed a significant increase in contact area when chamber height was increased from 30 to 100 μm ($P < 0.05$), but an analysis of variance performed over the entire trend revealed no statistical significance ($P > 0.05$). When wall shear stress was increased to 2 or 8 dynes/cm^2, increasing chamber height (20 – 100 μm) had a much more significant impact on average contact area with overall increases of 17% and 33%, respectively (Fig. 32A). Statistical analysis confirmed the significance of the increase at both shear stresses (ANOVA, $P < 0.05$). Specifically, significant increases in contact area were observed when chamber height increased from 30 to 75 μm at 2 dynes/cm^2 and between 30 to 75 μm and 75 to 100 μm at 8 dynes/cm^2 (Student's t-test, $P < 0.001$).

Alternatively, we compared contact areas for varying wall shear stress at a constant channel height. Figure 32B shows that for 20 and 30 mm tall channels, increasing wall shear stress from 0.5 to 2 dynes/cm^2 had little effect on contact area with increases of 4% and 8%, respectively. Meanwhile, increasing wall shear stress from 2 to 8 dynes/cm^2 in these channels yielded statistically significant increases of

24% and 22%, respectively (Student's t-test, $P < 0.001$). In 75 and 100 μm tall channels, increasing wall shear stress from 0.5 to 2 dynes/cm^2 resulted in contact area increases of 17% and 12%, while increasing from 2 to 8 dynes/cm^2 resulted in contact area increases of 25% and 40%. All of these increases were determined to be statistically significant (Student's t-test, $P < 0.001$).

Discussion

We report here the fabrication and characterization of microfluidic chambers of varying heights (20 – 250 μm) but with a constant channel width:height ratio of 10:1. The dimensions of these channels were designed to investigate neutrophil rolling in chambers which required very low perfusion volumes. Our results indicate that the ratio of cell diameter to channel height (D_c/H) is an important parameter in leukocyte rolling assays and that the associated changes in leukocyte rolling are related to leukocyte deformation. The microfluidic studies we have reported here are novel for three reasons: (i) the smallest chambers require 13 – 390 times less perfusion volume than other previously reported microfluidic leukocyte rolling studies[40, 52, 215] (Table 3), making them ideal for applications with limited sample; (ii) these results provide experimental support for the theoretical studies of Khismatullin and Truskey, who reported increases in both contact time and contact area of monocytes when chamber height was decreased from 80 μm to 20μm[111] and related these effects to leukocyte deformation, and (iii) the 200 μm x 20 μm microfluidic chambers approach the dimensions that a rolling leukocyte would experience in a post capillary vessel. Evidence for the importance of D_c/H is that as the channel height was reduced from 100 μm to 20 μm thereby approaching the diameter of a human neutrophil (8 μm) both the average rolling velocity as well as the variance in rolling velocity of neutrophils on P-selectin coated surfaces decreased (Figure 28) by as much as 72%. This trend of decreasing rolling velocity with increased D_c/H was observed experimentally at three distinct shear stresses and in numerical simulations (Figures 29, 30). Evidence that the decreases in rolling

velocities were related to cell deformation is supported by the observations that the rolling velocity of paraformaldehyde fixed neutrophils or rigid polystyrene beads coated with PSGL-1 decreased by only 23% or 10% respectively (Figure 31).

The role deformation plays in leukocyte adhesion has been examined through the study of fluid flow and the forces it exerts on objects within the flow field. A considerable effort has been devoted to modeling cells in flow to better understand how they react to shear force and what role this plays in various types of adhesion. Goldman, Cox and Brenner (GCB) originally determined the drag force for a rigid spherical body in simple shear flow near a wall as:

$$F_{drag} = 6k\pi z R\tau_w \qquad (12)$$

where z is the distance between the wall and the center of the sphere, k is a correction factor that takes wall effects into account, R is the radius of the sphere and τ_w is the wall shear stress.[87] This solution was later found to be inadequate for biological cells, however, as they do not behave like rigid spheres. Indeed, previous studies have observed the deformation of rolling and adherent leukocytes.[43, 49-50] Both Templeman and Yago have reported the importance of cell deformation in maintaining rolling adhesion, especially under high shear stress conditions.[239, 259] These results suggest that the deformability of cells affects their response to the forces that act on them in flow.

Another assumption of the GCB solution for drag force is that the object experiences simple shear or couette flow. This assumes a linear velocity profile and constant shear rate with respect to distance from the wall, which is only possible when the ratio of cell diameter to channel diameter is small. Most in vitro flow

chambers have heights greater than ten times the diameter of a leukocyte, however, post-capillary venules may only have diameters three to four times the size of a leukocyte. To correctly model adhesion in these cases, the effects of chamber height must be taken into account. When flow through a chamber is bounded on the top and bottom, the velocity profile changes from simple shear flow to a parabolic profile. Therefore, an additional correction must be considered to account for the effects of parabolic flow. Pozrikidis showed that for a rigid sphere near the wall in parabolic flow, the corrected drag force is[194]:

$$F_{corrected,\ drag} = F_{drag} - 11.64\pi(R^3/H)\tau_w \qquad (13)$$

The Pozrikids solution suggests that drag force decreases with a decrease in channel height. When the vessel size or chamber height is close to the diameter of a leukocyte, adherent cells will occlude the flow. This flow occlusion results in an increased pressure drop across the surface of the cell and, consequently, an increase in the drag force the cell experiences. Khismatullin and Truskey predicted that an increase in drag force would increase cell deformation in the region where it contacts the substrate.[111] Their theoretical model showed that this resulted in increased contact time when the cell took up a greater portion of the channel height (i.e. the ratio of cell diameter to chamber height increased). Similarly, Lei et al predicted that a decrease in channel height will lead to a significant increase in the shear stress at the top of the cell[132]. This increase in shear stress would increase the torque acting on the cell, bringing the front of the cell in closer contact

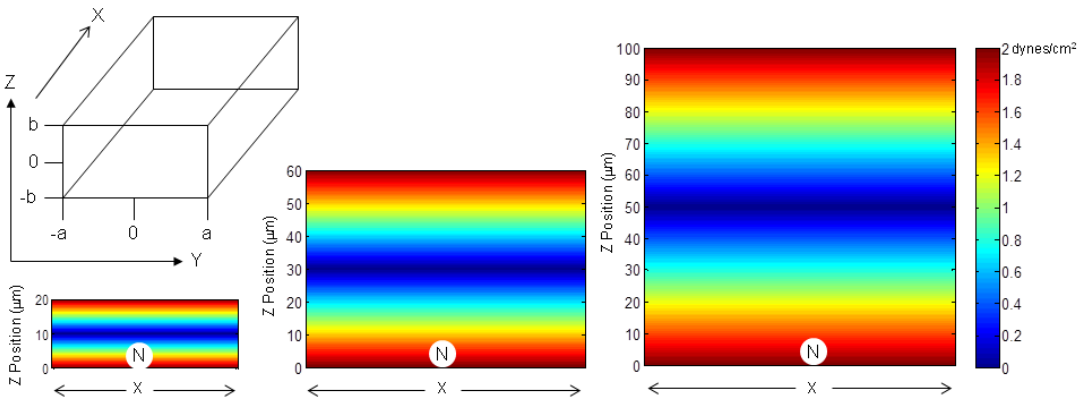


Figure 33: Here we present the shear stress gradients in 20 μm, 60 μm and 100 μm tall microfluidic chambers. When wall shear stress is held constant at 2 dynes/cm^2, it can be seen that the shear stress gradient is significantly dependent on chamber height. Also of note is that the average shear stress across the height of an adherent cell decreases significantly with decreasing chamber height.

with the substrate, resulting in slower rolling. Conversely, when the ratio of cell diameter to chamber height was decreased Khismatullin and Truskey predicted that cells would contact the substrate for shorter periods of time. They suggested this would occur as a result of a decreased shear stress gradient. In Figure 33, we show how the shear stress gradient varies with channel height. While there will still be some slight flow occlusion when a cell adheres to the bottom channel wall, the shear stress increase at the top of an adherent cell in a taller channel will be less than in a smaller channel[132]. Khismatullin and Truskey predicted that the change in the shear stress gradient combined with less torque acting on a cell in a taller channel would result in the deformation of the overall cell body into a teardrop shape[111]. This corresponds to other theoretical studies which have predicted that global cell deformation occurs as a response to shear. In smaller channels, however, the shear stress acting on the top of the cell is less and the overall body of the cell deforms less. Cells that undergo less bulk deformation have been shown to remain in contact with the substrate for longer periods of time.

Theoretical models have predicted two ways in which cells can deform and behave differently from the theory presented by Goldman et al: (I) global cell deformation and (II) contact zone deformation. In the first case, the entire body of the cell can deform in the direction of flow. In vivo observations of neutrophils rolling in postcapillary venules have shown that cells deform in the direction of flow.[43, 231] This bulk cell deformation has been quantified in previous studies as a change in the ratio of cell length to cell height. Recent theoretical models have produced three-dimensional projections of rolling cells which predict this deformation results in a change in the cell shape from a sphere to a teardrop-like shape.[101, 112] Jadhav et al[101] also demonstrated that this deformation increases with increasing fluid shear rate. Furthermore, stiffness of the cell membrane has also been shown to affect bulk cell deformation as well as rolling velocity and contact area.[168, 186]

In the second case, deformation occurs in the contact zone between the adhering cell and the underlying substrate as a result of drag force exerted on the surface of the leukocyte. Because drag force increases when adherent cells occlude more of the flow in a channel, increasing the cell size or decreasing the channel height can cause changes in the drag force and, consequently, cell deformation.

A surprising finding in the current study was that we observed a slight decrease in rolling velocity when D_c/H was further decreased from 0.08 to 0.053 in the microfluidic channels or 0.032 in the Glycotech flow chamber. This decrease translates to an increase in the microfluidic channel height from 100 μm to 150μm or 250 μm in the Glycotech flow chamber. The assumption of semi-infinite flow has

been shown to be valid in cases around this point, where the height of the chamber is greater than ten times the diameter of the cell. Assuming semi-infinite flow means the velocity profile of the fluid can be modeled linearly, which gives a constant shear stress across the body of the cell. Because theoretical models have predicted that bulk cell deformation occurs as a result of differences in shear stressed experienced at the top and bottom of the cell, it stands that there will be less bulk cell deformation when there is constant shear stress across the cell body. Less bulk cell deformation as a result of constant shear stress explains the drop in rolling velocity observed between H = 100 μm and H = 150 μm. The fact that the numerical simulations also exhibited a decrease in rolling velocity for chamber heights above 100 μm, provides evidence that the experimental results were not an artifact.

To test whether cell deformation was involved in the changes in rolling velocity observed in the smaller microfluidic channels, we performed two complementary experiments with paraformaldehyde-fixed neutrophils and rigid polystyrene beads coated with PSGL-1. When perfused at a shear stress of 2 dynes/cm^2, fixed neutrophils rolled significantly faster than untreated neutrophils in all of the microfluidic channels tested (Figure 31). This observation is consistent with previous studies that have shown that chemical fixation increases the rigidity of the cell membrane thereby increasing rolling velocities on P-selectin surfaces.[259] In contrast to untreated neutrophils the reduction in rolling velocity for the fixed neutrophils (22%) was significantly less as the channel height was reduced. These results suggest that fixation-sensitive cellular features were involved in the

stabilization of rolling velocities. The exact nature of these cellular features was not determined in this study, but is currently under investigation. Previous studies have demonstrated that cell contact area[49-50], microvillus extension[182, 224], and membrane tether formation[197, 219, 236] are likely involved.

Similar to the results with fixed neutrophils, perfusion of PSGL-1 coated beads with PSGL-1 surface densities similar to that of untreated neutrophils resulted in significantly higher rolling velocities. This result is consistent with other microbead studies.[182, 207, 259] The observation that a smaller reduction (9%) in rolling velocity with channel height compared with untreated neutrophils (72%) also supports the notion that the reduction in rolling velocity in untreated neutrophils is related to cell deformation.

To better understand how cell deformation and rolling velocity correlate, we used interference reflection microscopy (RICM) to observe the areas of rolling neutrophils that were in close contact with the bottom wall of the chamber. This technique has been previously used to observe the interfaces between cells and glass surfaces[42, 190] and is similar to a footprinting technique recently reported by Sundd et al which uses variable angle total internal reflection fluorescence microscopy.[236] Using RICM in combination with frame-by-frame analysis, we were able to determine the average footprint areas of rolling neutrophils in chambers of various heights. Intuition would suggest that these average footprint areas should relate inversely to rolling velocity, resulting in a decrease in footprint area with an increase in chamber height. However, we observed an increase in footprint area that correlated not only with increasing wall shear stress but also with increasing

chamber height (Figure 32).

Although this result is counter-intuitive, it can be explained by examining the shear stress that acts on the top of an adherent cell. Figure 33 shows that in chambers with heights much greater than the cell diameter (H = 100 μm), there is only a slight difference between the wall shear stress and the shear stress acting on the top of the cell. Therefore, there is less torque acting on this cell than on a cell in a small channel (H = 20 μm) meaning that selectin-ligand bonds will not form as fast at the cell's leading edge. Meanwhile, there is more global cell deformation that occurs in the tall channel which increases the overall footprint area. The overall net result is an increase in rolling velocity even though there is more cellular surface area available for selectin-ligand interaction. This can be seen not only in our comparisons of channel height at constant wall shear stress, but also by comparing increasing wall shear stress at constant channel height.

When channel height is small (< 30 μm) and wall shear stress is low (< 2 dynes/cm^2), there is little change in contact area. However, when wall shear stress is high (8 dynes/cm^2) the shear stress impacting the top of the cell increases to the point that significant contact area increases are observed. This effect can also be seen in tall channels, but the increase in channel height means the shear stress gradient is less steep. As a result, there will be significant global deformation, even if the wall shear stress is low. Therefore, an increase in wall shear stress from 0.5 to 2 dynes/cm^2 results in a significant increase in contact area in taller channels (H ≥ 75 μm) but not in smaller ones (H ≤ 30 μm). These results suggest that the rolling velocity of a cell is not dependent solely on cellular contact area, but that there is a

balance between contact area and the shear stress that acts on the top of the cell. Because the shear stress at the top of the cell is dependent on D_c/H, this places greater significance on chamber height as a design parameter in microfluidic cell adhesion assays.

In summary, our results have experimentally demonstrated the importance of channel height in microfluidic based leukocyte rolling assays. As the channel height approaches the cell diameter the cell rolling velocity slows down and becomes more stable. These results are important because they (i) begin to explain some of the differences in rolling velocities observed between in vitro (small D_c/H ratios) and in vivo (large D_c/H ratios) leukocyte rolling assays; (ii) point to the D_c/H ratio as an important parameter in the design of microfluidic based assays as well as the interpretation of the results; and (iii) should be applicable to not only leukocyte rolling assays but to rolling assays that involve other cell types such as platelets or cancer cells.

CHAPTER 5: Shear Stress at Bifurcations and its Effects on Neutrophil Adhesion

Introduction

Atherosclerosis is a cardiovascular disease characterized by the accumulation of lipoprotein, cholesterol and cellular products on the vascular wall [183, 205]. These accumulations, also known as atherosclerotic plaques, often incorporate inflammatory cells (e.g. macrophages and polymorphonuclear leukocytes) and platelets [17, 59, 102, 209-210]. During inflammation and thrombosis, leukocytes are recruited to the endothelium through interactions between PSGL-1 expressed on leukocyte microvilli and P- and E-selectins expressed by activated endothelial cells and platelets. Similarly, leukocytes have been shown to adhere to and infiltrate atherosclerotic plaques through P-/E-selectin-mediated binding [51, 210]. Previous studies have demonstrated that mice lacking P-selectin exhibit reduced fatty streak formation, one of the first signs of atherogenesis [51, 104]. Leukocyte-leukocyte interactions through PSGL-1/L-selectin binding have also been implicated in the growth of atherosclerotic plaques [143]. Additionally, leukocyte microparticles can infiltrate atherosclerotic plaques through the PSGL-1/selectin mechanism of adhesion [73, 167]. Once recruited, these microparticles can release tissue factor and other procoagulant markers [146]. These studies indicate a clear role for adhesive inflammatory cell interactions in atherosclerotic plaque formation and growth.

In addition to molecular interactions, shear stress also affects cell adhesion and atherosclerotic plaque formation. Previous studies have observed that atherosclerotic plaques typically originate in regions of the vascular system that are

characterized by recirculating flow [8], boundary layer separation [66] or abnormally low or high shear stress [27, 237, 265]. In vitro studies performed with sudden expansion flow chambers have demonstrated the effects of unsteady shear stress on endothelial cells [155, 240] and leukocytes [9, 37]. Recently, Hsiai et al demonstrated that oscillatory flow increases the probability of leukocyte-endothelial cell binding and also up-regulates MCP-1 mRNA expression [98]. Conversely, steady shear has been shown to promote endothelial cell expression of anti-inflammatory molecules such as nitric oxide and prostacyclin, as well as other molecules that help to neutralize oxygen free radicals [69, 243]. Although these studies demonstrate a potential for cell adhesion to occur in regions of unsteady shear, only a few studies have investigated the effects of shear stress on adhesion at bifurcations.

Previous computational [140, 159, 180, 266] and in vitro [34, 110, 120, 188] studies have suggested that the apexes of bifurcations are susceptible to points of stagnation. This suggests that leukocyte rolling and adhesion can potentially occur in these stagnation zones even when the overall shear stress is very high. However, these in vitro studies investigated flow visualization rather than cell adhesion patterns. Furthermore, many of the models used glass chambers which required large perfusion volumes. Recently, microfluidic chambers with significantly smaller dimensions have been used to model leukocyte adhesion [89, 103, 215-216] as well as the complex geometrical structures found in the vascular system [195, 211, 263]. Prabhakarpandian et al showed that biotinylated microspheres in avidin coated microvascular networks tended to adhere more at bifurcation apex sites than in

linear channel sections [196]. However, they only tested shear stresses in the range of 0.1 – 2.5 dynes/cm^2. Urschel et al also reported increased monocyte adhesion to endothelial cell layers cultured in bifurcations but only on the outer channel walls and at shear stresses less than 10 dynes/cm^2 [245]. They did not report whether adhesion was observed at the bifurcation apex.

A previous master's student in Dr. Schmidtke's group investigated cell adhesion at bifurcations, however a number of design parameters for these microfluidic devices may have unknowingly influenced the results[156]. The devices used in the previous studies consisted of a single inlet channel that diverged into two asymmetric daughter channels. Although asymmetric bifurcations are common throughout the circulatory tree, asymmetry likely leads to uneven flow distribution. This was evident in the previous work in that perfusion experiments carried out over a lengthy time period often led to the complete occlusion of one of the daughter channels. The cross-sectional dimensions of these devices (100 x 50 μm, W x H) may have also affected the cell adhesion pattern. As we have shown in the previous chapter, significant differences in selectin-mediated rolling can arise when the ratio of cell diameter to chamber height (D_c/H) is greater than 0.1. Additionally, a channel width to channel height ratio (W/H) less than 10 makes an accurate estimation of shear stress increasingly difficult as the velocity gradient along the channel width becomes significantly steeper.

To overcome these difficulties, we fabricated bifurcated microfluidic devices with a simple design consisting of a single inlet channel that diverges into two symmetric daughter channels which then converge downstream into a single exit

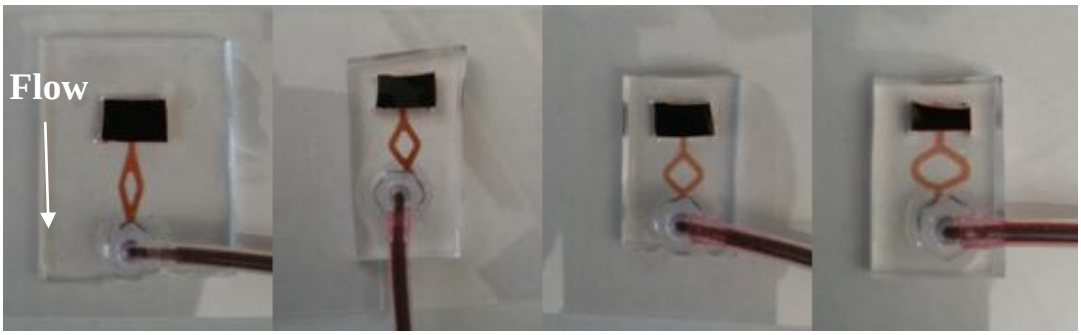


Figure 34: We fabricated microfluidic chambers consisting of a single inlet channel that diverged into two daugther channels that reconverged downstream to form a single exit channel. Devices were fabricated with bifurcation angles of 30, 60, 90 and 120º (left to right).

channel (Fig. 34). We demonstrate that the stagnation point at a bifurcation apex can sustain PSGL-1/P-selectin adhesion interactions even when the overall cell suspension is perfused at a very high wall shear stress. Antibody control experiments revealed that neutrophil adhesion at the bifurcation apex was dependent on PSGL-1/P-selectin interactions and not simply a result of the fluid mechanics. Furthermore, we show that the accumulation of adherent neutrophils at the bifurcation apex is dependent on PSGL-1/L-selectin interactions between leukocytes and cellular deformability as well as the concentration of P-selectin immobilized on the chamber walls. We also demonstrate that geometrical properties such as bifurcation angle and channel cross-sectional dimensions play a role in neutrophil accumulation. These results taken together demonstrate the significant effect of shear stress on leukocyte adhesion at bifurcations.

Methods

Proteins and Reagents

Human P-selectin, anti-PSGL-1 mAb P1, anti-P-selectin mAb G1 and anti-L-selectin mAb Dreg56 were kindly provided by Dr. Rodger McEver (Oklahoma Medical Research Foundation, Oklahoma City, OK).

Fabrication of Microfluidic Chambers

Master templates for microfluidic chambers were fabricated with SU8 photoresists (Microchem Corporation), using a previously described protocol. Polydimethylsiloxane (PDMS) from Sylgard 184 Silicone Elastomer kits was mixed at a 10:1 elastomer base:curing agent ratio and cured over the photoresist templates at 200°C for 30 minutes to create stamps with channels that were inverses of the templates. A polystyrene elbow (Small Parts) was inserted at one end of each template prior to curing to serve as an outlet port. After curing, PDMS was removed from the insides of the outlet ports and an inlet reservoir large enough to hold approximately 200 μL of fluid was cut out of the opposite end of each channel. Stamps were cleaned in 20% HCl and 70% ethanol, dried at 200°C for 10 minutes and sealed to clean glass cover slips by treating both stamp and cover slip with a high frequency generator.

Neutrophil Isolation

Human venous whole blood was obtained by venipuncture from healthy donors after informed consent was given and anticoagulated with sodium heparin. Whole

blood was layered on top of a cell separation medium (Lympholyte-poly, Cedarlane Laboratories) and spun at 400 g for 30 minutes. The resulting neutrophil layer was removed and diluted with 0.4% sodium chloride followed by Hank's balanced salt solution with Ca^{2+} and Mg^{2+} (HBSS, Lonza). Remaining erythrocytes were lysed with sodium chloride solutions, and neutrophils were washed two more times with a 0.5% solution of HSA in HBSS and re-suspended in the same solution at 10^6 cells/mL. Cell counts were verified using a manual hemocytometer set (Hausser Scientific). Neutrophils for antibody experiments were incubated with 20 μg/mL anti-PSGL-1 mAb PL1 or anti-L-selectin mAb Dreg56 for 30 minutes prior to use. For experiments requiring fixed cells, the above protocol was modified by replacing HSA solutions with only HBSS. After isolation, neutrophils were incubated in a solution of 1% paraformaldehyde for 5 minutes and then washed five times with HBSS to remove any remaining paraformaldehyde. The blood collection protocol was approved by the Institutional Review Board of the University of Oklahoma, and informed consent was obtained from all donors.

Perfusion Experiments

Microfluidic chambers were treated with a solution of 1% Aquasil (Thermo Scientific) and washed with distilled water to create a uniform hydrophobic surface. Chambers were then incubated for 3 h with a solution of 3.0 μg/mL P-selectin, and then washed and incubated with a 0.5% solution of HSA in HBSS for 30 min to prevent non-specific binding. Chambers for antibody experiments were treated with 20 μg/mL anti-P-selectin mAb G1 for 30 minutes prior to use. 1.5 μg/mL and 0.75

μg/mL solutions were also used for P-selectin concentration experiments. Cell suspensions of isolated neutrophils (untreated, antibody treated or fixed, 10^6 cells/mL) were then perfused through P-selectin coated chambers at a constant inlet channel wall shear stresses (τ_w) ranging from 1 - 100 dyn/cm^2 for 2 minutes. A fresh chamber was used each time the shear stress was changed. Neutrophil adhesion was observed both in the inlet channel and at the bifurcation apex. Adhesive interactions were recorded onto VHS tapes using a CCD camera (DAGE-MTI CCD-300) and a Sony S-VHS videocassette recorder.

Analysis of Adhesion Pattern

VHS recordings of perfusion experiments were digitized using Metamorph version 7.5 (Molecular Devices). Video segments (t = 2 minutes) were then analyzed at 10 second intervals using the threshold function in the Metamorph software to determine the total area of the cells adhering in a defined region of the inlet channel (SA_{inlet}) and at the bifurcation apex (SA_{apex}). The total threshold area was then divided by the two-dimensional area of a perfectly round neutrophil (D = 8 μm) to obtain an estimate of the total cell number (N_{cells}). Cell adhesion (cells/mm^2) was calculated by dividing N_{cells} by SA_{inlet} or SA_{apex}. It should be noted that this method assumes that adhering cells remain perfectly spherical and only adhere at the bottom wall of the chamber.

Results

Leukocyte Aggregate Formation is Dependent on Channel Cross-Sectional Dimensions. Previous studies have shown that bifurcations in the vascular system are especially prone to the development of atherosclerotic plaque.[82, 85, 121, 265] Indeed, unsteady shear along the vascular wall, such as that found at bifurcations in the vascular system, has been demonstrated to affect endothelial cells.[98, 155, 240] In vitro studies have also demonstrated that unsteady shear can increase the likelihood that a leukocyte will be recruited to and roll on the vascular endothelium.[9, 37, 98] Although the outside walls of bifurcations are characterized by unsteady shear, some theoretical studies have also demonstrated the presence of a stagnation point at the apex of a bifurcation[140, 159, 180, 266]. Since the pathogenesis of atherosclerosis can be affected by leukocyte and platelet adhesion, these areas may potentially serve as recruitment sites for cell adhesion even under high shear stress conditions.

A previous master's student in Dr. Schmidtke's group investigated the adhesive interactions of human neutrophils at the apexes of bifurcations coated with P-selectin[156]. However, the microfluidic devices used in these studies had very small channel cross-sectional dimensions (100 μm x 50 μm, W x H). The daughter channels downstream of the bifurcation were also asymmetric in channel width (~ 130 and 80 μm, respectively). This led to the preferential formation of neutrophil aggregates in one daughter channel before the other. We fabricated diamond-shaped microfluidic devices similar to those in Figure 34, but with channel dimensions similar to those previously used (100 μm x 50 μm, W x H).

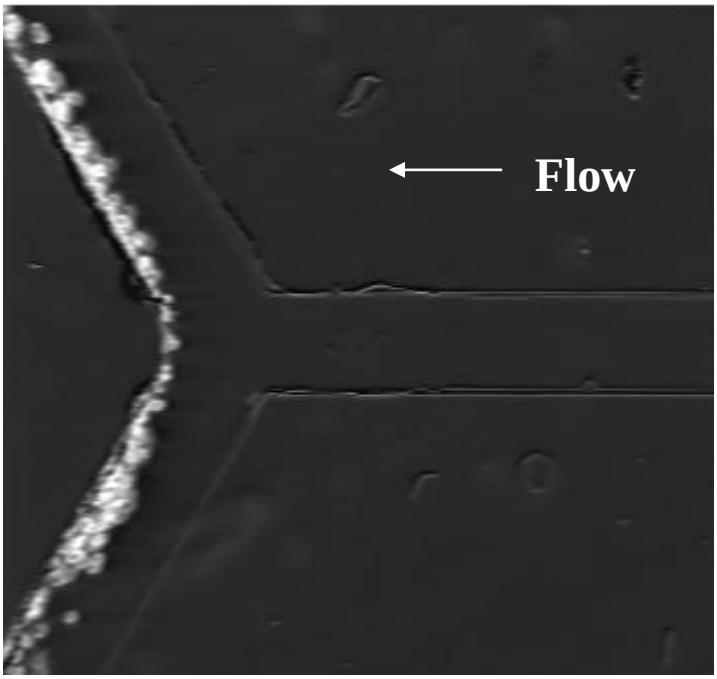


Figure 35: We observed the buildup of adherent neutrophils in the daughter channels of a 120º bifurcation with cross-sectional dimensions of 100 μm x 50 μm (W x H). Neutrophils were perfused at 50 dynes/cm^2 for 20 min, and the chamber was coated with 3 μg/mL P-selectin.

Additionally, our channels were designed with symmetric daughter channels. We coated these chambers with 3 μg/mL P-selectin and perfused human neutrophil suspensions through them at a shear stress of 50 dynes/cm^2. Similar to previous observations, we saw the buildup of neutrophil aggregates downstream of the bifurcation after 20 minutes of perfusion. However, the aggregate buildup in our channels occurred simultaneously and symmetrically in both daughter channels (Fig. 35).

To determine whether neutrophil aggregate formation was dependent on channel cross-sectional dimensions, we also fabricated diamond-shaped chambers with cross-sectional dimensions of 1000 μm x 100 μm (W x H). When neutrophil suspensions were perfused through these chambers at 50 dynes/cm^2, we observed

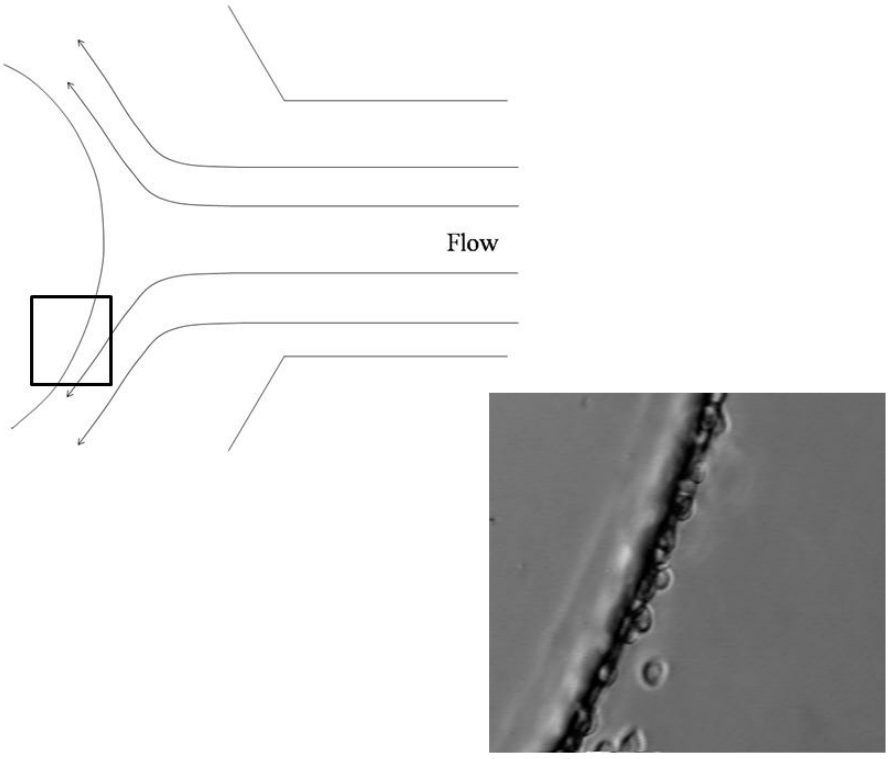


Figure 36: In a chamber with cross-sectional dimensions of 1000 μm x 100 μm (W x H), we observed only a thin layer of adherent neutrophils after 20 minutes of perfusion at 50 dynes/cm^2. The chamber was coated with 3 μg/mL P-selectin.

that neutrophils only adhered along the wall of the bifurcation apex. In contrast to the smaller channels, neutrophils did not aggregate in the daughter channels. Instead, we observed only a thin layer of adherent cells along the inside walls of the daughter channels after 20 minutes of perfusion (Fig. 36). It should be noted that in both size channels we did not observe any neutrophil adhesion in the inlet channel.

Cells Adhere at Bifurcation Apex at High Shear but Not in Main Channel. To quantify the observed adhesion patterns in the larger bifurcation chambers (1000 x 100 μm), we estimated the number of adherent cells at 10 s intervals in the inlet channel and around the chamber wall at the bifurcation apex (Fig. 37a). At $\tau_w = 1$

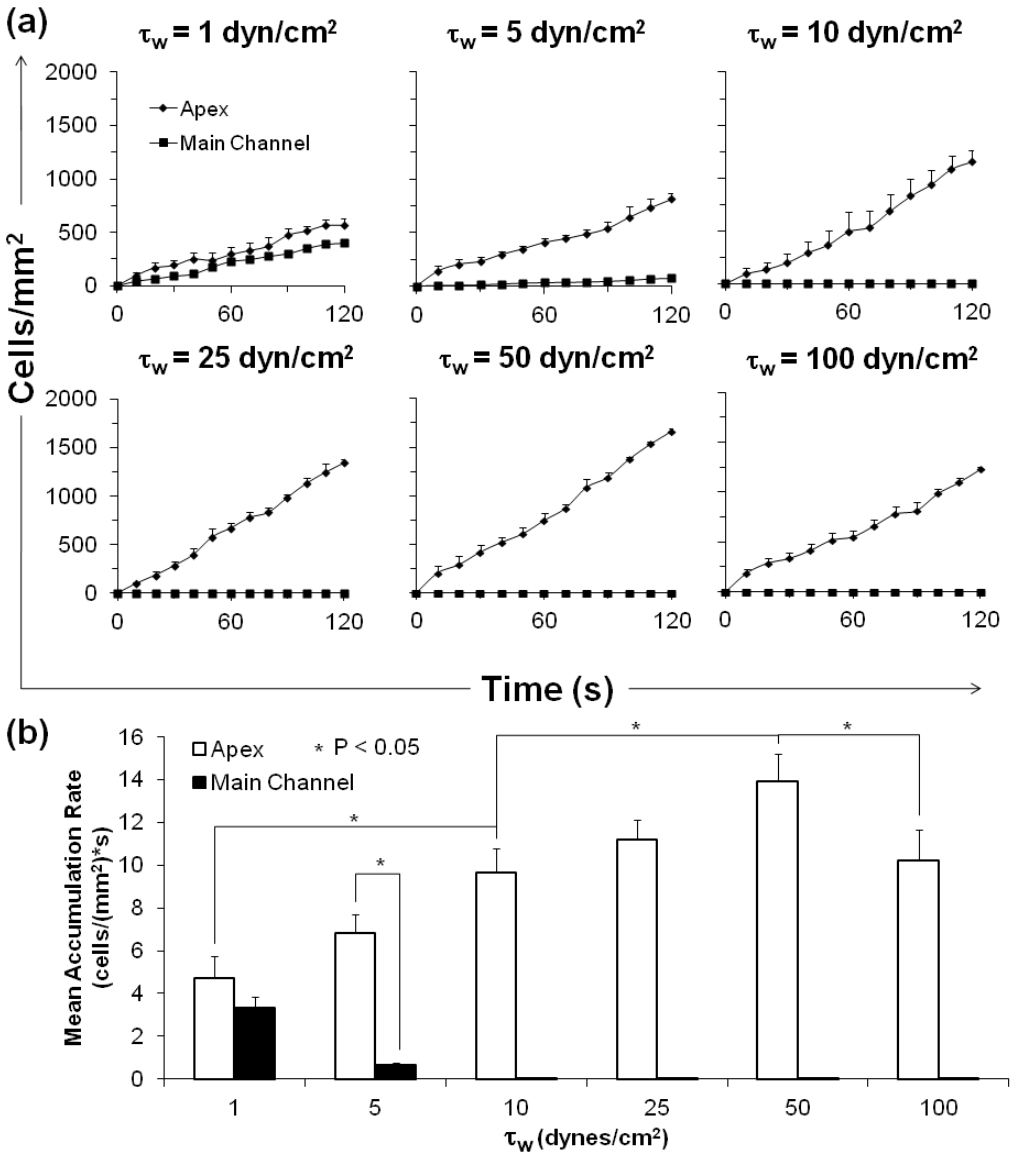


Figure 37: (a)Neutrophils accumulated at the apex of a 120° bifurcated microfluidic chamber at τ_w = 1 – 100 dynes/cm^2, while adhesion in the inlet channel was not observed at τ_w > 5 dynes/cm^2. (b)Increased neutrophil accumulation rate at the apex correlated with increasing tw from 1 – 50 dynes/cm^2 at the apex and then decreased at τ_w = 100 dynes/cm^2. The accumulation rate in the inlet channel decreased with increasing τ_w.

dyn/cm^2, adherent cells accumulated at both sites with adhesion at the apex being slightly greater than in the inlet channel. After two minutes of perfusion, the average number of adherent cells in the inlet channel and at the bifurcation apex was approximately 400 and 550 cells/mm^2, respectively. As τ_w was increased, we

observed a significant decrease in cell adhesion in the inlet channel with no adhesion observed at $\tau_w > 5$ dynes/cm^2. At the bifurcation apex, however, cell adhesion significantly increased with increasing τ_w up to 50 dynes/cm^2. At this shear stress, the number of cells observed adhering at the apex increased steadily during two minutes of perfusion to an average value of approximately 1700 cells/mm^2.Further increasing τ_w to 100 dynes/cm^2 resulted in a slight decrease in the number of cells adhering at the apex to approximately 1300 cells/mm^2.

We also calculated the average rate of neutrophil accumulation in the inlet channel and at the bifurcation apex (Fig. 37b). At $\tau_w = 1$ dyn/cm^2, the accumulation rate was slightly decreased in the inlet channel compared to the apex. Increasing τ_w to 5 dyn/cm^2 and beyond brought about a significant difference in the accumulation rates at the two sites. The accumulation rate at the apex was also dependent on the shear stress level. Significant increases in accumulation rate were observed when τ_w was increased from 1 – 10 dyn/cm^2 and from 10 – 50 dyn/cm^2 ($P < 0.05$). The decrease in accumulation rate when τ_w was increased from 50 – 100 dyn/cm^2 was also statistically significant.

Antibody Control Experiments. To confirm that cell accumulation at the apex occurred as a result of interactions between immobilized P-selectin and cellular PSGL-1, we performed various antibody control experiments. P-selectin coated chambers with a bifurcation angle of 120° were treated with anti-P-selectin mAb G1, a blocking antibody to P-selectin. Likewise, we incubated isolated human neutrophils with anti-PSGL-1 mAb PL1, a blocking antibody to PSGL-1. PL1-

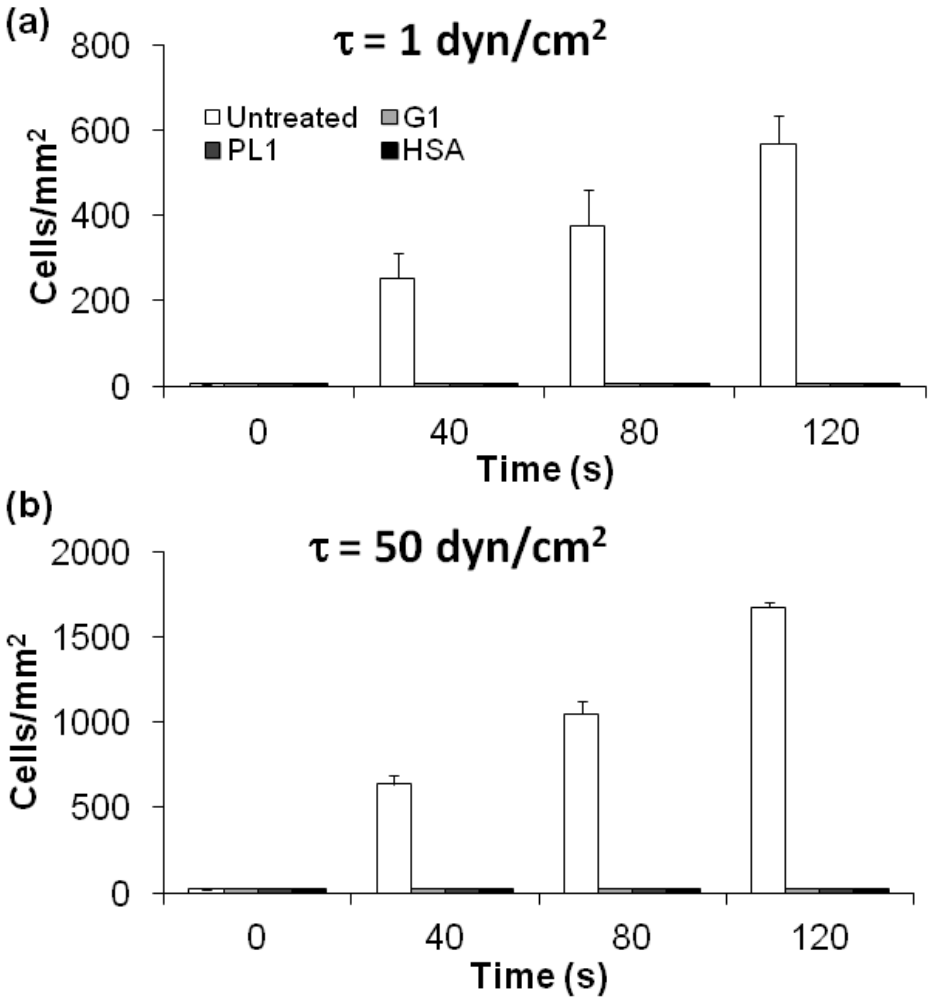


Figure 38: Neutrophil adhesion at the bifurcation apex was abolished when P-selectin or PSGL-1 were blocked with monoclonal antibodies. Neutrophils also failed to adhere at the bifurcation apex in chambers coated only with HSA. Cells were perfused at $\tau_{w,\,main}$ = (a)1 and (b)50 dynes/cm^2. Bifurcation angle = 120°.

treated and untreated neutrophils were perfused through individual P-selectin coated chambers and G1-treated P-selectin coated chambers at low shear stress (τ_w = 1 dyn/cm^2, Fig. 38a) and high shear stress (50 dyn/cm^2, Fig. 38b).

No adhesion was observed in the inlet channels or at the bifurcation apexes of G1-treated chambers. Similarly, PL1-treated neutrophils failed to adhere in either the inlet channels or at the bifurcation apexes of P-selectin coated chambers at both

shear stresses. Following perfusion of PL1-treated cells, we flushed each chamber with a 0.5% solution of HSA in HBSS and perfused untreated neutrophils for two minutes. Untreated neutrophils adhered in expected patterns at both shear stresses where PL1-treated neutrophils previously had not.

To test whether adhesion at the bifurcation apex could simply be a result of the fluid mechanics alone, we incubated chambers with 120° bifurcations with only a 0.5% solution of HSA in HBSS. Untreated neutrophils were perfused through these chambers at shear stresses of 1 and 50 dyn/cm^2. No cells were observed adhering in the inlet channels or at the bifurcation apexes of HSA-coated chambers after two minutes at either shear stress (Fig. 38).

Apex Adhesion Decreases with Paraformaldehyde Fixation and L-selectin Blocking. Given that neutrophil adhesion at the bifurcation apex is the result of specific molecular interactions, we also investigated the role of L-selectin/PSGL-1 mediated leukocyte-leukocyte interactions in apex accumulation. Isolated neutrophils were incubated with Dreg56, a blocking mAb to L-selectin, and perfused through 120° bifurcated chambers coated with 3μg/mL P-selectin at τ_w = 1 and 50 dyn/cm^2. At 1dyn/cm^2, we estimated Dreg56-treated cell adhesion to be approximately 325 cells/mm^2 after two minutes, which was approximately 44% less than untreated cells (Fig. 39a). Interestingly, we observed little change in adhesion for Dreg56-treated cells with respect to shear stress. When Dreg56-treated cells were perfused at 50 dyn/cm^2, we estimated approximately 400 cells/mm^2 adhering after two minutes (Fig. 39b). This represents drop in adhesion of approximately 78% between Dreg56-treated cells and untreated cells. We also estimated the number of adherent Dreg56-

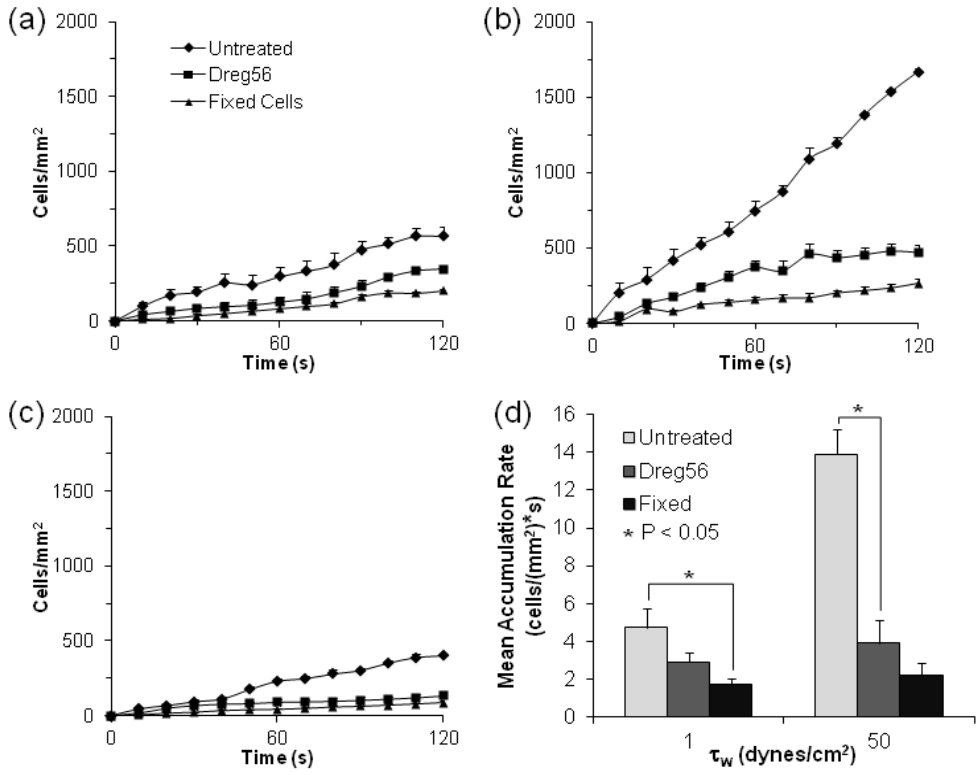


Figure 39: Neutrophil accumulation at the bifurcation apex was significantly reduced when cells were fixed with paraformaldehyde or treated with anti-L-selectin mAb Dreg56. τ_w = (a)1 and (b)50 dynes/cm^2. (c)Paraformaldehyde fixation or incubation with anti-L-selectin mAb Dreg56 also significantly reduced neutrophil accumulation in the inlet channel at 1 dyne/cm^2. (d)Apex accumulation rates for fixed and Dreg56 cells also decreased at low and high τ_w. Bifurcation angle = 120°.

treated cells in the inlet channel. At 1 dyne/cm^2, there were approximately 125 cells/mm^2 in the inlet channel after 120 s representing a 64% decrease compared to untreated cells (Fig. 39c). Meanwhile at 50 dynes/cm^2, we did not observe any Dreg56-treated cells adhering in the inlet channel. In addition, we calculated the accumulation rate of Dreg56-treated cells at both shear stresses (Fig. 39d). At τ_w = 1dyn/cm^2, the average accumulation rate was approximately 2.9 (cells/mm^2)/s compared to 4.7 (cells/mm^2)/s for untreated cells. Increasing τ_w to 50 dyn/cm^2 slightly increased in the accumulation rate for Dreg56-treated cells to 3.9

(cells/mm^2)/s, however, this result was significantly lower than the untreated cell accumulation rate of 13.9 (cells/mm^2)/s ($P < 0.05$).

We also investigated whether physical cellular properties play a role in adherent cell accumulation at the apex. Previously, paraformaldehyde fixation has been shown to increase leukocyte rolling velocity which is likely due to decreased cell deformability[259]. To determine whether paraformaldehyde fixation can affect leukocyte adhesion at bifurcations, we fixed isolated neutrophils with a 1% paraformaldehyde solution and perfused the fixed cells through 120° bifurcated chambers at τ_w of 1 dyn/cm^2 (Fig. 39a) and 50 dyn/cm^2 (Fig. 39b).

At τ_w = 1dyn/cm^2 we observed a decrease in apex adhesion from approximately 600 cells/mm^2 to 175 cells/mm^2. This represents a decrease of approximately 72% in leukocyte adhesion at the bifurcation apex. At τ_w = 50 dyn/cm^2 we estimated approximately 200 cells/mm^2 adhering at the apex after two minutes, which represents an approximately 88% drop in adhesion between untreated cells and fixed cells. Additionally, we estimated fixed cell adhesion in the inlet channel at approximately 90 cells/μm^2 (1 dyne/cm^2, Fig. 39c), representing a 75% decrease compared to untreated cells. Fixed cells also did not adhere in the inlet channel at 50 dynes/cm^2. We also calculated the accumulation rates for fixed cells at both shear stresses. Similar to Dreg56-treated cells, fixed cells exhibited significant decreases in accumulation rate compared to untreated cells at τ_w = 1 and 50 dyn/cm^2 (Fig. 39d).

Adhesion at the Bifurcation Apex Decreases with Decreasing P-selectin Concentration. Leukocyte rolling is dependent not only on the effects of shear stress

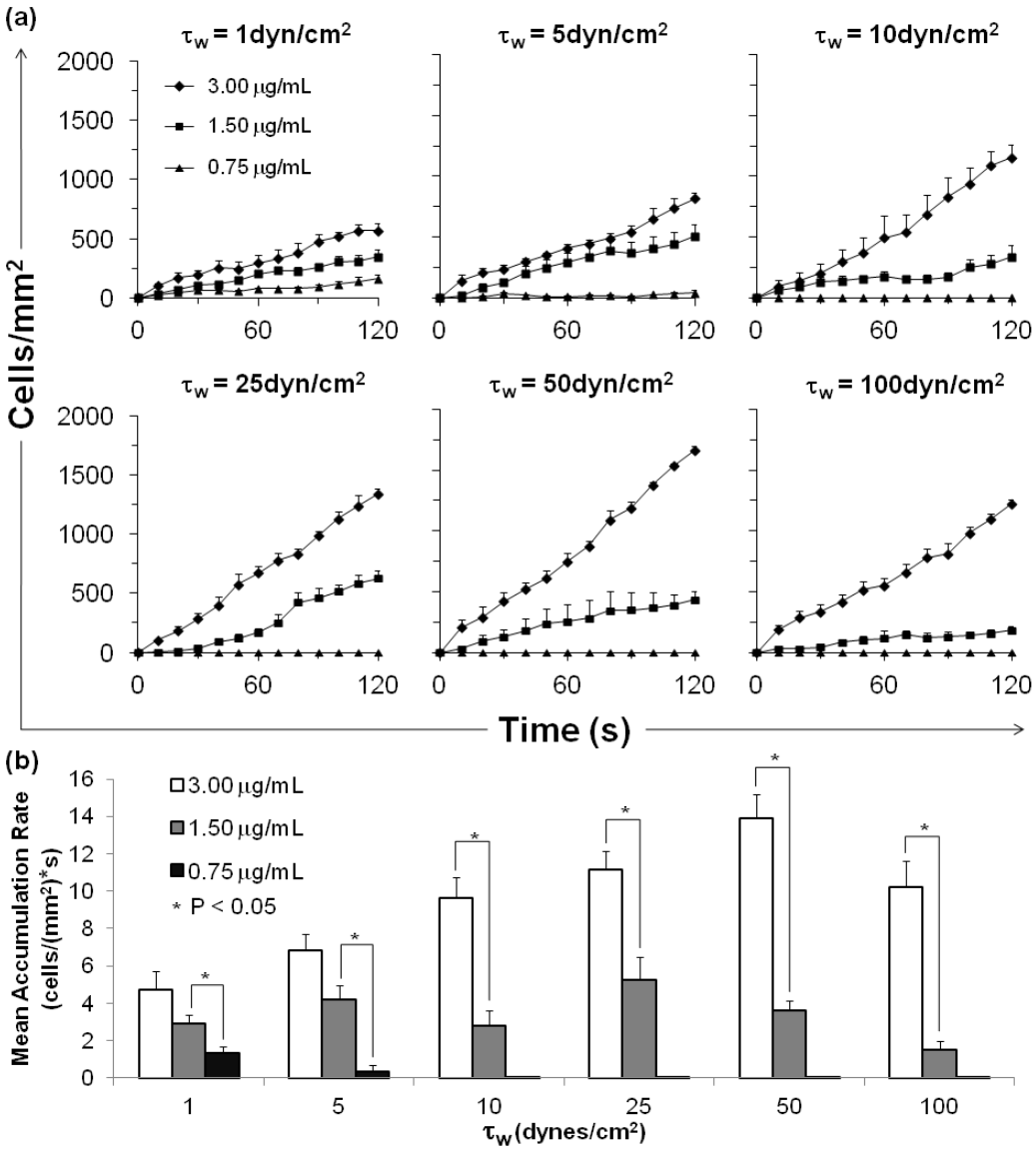


Figure 40: (a)Neutrophil accumulation at the bifurcation apex decreased significantly with decreasing P-selectin concentration, especially at high τ_w. (b)Accumulation rate was also significantly dependent on P-selectin concentration. Bifurcation angle = 120°.

but also on the number of P-selectin sites available for binding. To determine whether leukocyte adhesion at a bifurcation is dependent on P-selectin site density, we coated 120° bifurcated chambers with varying concentrations of P-selectin (0.75 – 3.00 μg/mL). Isolated neutrophil suspensions were perfused through these chambers at the same τ_w as previous experiments. We observed that decreased

adhesion at the apex correlated significantly with decreasing P-selectin concentration at all shear stress levels (Fig. 40a).

At 1dyn/cm^2, neutrophils adhered at the bifurcation apex in chambers coated with all three P-selectin concentrations. As expected, adhesion was the greatest in the 3.00 μg/mL chambers, with approximately 600 cells/mm^2 adhering at the apex. When the coating concentration was decreased to 1.50 μg/mL, apex adhesion decreased to approximately 350 cells/mm^2. A further decrease in the P-selectin concentration to 0.75 μg/mL decreased apex adhesion to approximately 150 cells/mm^2. We also measured adhesion in the inlet channel at all three P-selectin concentrations. As expected, a decrease in the number of adherent cells correlated with a decrease in P-selectin concentration.

While increasing shear stress led to increasing apex adhesion in chambers coated with 3.0 μg/mL P-selectin, apex adhesion did not significantly increase with increasing shear stress when P-selectin concentration was decreased to 1.5 μg/mL (Fig. 40a). Indeed, apex adhesion only increased to approximately 630 cells/mm^2 at τ_w = 25 dyn/cm^2 and then decreased to approximately 200 cells/mm^2 at τ_w = 100 dyn/cm^2. Further decreasing the P-selectin concentration to 0.75 μg/mL resulted in a significant decrease in apex adhesion at 5 dyn/cm^2 and no adhesion was observed at the apex at $\tau_w \geq 10$ dyn/cm^2. Fig. 40b shows that, at τ_w = 1 and 5 dyn/cm^2, accumulation rate did not decrease significantly until P-selectin concentration decreased from 1.50 – 0.75 μg/mL. However, at $\tau_w \geq 10$ dyn/cm^2 there was a significant decrease in accumulation rate when P-selectin concentration was decreased from 3.00 – 1.50 μg/mL.

Adhesion at the Bifurcation Apex Decreases with Decreasing Bifurcation Angle. To investigate how changes in channel geometry would affect the pattern of cell adhesion, we fabricated diamond-shaped channels with bifurcation angles ranging from 90 – 30° to complement our 120° bifurcation studies. Isolated neutrophils were perfused through P-selectin coated chambers at τ_w = 1 – 100 dynes/cm^2. Figure 41a shows a slight decrease in adhesion at the bifurcation apex between 120° and 90° bifurcated channels at each of the shear stresses tested. At low shear stress (1 dyne/cm^2), we observed an estimated difference in adhesion of approximately 30% after two minutes. At high shear stress (50 dynes/cm^2) that difference increased to approximately 35%.

Between 90 degree and 60 degree bifurcated channels we continued to see a decrease in adhesion at the apex (Fig. 41a). At all shear stresses except the lowest, we observed almost no difference in the amount of adhesion at the apex between these angles until approximately one minute after the start of perfusion. After one minute, we observed a leveling off in adhesion in the 60 degree bifurcated channels, while apex adhesion in the 90 degree channels tended to continue increasing. The greatest difference we observed between these two angles after two minutes was at 5 dynes/cm^2, when apex adhesion decreased by approximately 40%. As shear stress was increased, we observed a decrease in the difference of apex adhesion, falling to only a 22% decrease at 100 dynes/cm^2.

A further decrease in the bifurcation angle from 60 degrees to 30 degrees brought about an even greater decrease in apex adhesion (Fig. 41a). At 1 dyne/cm^2, we observed an approximately 33% decrease in adhesion between 60 degree and 30

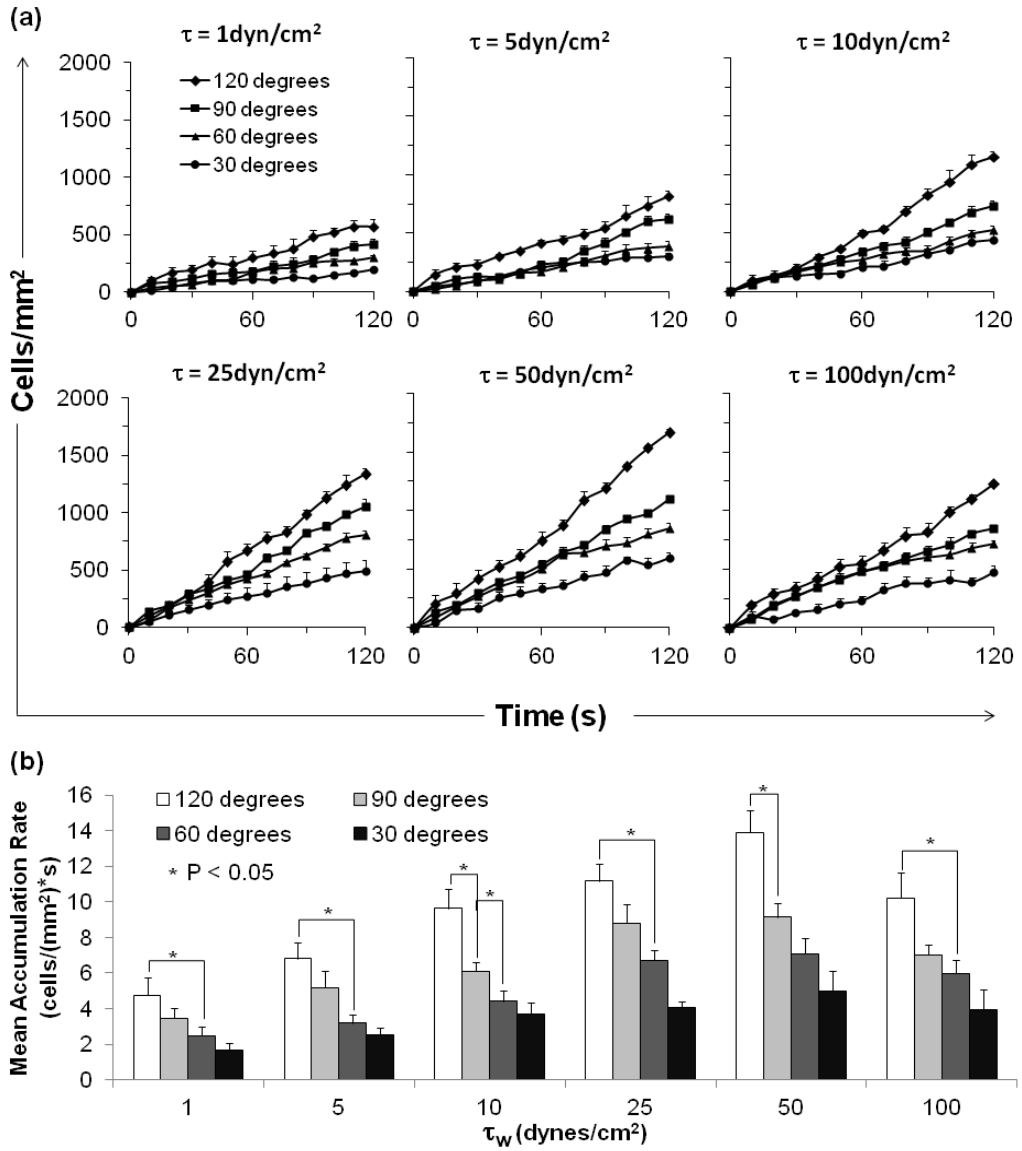


Figure 41: (a)Decreased neutrophil accumulation at the bifurcation apex correlated with decreasing bifurcation angle at constant τ_w. (b)Decreased accumulation rates also correlated with decreasing bifurcation angle.

degree channels and an estimated 65% decrease between 120 degree and 30 degree channels. These estimated decreases in adhesion remained consistent across the entire range of shear stresses. As a control test, we also quantified adhesion in the inlet channels for channels with all four bifurcation angles. Inlet channel adhesion

remained consistent for each stress independent of the bifurcation angle. In addition, we observed no adhesion at shear stresses above 5 dynes/cm^2 in any of the channels.

Discussion

Here we report the fabrication of diamond-shaped microfluidic chambers with a single inlet and a single outlet channel to determine whether selectin-mediated leukocyte rolling can be supported at the apex of a bifurcation. Computational studies have shown that a stagnation point exists at the apex of a bifurcation (Fig. 42)[140, 159, 180, 266]. This suggests that selectin-mediated neutrophil adhesion could occur at this point at both low and high wall shear stresses. Indeed, a previous master's thesis described the adhesion of CHO cells expressing human PSGL-1 and isolated human neutrophils at the apexes of asymmetrical bifurcations. While this study observed significant adhesion at the bifurcation apex even at significantly high shear stress (100 dynes/cm^2), there were significant drawbacks to the design of the microfluidic devices.

This study used bifurcations that split into asymmetric daughter channels. Even though this asymmetry is common through the arterial tree, it leads to uneven flow which was observed in the preferential occlusion of one daughter channel over the other. To eliminate the effects of uneven flow distribution, we fabricated our channels with symmetric daughter channels. The cross-sectional dimensions of the devices used in the previous study (100 μm x 50 μm, W x H) also presented significant challenges in estimating the shear stress. Similar to the previous neutrophil adhesion experiments reported in the master's thesis, we observed the significant buildup of neutrophil aggregates in the daughter channels of 100 x 50 μm (W x H) chambers after 10 minutes of perfusion at 50 dynes/cm^2 (Fig. 35).

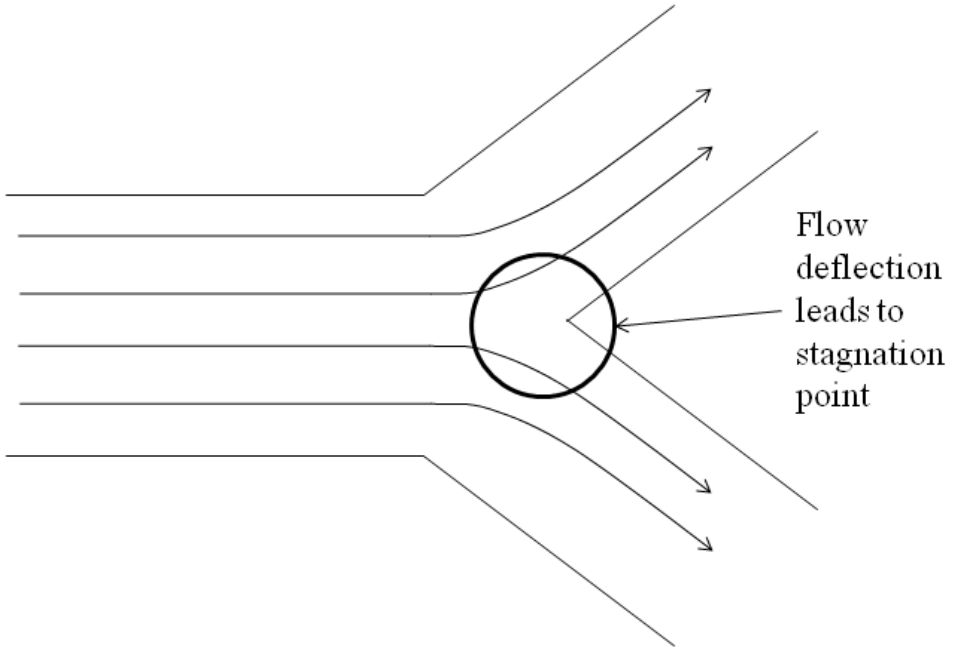


Figure 42: Flow deflection at the bifurcation apex creates a stagnation point

Previous studies have demonstrated that flow velocities in a rectangular channel with a width to height ratio (W/H) less than 10 are dependent on both the vertical and lateral position. We also fabricated our channels with cross-sectional dimensions of 1000 μm x 100 μm (W x H) to negate the dependence of velocity on the lateral position. In these channels, we did not observe the buildup of neutrophil aggregates. Rather, after 10 minutes of perfusion we observed only a thin layer of neutrophils adhering along the inner walls of the daughter channels (Fig. 36). In the previous chapter of this work, we also demonstrated the dependence of selectin-mediated rolling on the ratio of cell diameter to channel height (D_c/H). Specifically, we showed that neutrophils rolled significantly slower on P-selectin for $D_c/H > 0.1$. This was true for the previous devices which would have had D_c/H ratios of 0.16 for neutrophils ($D_c \sim 8$ μm) or 0.30 for CHO cells ($D_c \sim 15$ μm). Because our devices

were fabricated with a height of 100 μm, we were able to eliminate the additional affects that the D_c/H parameter can have on rolling.

As expected, at low $\tau_{w, main}$ (1 – 5 dyn/cm^2) we observed consistent neutrophil rolling along the length of the inlet channel, as well as at the bifurcation apex. In addition, there was no significant difference between the number of cells rolling in the inlet channel and at the apex, suggesting that at low inlet channel wall shear there is little difference between this shear stress and the shear stress at the bifurcation apex. As $\tau_{w, main}$ was increased, the number of cells observed rolling in the inlet channel decreased significantly. In fact, at $\tau_{w, main}$ = 10 dyn/cm^2 or greater, neutrophil rolling in the inlet channel is entirely abolished. Neutrophil rolling on P-selectin coated surfaces occurs when PSGL-1/P-selectin bonds are able to form at the leading edge of the cell before the bonds at the trailing edge of the cell are completely broken. Our data suggest that inlet channel wall shear stresses of 10 dyn/cm^2 or greater create enough force to prevent the sustained interactions required to support neutrophil rolling.

At the bifurcation apex, however, we continued to see a significant increase in neutrophil adhesion with increasing shear stress. We attribute this increase to an increase in the momentum of cells as they leave the inlet channel and collide with the apex wall. In a comparable study, however, untreated neutrophils did not accumulate at the apexes of chambers coated with albumin suggesting that cells do not adhere at the apex solely as a result of their momentum. We confirmed that PSGL-1/P-selectin adhesive interactions were necessary for apex accumulation by performing further experiments with anti-PSGL-1 and anti-P-selectin blocking

mAbs. Indeed, there was no neutrophil accumulation present in chambers where P-selectin was blocked with anti-P-selectin mAb G1. Similarly, neutrophils treated with anti-PSGL-1 mAb PL1 failed to accumulate at the apexes of P-selectin coated chambers. These studies showed that PSGL-1/P-selectin interactions were necessary for neutrophils to adhere at the apex.

As the cells collide with the apex wall, cellular deformation may play a role in adhesion by increasing the surface area of the cell available for binding with P-selectin immobilized at the apex wall. In addition, the build-up of adherent cells at the apex wall could increase the potential for secondary leukocyte-leukocyte adhesion through PSGL-1/L-selectin binding.

In order to determine whether cell deformation plays a role in neutrophil adhesion at the bifurcation apex, we performed perfusion experiments with neutrophils fixed with 1% paraformaldehyde in 120-degree bifurcated channels. Previous studies have shown that paraformaldehyde fixation significantly increases neutrophil rolling velocities on P-selectin coated surfaces.[259] Although this may be due in part to changes in the way PSGL-1 binds to P-selectin after fixation, it has also been suggested that fixing a cell with paraformaldehyde limits its ability to deform. Therefore, we investigated the adhesion pattern of neutrophils fixed with 1% paraformaldehyde at the bifurcation apex under low and high shear stress. We observed a significant decrease between untreated neutrophil and fixed neutrophil adhesion under both low and high shear conditions. Additionally, we observed little difference between fixed cell adhesion at low and high shear, which contrasted the untreated cell adhesion (Fig. 39). This significant decrease in adhesion suggests that

cell deformation is indeed important for cells adhering at the bifurcation apex. The insignificant difference in adhesion of fixed cells between low and high shear conditions may also suggest that the increase in untreated cell adhesion with increasing shear stress is related to cell deformation.

We also investigated the role of secondary leukocyte-leukocyte interactions in the cell adhesion pattern. To accomplish this, isolated neutrophils were incubated with Dreg56, an mAb that has been shown to block binding between L-selectin and PSGL-1. These cells were then perfused through 120-degree bifurcated chambers at low and high shear stress. Under low shear stress, we observed a decrease in adhesion of Dreg56-treated cells compared with untreated cells. At high shear stress, we observed nearly the same level of Dreg56-treated cell adhesion as at low shear stress. Under high shear stress, however, we found that adhesion appeared to level off after 80s of perfusion. In contrast, under low shear stress we observed a continual increase in cell adhesion for the entire 120s of perfusion. This suggests that as cells collide with the apex wall and adhere, they prevent other cells from interacting with the wall. Therefore, without the ability of neutrophils to interact with one another, the build-up of adhering cells was severely limited.

Although cellular properties clearly play a role in neutrophil adhesion at the apex of a bifurcation, we also investigated how the characteristics of the apex could affect adhesion. Specifically, we investigated the effect that decreasing the bifurcation angle could have on the flow dynamics around the apex wall. We fabricated diamond-shaped chambers with bifurcation angles of 30, 60 and 90 degrees, to test alongside our original 120-degree bifurcation design. Isolated

neutrophils were perfused through these chambers at varying inlet channel wall shear stresses. We observed that increasing the bifurcation angle increased the number of cells that adhered at the apex, however, these increases did not always occur right away. While cell adhesion was always significantly higher in the 120-degree channels, the 90-degree and 60-degree channels almost always exhibited the same level of adhesion through the first 60s of perfusion. At all shear stresses tested, we did not observe a significant difference between 90-degree and 60-degree chambers until between 60 and 90s of perfusion. Additionally, we observed little difference in the 30-degree chambers during the first 60 s of perfusion at low shear stress. As shear stress increased, we began to see a significant difference between 30 and 60-degree chambers as early as 20 s into perfusion.

These data suggest that bifurcation angle does play a role in cell adhesion at the apex, however, it does not always have an immediate effect. As cells near the bifurcation, they will experience a loss of momentum as the fluid decelerates. In the case of a thinner bifurcation angle, this deceleration means that cells will collide with the apex wall with less force. For a wider bifurcation angle, the fluid deceleration will occur in a much smaller space. Therefore, cells will collide with the apex wall with greater force. Our data agree with this hypothesis in that we observe the greatest cell adhesion at the widest bifurcation angle and the least adhesion at the thinnest angle. Furthermore, although increased fluid velocity can provide cells with additional momentum, the effects of the bifurcation angle still play a role as evidenced by the observation of this trend at both low and high shear stress.

While the bifurcation angle can play a role in the overall fluid dynamics surrounding the apex, we have also shown that cell adhesion at the apex is dependent on the presence of immobilized adhesive protein (P-selectin). To investigate whether the concentration of P-selectin during chamber incubation affects cell adhesion, we coated 120-degree bifurcation chambers with varying concentrations of P-selectin. We hypothesized that decreasing the concentration of P-selectin should in turn decrease the number of immobilized P-selectin sites available for binding with cellular PSGL-1. Therefore, chambers were coated with P-selectin solutions of 1.5 μg/mL and 0.75 μg/mL to compare to our original results with 3.0 μg/mL.

Indeed, we observed that decreasing the coating concentration of P-selectin results in a decrease in neutrophil adhesion at the apex. This further demonstrates that the number of P-selectin sites available for binding plays a significant role in the neutrophil apex adhesion pattern. Even at high shear when the cells strike the apex wall with greater force, our data suggests that a certain number of P-selectin sites must be available for binding. This appears evident from our observation that neutrophil adhesion can be abolished at a shear stress of 10 dyn/cm^2 or greater when the P-selectin concentration is decreased to 0.75 μg/mL.

In summary, we have reported the observation of selectin-mediated leukocyte adhesion at the apex of bifurcations at wall shear stresses as high as 100 dynes/cm^2. Using blocking antibodies to P-selectin and PSGL-1, we confirmed the specificity of these interactions. Furthermore, we determined that adhesion is dependent on the density of P-selectin sites available at the apex. We also

demonstrate that adhesion at the bifurcation apex is aided by cellular deformation as well as secondary L-selectin/PSGL-1 interactions. In addition, we have shown that chamber geometry plays an important role in that increased adhesion correlates with steeper bifurcation angles. These results are significant in that they provide a better understanding of leukocyte adhesion at bifurcations and will aid in the development of in vitro models of atherosclerosis.

Chapter 6: Conclusions and Future Directions

Conclusions

The studies presented here investigated the effects of shear stress on selectin-mediated neutrophil rolling as it relates to localized and global cellular deformation. In the case of localized contact zone deformation, the studies presented in chapter 2 demonstrate that reflective interference contrast microscopy (RICM) can be used as a low-cost alternative to quantitative dynamic footprinting to visualize the footprints of rolling neutrophils. These studies demonstrate that contact area is a dynamic quantity that is dependent on the separation distance between cell and substrate. We used this technique to show that the footprint area of a rolling neutrophil ($z < 137$ nm) increases from approximately 11 μm^2 at a wall shear stress of 1 dyne/cm^2 to 20 μm^2 at 8 dynes/cm^2. Plots of contact area against time at multiple separation distances also revealed that a majority of the footprint was more than 75 nm above the substrate surface. This was further observed by plotting instantaneous velocities against contact areas. Here, we also observed what appeared to be a general trend where increased rolling velocity corresponded to lower contact area measurements. To further characterize this trend, we assumed a microvillus tip area of 0.06 μm^2 and calculated the number of microvilli interacting with the substrate from the contact area measurements at $z < 50$ nm. Typically, there were 10 – 20 microvilli interacting at 1 dyne/cm^2 and 50 – 100 microvilli at 8 dynes/cm^2.

In addition to footprint visualization, we also observed the formation of membrane tethers with RICM. These tether structures formed when regions of the

footprint with a very low separation distance remained stationary while the cell continued to translocate downstream. While tethers typically released from the substrate and retracted back to the cell body, on rare occasions we observed the breakage of tethers along their lengths resulting in the deposition of membrane pieces. We found that increased membrane tether formation correlated with increased shear stress and tether breakage events were more likely to be observed under high shear stress conditions (> 4 dynes/cm^2). We also demonstrated that tether formation and overall footprint area are dependent on shear stress rather than shear rate by using Ficoll to vary the viscosities of cell suspensions, thereby allowing us to vary shear stress independently of shear rate. These studies demonstrated that shear stress plays a clear role in two types of localized cell deformation: contact zone deformation and membrane tether formation.

However, there are factors in addition to shear stress that mediate membrane tether extraction. In chapter 3 we presented studies that investigated the role of ligand density and ligand type in membrane tether formation. Average membrane tether lifetime nearly doubled with increasing P-selectin concentration as well as increasing shear stress. Membrane tether length also increased with increasing shear stress but did not display any trend with varying P-selectin concentration. This demonstrated that tether length is dependent on the shear stress applied to the cell while tether lifetime is dependent on both shear force and the strength of the selectin/ligand interactions. Therefore, increased P-selectin site availability resulted in an increase in tether lifetime but not tether length.

We also demonstrated the effects of ligand density on membrane tether formation with two other ligand types: a recombinant human P-selectin-Fc chimera and a recombinant human E-selectin-Fc chimera. The results with the P-selectin chimera were very similar the multimeric P-selectin which suggests that the presentation of the ligand does not necessarily affect membrane tether lengths or lifetimes. Alternatively, average membrane tether lifetimes were nearly three times greater on E-selectin compared to P-selectin. Average tether length, however, remained unchanged regardless of ligand type. Additionally, neutrophils treated with anti-PSGL-1 mAb PL1 rolled faster and exhibited decreased tether lengths and lifetimes on P-selectin. However, PL1-treated neutrophils did not exhibit any of these changes when rolled on E-selectin coated surfaces. These observations lend support to the suggestion that ligands distinct from PSGL-1 mediate rolling on E-selectin[258, 262] and suggest that these ligands can also mediate membrane tether formation.

In the study of cell adhesion in vitro, microfluidic devices are becoming extremely popular. However, there are significant trade-offs between sample volume requirements and channel geometry. When manipulating design parameters such as channel dimensions to achieve lower sample volume requirements, previous studies have predicted that this will also have an impact on cell adhesion by affecting global deformation[112, 132]. The studies in chapter 4 demonstrate that this deformation is indeed related to the ratio of cell diameter to chamber height (D_c/H). We demonstrated that decreasing chamber height from 100 – 30 μm (D_c/H = 0.08 – 0.27) resulted in a 41 – 62% decrease in rolling velocity at shear stresses

ranging from 0.5 – 8 dynes/cm^2. Decreasing chamber height further to 20 μm (D_c/H = 0.40) resulted in a further velocity decrease of 44 – 55% at the same shear stress levels. These results confirmed a previous theoretical study which suggested that an adherent neutrophil in a tall channel will roll faster due to increased shearing at the top of the cell[111]. Simulations of neutrophil rolling with VECAM confirmed that decreasing chamber height correlates with a decrease in rolling velocity.

In complementary studies, neutrophils fixed with paraformaldehyde and PSGL-1 coated polystyrene microspheres did not display significant changes in rolling velocity when channel height was decreased (22% and 9% decreases, respectively). This demonstrated that the decrease in rolling velocities observed with untreated cells was related to their ability to deform. Observations with IRM also showed that neutrophil contact area increases with increasing chamber height. Even though the increasing contact area correlates with increasing rolling velocity, the force applied by the shear stress balances the increased contact area from cellular deformation leading to faster rolling.

The studies in chapter 5 demonstrate that shear induced cellular deformation is dependent not only on channel height but also on channel geometry. Previous studies have shown that atherosclerotic plaques tend to localize at sites of unsteady shear including bifurcations[66, 170, 183]. These plaques have also been shown to incorporate inflammatory cells through selectin/ligand interactions[51, 210]. Our microfluidic studies with bifurcated chambers demonstrate that the stagnation point at the bifurcation apex is able to support neutrophil adhesion even when the inlet channel shear stress is very high. Indeed, neutrophil accumulation at the apex

correlated with increased wall shear stress with approximately 1300 cells/mm^2 adhering at a shear stress of 100 dynes/cm^2.

We demonstrated with blocking antibodies that neutrophil accumulation at the apex is the result of specific molecular interactions between PSGL-1 and P-selectin. We also used albumin coated channels to show that apex accumulation was not the result of momentum from high shear stress. To investigate the effects of cellular deformation, neutrophils were fixed with 1% paraformaldehyde. Fixed neutrophils adhered at the bifurcation apex, but in significantly fewer numbers compared to untreated cells. Neutrophils treated with anti-L-selectin mAb Dreg56 also exhibited decreased adhesion at the apex. Both of these studies demonstrated that neutrophil accumulation at the apex is dependent to a degree on cellular deformation and PSGL-1/L-selectin interactions. Neutrophil accumulation was also dependent on P-selectin coating concentration. Decreasing P-selectin concentration to 1.5 mg/mL resulted in a 38 – 85% decrease in accumulation at shear stresses ranging from 1 – 100 dynes/cm2. Further decreasing the concentration to 0.75 mg/mL resulted in a further decrease of 53% and 92% at shear stresses of 1 and 5 dynes/cm^2, respectively and completely abolished accumulation at shear stresses greater than 10 dynes/cm^2.

Lastly, we showed that apex accumulation is also dependent on chamber geometric properties including bifurcation angle and cross-sectional dimensions. A decrease in the bifurcation angle from 120 – 30 degrees correlated with a reduction in neutrophil accumulation of approximately 65% at shear stresses from 1 – 100 dynes/cm^2. Alternatively, decreasing the channel cross-sectional dimensions did not

significantly impact initial (t = 120 s) accumulation at the apex but resulted in aggregate build-up in the daughter channels leading to approximately 40% coverage of the bottom channel wall regardless of bifurcation angle after 60 minutes of perfusion.

Future Directions

There are numerous possibilities for extending these projects in the future. In the case of membrane tether extrusion, our studies with ligand type can be extended to characterize tether formation as a result of PSGL-1/L-selectin interactions. These interactions are significant because both molecules are expressed on the surface of leukocytes, meaning that tether formation could be observed on L-selectin or PSGL-1 coated surfaces. Furthermore, L-selectin would be significant in that it is shed from leukocyte membranes under certain conditions[33, 249]. While little is known about tether formation involving L-selectin, previous studies have demonstrated that L-selectin can mediate tether formation during leukocyte-leukocyte collisions[47, 109]. Additionally, we have observed tether formation on L-selectin coated surfaces, but we have not published these reports or engaged in any characterization of L-selectin membrane tethers.

Our tether extraction studies could also be extended to observe and characterize tether formation during integrin-mediated slow rolling. Previous studies have shown that neutrophils roll slower on substrates coated with P-selectin and ICAM-1 compared to P-selectin alone[160, 264]. However, little is known about tether formation during rolling on such substrates. We can also extend these studies to include multiple cell types such as monocytes, basophils, eosinophils or even

CHO cells. CHO cells expressing human PSGL-1 are indeed significant, as we have briefly used RICM to observe differences in the footprints of these cells compared to neutrophils.

In regard to the microfluidic studies, the possibilities for cell adhesion in microfluidic chambers are virtually endless. In one case, we have developed patterns for microfluidic channels with a constriction to study the effects of contracting and expanding flow on both leukocyte and platelet adhesion. In addition, the dimensions of these chambers allow for ultra-high shear stresses ($> 10^3$ dynes/cm^2) to be achieved with minimal sample volume. These studies could be useful in helping to model the high shear flow in ventricular assist devices to better understand the effects of high shear on leukocyte and platelet adhesion as well as morphology and signaling.

Finally, there is further work that can be done with our diamond-shaped microfluidic channels. Because these devices have a single entrance and exit, they provide a unique opportunity to study cell adhesion not only at diverging bifurcations but also at points of convergence between two flow streams. A recent study by Lamkin-Kennard et al characterized the distribution of adherent leukocytes at venular convergences *in vivo*[125]. However, this study did not quantitatively investigate the specific hydrodynamic contributions to the adhesion pattern. Our devices would provide a simple in vitro system that could be used to model cell adhesion at convergence points and determine the hydrodynamic effects on such adhesion.

REFERENCES

1. Aigner, S., et al., *CD24 mediates rolling of breast carcinoma cells on P-selectin.* FASEB J, 1998. **12**(12): p. 1241-51.

2. Alon, R., et al., *The kinetics and shear threshold of transient and rolling interactions of L-selectin with its ligand on leukocytes.* Proc Natl Acad Sci U S A, 1998. **95**(20): p. 11631-6.

3. Alon, R., et al., *The kinetics of L-selectin tethers and the mechanics of selectin-mediated rolling.* The Journal of cell biology, 1997. **138**(5): p. 1169-80.

4. Alon, R., et al., *Glycolipid ligands for selectins support leukocyte tethering and rolling under physiologic flow conditions.* J Immunol, 1995. **154**(10): p. 5356-66.

5. Alon, R., D.A. Hammer, and T.A. Springer, *Lifetime of the P-selectin-carbohydrate bond and its response to tensile force in hydrodynamic flow.* Nature, 1995. **374**(6522): p. 539-42.

6. Annane, D., E. Bellissant, and J.M. Cavaillon, *Septic shock.* Lancet, 2005. **365**(9453): p. 63-78.

7. Asako, H., et al., *Indomethacin-induced leukocyte adhesion in mesenteric venules: role of lipoxygenase products.* Am J Physiol, 1992. **262**(5 Pt 1): p. G903-8.

8. Asakura, T. and T. Karino, *Flow patterns and spatial distribution of atherosclerotic lesions in human coronary arteries.* Circ Res, 1990. **66**(4): p. 1045-66.

9. Barber, K.M., A. Pinero, and G.A. Truskey, *Effects of recirculating flow on U-937 cell adhesion to human umbilical vein endothelial cells.* Am J Physiol, 1998. **275**(2 Pt 2): p. H591-9.

10. Batchelor, G.K., *An introduction to fluid dynamics*. 1973, Cambridge: Cambridge University Press. xviii, 615 p.

11. Bell, G.I., *Models for the specific adhesion of cells to cells.* Science, 1978. **200**(4342): p. 618-27.

12. Belval, T., J.D. Hellums, and R.T. Solis, *The kinetics of platelet aggregation induced by fluid-shearing stress.* Microvascular research, 1984. **28**(3): p. 279-88.

13. Berg, E.L., et al., *Comparison of L-selectin and E-selectin ligand specificities: the L-selectin can bind the E-selectin ligands sialyl Le(x) and sialyl Le(a).* Biochem Biophys Res Commun, 1992. **184**(2): p. 1048-55.

14. Bevilacqua, M.P., et al., *Endothelial leukocyte adhesion molecule 1: an inducible receptor for neutrophils related to complement regulatory proteins and lectins.* Science, 1989. **243**(4895): p. 1160-5.

15. Bienvenu, K. and D.N. Granger, *Molecular determinants of shear rate-dependent leukocyte adhesion in postcapillary venules.* Am J Physiol, 1993. **264**(5 Pt 2): p. H1504-8.

16. Birchall, D., et al., *Analysis of haemodynamic disturbance in the atherosclerotic carotid artery using computational fluid dynamics.* Eur Radiol, 2006. **16**(5): p. 1074-83.

17. Blann, A.D., S.K. Nadar, and G.Y. Lip, *The adhesion molecule P-selectin and cardiovascular disease.* Eur Heart J, 2003. **24**(24): p. 2166-79.

18. Borsig, L., et al., *Synergistic effects of L- and P-selectin in facilitating tumor metastasis can involve non-mucin ligands and implicate leukocytes as enhancers of metastasis.* Proc Natl Acad Sci U S A, 2002. **99**(4): p. 2193-8.

19. Bose, S., *A Microvillus Based Approach to Model Cell Rolling*, in *Department of Mechanical Engineering*. 2009, Massachusetts Institute of Technology: Cambridge, MA.

20. Brakemeier, S., et al., *Shear stress-induced up-regulation of the intermediate-conductance Ca(2+)-activated K(+) channel in human endothelium.* Cardiovasc Res, 2003. **60**(3): p. 488-96.

21. Brooks, S.B. and A. Tozeren, *Flow past an array of cells that are adherent to the bottom plate of a flow channel.* Computers & Fluids, 1996. **25**(8): p. 741-757.

22. Brown, D.C. and R.S. Larson, *Improvements to parallel plate flow chambers to reduce reagent and cellular requirements.* BMC Immunology, 2001. **2**(9 Cited May 17, 2002): p. 1-7.

23. Bruehl, R.E., T.A. Springer, and D.F. Bainton, *Quantitation of L-selectin distribution on human leukocyte microvilli by immunogold labeling and electron microscopy.* J Histochem Cytochem, 1996. **44**(8): p. 835-44.

24. Brunk, D.K., D.J. Goetz, and D.A. Hammer, *Sialyl Lewis(x)/E-selectin-mediated rolling in a cell-free system.* Biophys J, 1996. **71**(5): p. 2902-7.

25. Caputo, K.E. and D.A. Hammer, *Effect of microvillus deformability on leukocyte adhesion explored using adhesive dynamics simulations.* Biophys J, 2005. **89**(1): p. 187-200.

26. Carmassi, F., et al., *Coagulation and fibrinolytic system impairment in insulin dependent diabetes mellitus.* Thrombosis research, 1992. **67**(6): p. 643-54.

27. Caro, C.G., *Discovery of the role of wall shear in atherosclerosis.* Arterioscler Thromb Vasc Biol, 2009. **29**(2): p. 158-61.

28. Celi, A., et al., *Thrombus formation: direct real-time observation and digital analysis of thrombus assembly in a living mouse by confocal and widefield intravital microscopy.* J Thromb Haemost, 2003. **1**(1): p. 60-8.

29. Chang, K.C. and D.A. Hammer, *The forward rate of binding of surface-tethered reactants: Effect of relative motion between two surfaces.* Biophysical Journal, 1999. **76**(3): p. 1280-1292.

30. Chapman, G. and G. Cokelet, *Model studies of leukocyte-endothelium-blood interactions. I. The fluid flow drag force on the adherent leukocyte.* Biorheology, 1996. **33**(2): p. 119-38.

31. Chapman, G.B. and G.R. Cokelet, *Model studies of leukocyte-endothelium-blood interactions. II. Hemodynamic impact of leukocytes adherent to the wall of post-capillary vessels.* Biorheology, 1997. **34**(1): p. 37-56.

32. Chapman, G.B. and G.R. Cokelet, *Flow resistance and drag forces due to multiple adherent leukocytes in postcapillary vessels.* Biophys J, 1998. **74**(6): p. 3292-301.

33. Chen, A., P. Engel, and T.F. Tedder, *Structural requirements regulate endoproteolytic release of the L-selectin (CD62L) adhesion receptor from the cell surface of leukocytes.* The Journal of experimental medicine, 1995. **182**(2): p. 519-30.

34. Chen, J., X.Y. Lu, and W. Wang, *Non-Newtonian effects of blood flow on hemodynamics in distal vascular graft anastomoses.* J Biomech, 2006. **39**(11): p. 1983-95.

35. Chen, S. and T.A. Springer, *An automatic braking system that stabilizes leukocyte rolling by an increase in selectin bond number with shear.* J Cell Biol, 1999. **144**(1): p. 185-200.

36. Chen, S. and T.A. Springer, *Selectin receptor-ligand bonds: Formation limited by shear rate and dissociation governed by the Bell model.* Proc. Natl. Acad. Sci. U.S.A., 2001. **98**(3): p. 950-5.

37. Chiu, J.J., et al., *Analysis of the effect of disturbed flow on monocytic adhesion to endothelial cells.* J Biomech, 2003. **36**(12): p. 1883-95.

38. Chiu, J.J., et al., *Effects of disturbed flow on endothelial cells.* J Biomech Eng, 1998. **120**(1): p. 2-8.

39. Christ, K., et al., *Measurement of single-cell adhesion strength using a microfluidic assay.* Biomedical Microdevices, 2010. **12**(3): p. 443-455.

40. Christophis, C., et al., *Shear stress regulates adhesion and rolling of CD44+ leukemic and hematopoietic progenitor cells on hyaluronan.* Biophys J, 2011. **101**(3): p. 585-93.

41. Chung, B.J., A.M. Robertson, and D.G. Peters, *The numerical design of a parallel plate flow chamber for investigation of endothelial cell response to shear stress.* Comput Struct, 2003. **81**(8-11): p. 535-546.

42. Curtis, A.S., *The Mechanism of Adhesion of Cells to Glass. A Study by Interference Reflection Microscopy.* J Cell Biol, 1964. **20**: p. 199-215.

43. Damiano, E.R., et al., *Variation in the velocity, deformation, and adhesion energy density of leukocytes rolling within venules.* Circulation Research, 1996. **79**(6): p. 1122-1130.

44. Davies, P.F., *Flow-mediated endothelial mechanotransduction.* Physiol Rev, 1995. **75**(3): p. 519-60.

45. Davis, D.M. and S. Sowinski, *Membrane nanotubes: dynamic long-distance connections between animal cells.* Nature Reviews Molecular Cell Biology, 2008. **9**(6): p. 431-436.

46. Dembo, M., et al., *The reaction-limited kinetics of membrane-to-surface adhesion and detachment.* Proc R Soc Lond B Biol Sci, 1988. **234**(1274): p. 55-83.

47. Diamond, S., et al., *Cellular Aggregation in Blood Flow.* Comments on Theoretical Biology, 2000. **5**(6): p. 413-35.

48. Disdier, M., et al., *Cytoplasmic domain of P-selectin (CD62) contains the signal for sorting into the regulated secretory pathway.* Mol Biol Cell, 1992. **3**(3): p. 309-21.

49. Dong, C., et al., *Mechanics of leukocyte deformation and adhesion to endothelium in shear flow.* Ann Biomed Eng, 1999. **27**(3): p. 298-312.

50. Dong, C. and X.X. Lei, *Biomechanics of cell rolling: shear flow, cell-surface adhesion, and cell deformability.* J Biomech, 2000. **33**(1): p. 35-43.

51. Dong, Z.M., et al., *The combined role of P- and E-selectins in atherosclerosis.* J Clin Invest, 1998. **102**(1): p. 145-52.

52. Edington, C., et al., *Tailoring the trajectory of cell rolling with cytotactic surfaces.* Langmuir, 2011. **27**(24): p. 15345-51.

53. Eppihimer, M.J. and H.H. Lipowsky, *Leukocyte Sequestration in the Microvasculature in Normal and Low-Flow States.* American Journal of Physiology, 1994. **267**(3): p. H1122-H1134.

54. Eriksson, E.E., et al., *Direct viewing of atherosclerosis in vivo: plaque invasion by leukocytes is initiated by the endothelial selectins.* Faseb J, 2001. **15**(7): p. 1149-57.

55. Eriksson, E.E., et al., *Importance of primary capture and L-selectin-dependent secondary capture in leukocyte accumulation in inflammation and atherosclerosis in vivo.* J Exp Med, 2001. **194**(2): p. 205-18.

56. Evans, E., et al., *Nano- to microscale dynamics of P-selectin detachment from leukocyte interfaces. I. Membrane separation from the cytoskeleton.* Biophys J, 2005. **88**(3): p. 2288-98.

57. Evans, E., et al., *Mechanical switching and coupling between two dissociation pathways in a P-selectin adhesion bond.* Proc Natl Acad Sci U S A, 2004. **101**(31): p. 11281-6.

58. Evegren, P., L. Fuchs, and J. Revstedt, *Wall shear stress variations in a 90-degree bifurcation in 3D pulsating flows.* Medical Engineering & Physics, 2010. **32**(2): p. 189-202.

59. Fagerberg, B., et al., *Differences in lesion severity and cellular composition between in vivo assessed upstream and downstream sides of human symptomatic carotid atherosclerotic plaques.* J Vasc Res, 2010. **47**(3): p. 221-30.

60. Falati, S., et al., *Accumulation of tissue factor into developing thrombi in vivo is dependent upon microparticle P-selectin glycoprotein ligand 1 and platelet P-selectin.* The Journal of experimental medicine, 2003. **197**(11): p. 1585-98.

61. Finger, E.B., et al., *A differential role for cell shape in neutrophil tethering and rolling on endothelial selectins under flow.* J Immunol, 1996. **157**(11): p. 5085-96.

62. Finger, E.B., et al., *Adhesion through L-selectin requires a threshold hydrodynamic shear.* Nature, 1996. **379**(6562): p. 266-9.

63. Firrell, J.C. and H.H. Lipowsky, *Leukocyte margination and deformation in mesenteric venules of rat.* Am J Physiol, 1989. **256**(6 Pt 2): p. H1667-74.

64. Fleming, J.C., et al., *The transmembrane domain enhances granular targeting of P-selectin.* Eur J Cell Biol, 1998. **75**(4): p. 331-43.

65. Fong, A.M., et al., *Fractalkine and CX3CR1 mediate a novel mechanism of leukocyte capture, firm adhesion, and activation under physiologic flow.* J Exp Med, 1998. **188**(8): p. 1413-9.

66. Fox, J.A. and A.E. Hugh, *Localization of atheroma: a theory based on boundary layer separation.* Br Heart J, 1966. **28**(3): p. 388-99.

67. Foxall, C., et al., *The three members of the selectin receptor family recognize a common carbohydrate epitope, the sialyl Lewis(x) oligosaccharide.* The Journal of cell biology, 1992. **117**(4): p. 895-902.

68. Frangogiannis, N.G., C.W. Smith, and M.L. Entman, *The inflammatory response in myocardial infarction.* Cardiovasc Res, 2002. **53**(1): p. 31-47.

69. Frangos, J.A., et al., *Flow effects on prostacyclin production by cultured human endothelial cells.* Science, 1985. **227**(4693): p. 1477-9.

70. Friedman, M.H., V. O'Brien, and L.W. Ehrlich, *Calculations of pulsatile flow through a branch: implications for the hemodynamics of atherogenesis.* Circ Res, 1975. **36**(2): p. 277-85.

71. Fritz, J., et al., *Force-mediated kinetics of single P-selectin/ligand complexes observed by atomic force microscopy.* Proc. Natl. Acad. Sci. U.S.A., 1998. **95**(21): p. 12283-8.

72. Fukushima, T., et al., *Vortex Generation in Pulsatile Flow through Arterial Bifurcation Models Including the Human Carotid-Artery.* Journal of Biomechanical Engineering-Transactions of the Asme, 1988. **110**(3): p. 166-171.

73. Furie, B. and B.C. Furie, *Role of platelet P-selectin and microparticle PSGL-1 in thrombus formation.* Trends Mol Med, 2004. **10**(4): p. 171-8.

74. Furlow, M. and S.L. Diamond, *Interplay between membrane cholesterol and ethanol differentially regulates neutrophil tether mechanics and rolling dynamics.* Biorheology, 2011. **48**(1): p. 49-64.

75. Furman, M.I., et al., *Increased platelet reactivity and circulating monocyte-platelet aggregates in patients with stable coronary artery disease.* Journal of the American College of Cardiology, 1998. **31**(2): p. 352-8.

76. Gambaruto, A.M., D.J. Doorly, and T. Yamaguchi, *Wall shear stress and near-wall convective transport: Comparisons with vascular remodelling in a peripheral graft anastomosis.* Journal of Computational Physics, 2010. **229**(14): p. 5339-5356.

77. Gaver, D.P., 3rd and S.M. Kute, *A theoretical model study of the influence of fluid stresses on a cell adhering to a microchannel wall.* Biophys J, 1998. **75**(2): p. 721-33.

78. Gawaz, M., H. Langer, and A.E. May, *Platelets in inflammation and atherogenesis.* The Journal of clinical investigation, 2005. **115**(12): p. 3378-84.

79. Gerszten, R.E., et al., *MCP-1 and IL-8 trigger firm adhesion of monocytes to vascular endothelium under flow conditions.* Nature, 1999. **398**(6729): p. 718-23.

80. Gerszten, R.E., et al., *Adhesion of monocytes to vascular cell adhesion molecule-1-transduced human endothelial cells: implications for atherogenesis.* Circ Res, 1998. **82**(8): p. 871-8.

81. Gibson, C.M., et al., *Relation of vessel wall shear stress to atherosclerosis progression in human coronary arteries.* Arterioscler Thromb, 1993. **13**(2): p. 310-5.

82. Giddens, D.P., C.K. Zarins, and S. Glagov, *The Role of Fluid-Mechanics in the Localization and Detection of Atherosclerosis.* J Biomech Eng - Trans ASME, 1993. **115**(4): p. 588-594.

83. Gingell, D. and I. Todd, *Interference reflection microscopy. A quantitative theory for image interpretation and its application to cell-substratum separation measurement.* Biophys J, 1979. **26**(3): p. 507-26.

84. Girdhar, G. and J.Y. Shao, *Simultaneous tether extraction from endothelial cells and leukocytes: observation, mechanics, and significance.* Biophys J, 2007. **93**(11): p. 4041-52.

85. Glagov, S., et al., *Hemodynamics and Atherosclerosis - Insights and Perspectives Gained from Studies of Human Arteries.* Arch Pathol Lab Med, 1988. **112**(10): p. 1018-1031.

86. Goetz, D.J., et al., *Cell-cell adhesive interactions in an in vitro flow chamber.* Adhesion Protein Protocols, 1999. **96**: p. 137-145.

87. Goldman, A.J., R.G. Cox, and H. Brenner, *Slow Viscous Motion of a Sphere Parallel to a Plane Wall .2. Couette Flow.* Chemical Engineering Science, 1967. **22**(4): p. 653-&.

88. Granger, D.N. and P. Kubes, *The Microcirculation and Inflammation - Modulation of Leukocyte-Endothelial Cell-Adhesion.* Journal of Leukocyte Biology, 1994. **55**(5): p. 662-675.

89. Gutierrez, E. and A. Groisman, *Quantitative measurements of the strength of adhesion of human neutrophils to a substratum in a microfluidic device.* Anal Chem, 2007. **79**(6): p. 2249-2258.

90. Gutierrez, E., et al., *Microfluidic devices for studies of shear-dependent platelet adhesion.* Lab on a Chip, 2008. **8**(9): p. 1486-1495.

91. Hammer, D.A. and S.M. Apte, *Simulation of cell rolling and adhesion on surfaces in shear flow: general results and analysis of selectin-mediated neutrophil adhesion.* Biophys J, 1992. **63**(1): p. 35-57.

92. Hansson, G.K., *Immune mechanisms in atherosclerosis.* Arteriosclerosis, thrombosis, and vascular biology, 2001. **21**(12): p. 1876-90.

93. Hathcock, J.J., *Flow effects on coagulation and thrombosis.* Arteriosclerosis, thrombosis, and vascular biology, 2006. **26**(8): p. 1729-37.

94. Hattori, R., et al., *Stimulated secretion of endothelial von Willebrand factor is accompanied by rapid redistribution to the cell surface of the intracellular granule membrane protein GMP-140.* J Biol Chem, 1989. **264**(14): p. 7768-71.

95. Heinrich, V., A. Leung, and E. Evans, *Nano- to microscale dynamics of P-selectin detachment from leukocyte interfaces. II. Tether flow terminated by P-selectin dissociation from PSGL-1.* Biophys J, 2005. **88**(3): p. 2299-308.

96. Hidalgo, A., et al., *Complete identification of E-selectin ligands on neutrophils reveals distinct functions of PSGL-1, ESL-1, and CD44.* Immunity, 2007. **26**(4): p. 477-89.

97. House, S.D. and H.H. Lipowsky, *In vivo determination of the force of leukocyte-endothelium adhesion in the mesenteric microvasculature of the cat.* Circ Res, 1988. **63**(3): p. 658-68.

98. Hsiai, T.K., et al., *Monocyte recruitment to endothelial cells in response to oscillatory shear stress.* FASEB J, 2003. **17**(12): p. 1648-57.

99. Hung, T.C., et al., *Shear-induced aggregation and lysis of platelets.* Transactions - American Society for Artificial Internal Organs, 1976. **22**: p. 285-91.

100. Jadhav, S., B.S. Bochner, and K. Konstantopoulos, *Hydrodynamic shear regulates the kinetics and receptor specificity of polymorphonuclear leukocyte-colon carcinoma cell adhesive interactions.* J Immunol, 2001. **167**(10): p. 5986-93.

101. Jadhav, S., C.D. Eggleton, and K. Konstantopoulos, *A 3-D computational model predicts that cell deformation affects selectin-mediated leukocyte rolling.* Biophys J, 2005. **88**(1): p. 96-104.

102. Jander, S., et al., *Inflammation in high-grade carotid stenosis: a possible role for macrophages and T cells in plaque destabilization.* Stroke, 1998. **29**(8): p. 1625-30.

103. Jannat, R.A., et al., *Neutrophil adhesion and chemotaxis depend on substrate mechanics*, in *J Phys Condens Matter*. 2010. p. 194117.

104. Johnson, R.C., et al., *Absence of P-selectin delays fatty streak formation in mice.* J Clin Invest, 1997. **99**(5): p. 1037-43.

105. Johnston, B. and E.C. Butcher, *Chemokines in rapid leukocyte adhesion triggering and migration.* Semin Immunol, 2002. **14**(2): p. 83-92.

106. Johnston, B., T.B. Issekutz, and P. Kubes, *The alpha(4)-integrin supports leukocyte rolling and adhesion in chronically inflamed postcapillary venules in vivo.* Journal of Experimental Medicine, 1996. **183**(5): p. 1995-2006.

107. Johnston, G.I., R.G. Cook, and R.P. McEver, *Cloning of GMP-140, a granule membrane protein of platelets and endothelium: sequence similarity to proteins involved in cell adhesion and inflammation.* Cell, 1989. **56**(6): p. 1033-44.

108. Jou, L.D. and S.A. Berger, *Numerical simulation of the flow in the carotid bifurcation.* Theoretical and Computational Fluid Dynamics, 1998. **10**(1-4): p. 239-248.

109. Kadash, K.E., M.B. Lawrence, and S.L. Diamond, *Neutrophil string formation: hydrodynamic thresholding and cellular deformation during cell collisions.* Biophys J, 2004. **86**(6): p. 4030-9.

110. Keynton, R.S., S.E. Rittgers, and M.C. Shu, *The effect of angle and flow rate upon hemodynamics in distal vascular graft anastomoses: an in vitro model study.* J Biomech Eng, 1991. **113**(4): p. 458-63.

111. Khismatullin, D.B. and G.A. Truskey, *A 3D numerical study of the effect of channel height on leukocyte deformation and adhesion in parallel-plate flow chambers.* Microvasc Res, 2004. **68**(3): p. 188-202.

112. Khismatullin, D.B. and G.A. Truskey, *Three-dimensional numerical simulation of receptor-mediated leukocyte adhesion to surfaces: Effects of cell deformability and viscoelasticity.* Phys Fluids, 2005. **17**(3): p. 031505.

113. Khismatullin, D.B. and G.A. Truskey, *Leukocyte rolling on P-selectin: A 3D numerical study of the effect of cytoplasmic viscosity* Biophys J, 2012: p. (in press).

114. Kim, Y.J., et al., *Distinct selectin ligands on colon carcinoma mucins can mediate pathological interactions among platelets, leukocytes, and endothelium.* Am J Pathol, 1999. **155**(2): p. 461-72.

115. King, M.R., et al., *Nano-to-micro scale dynamics of P-selectin detachment from leukocyte interfaces. III. Numerical simulation of tethering under flow.* Biophys J, 2005. **88**(3): p. 1676-83.

116. Kirchhofer, D., M.A. Riederer, and H.R. Baumgartner, *Specific accumulation of circulating monocytes and polymorphonuclear leukocytes on platelet thrombi in a vascular injury model.* Blood, 1997. **89**(4): p. 1270-8.

117. Kochanek, P.M. and J.M. Hallenbeck, *Polymorphonuclear leukocytes and monocytes/macrophages in the pathogenesis of cerebral ischemia and stroke.* Stroke; a journal of cerebral circulation, 1992. **23**(9): p. 1367-79.

118. Ku, C.J., T. D'Amico Oblak, and D.M. Spence, *Interactions between multiple cell types in parallel microfluidic channels: monitoring platelet adhesion to an endothelium in the presence of an anti-adhesion drug.* Anal Chem, 2008. **80**(19): p. 7543-8.

119. Ku, D.N., *Blood flow in arteries.* Annual Review of Fluid Mechanics, 1997. **29**: p. 399-434.

120. Ku, D.N. and D.P. Giddens, *Pulsatile flow in a model carotid bifurcation.* Arteriosclerosis, 1983. **3**(1): p. 31-9.

121. Ku, D.N., et al., *Pulsatile flow and atherosclerosis in the human carotid bifurcation. Positive correlation between plaque location and low oscillating shear stress.* Arteriosclerosis, 1985. **5**(3): p. 293-302.

122. Kuczenski, R.S., H.C. Chang, and A. Revzin, *Dielectrophoretic microfluidic device for the continuous sorting of Escherichia coli from blood cells.* Biomicrofluidics, 2011. **5**(3): p. 032005-15.

123. Kuwano, Y., et al., *Rolling on E- or P-selectin induces the extended but not high-affinity conformation of LFA-1 in neutrophils.* Blood, 2010. **116**(4): p. 617-24.

124. Ladak, H.M., J.S. Milner, and D.A. Steinman, *Rapid three-dimensional segmentation of the carotid bifurcation from serial MR images.* J Biomech Eng, 2000. **122**(1): p. 96-9.

125. Lamkin-Kennard, K.A., et al., *The distribution of rolling neutrophils in venular convergences.* Biorheology, 2005. **42**(5): p. 363-83.

126. Langille, B.L. and F. O'Donnell, *Reductions in arterial diameter produced by chronic decreases in blood flow are endothelium-dependent.* Science, 1986. **231**(4736): p. 405-7.

127. Langille, B.L. and M. Ojha, *Blood flow dynamics, atherosclerosis and bypass graft failure.* Trends Cardiovasc Med, 1997. **7**(4): p. 111-8.

128. Laudanna, C., et al., *Rapid leukocyte integrin activation by chemokines.* Immunol Rev, 2002. **186**: p. 37-46.

129. Lawrence, M.B., et al., *Threshold levels of fluid shear promote leukocyte adhesion through selectins (CD62L,P,E).* J Cell Biol, 1997. **136**(3): p. 717-27.

130. Lawrence, M.B. and T.A. Springer, *Leukocytes roll on a selectin at physiologic flow rates: distinction from and prerequisite for adhesion through integrins.* Cell, 1991. **65**(5): p. 859-73.

131. Lawrence, M.B. and T.A. Springer, *Neutrophils Roll on E-Selectin.* Journal of Immunology, 1993. **151**(11): p. 6338-6346.

132. Lei, X., M.B. Lawrence, and C. Dong, *Influence of cell deformation on leukocyte rolling adhesion in shear flow.* J Biomech Eng, 1999. **121**(6): p. 636-43.

133. Leppanen, A., et al., *Binding of glycosulfopeptides to P-selectin requires stereospecific contributions of individual tyrosine sulfate and sugar residues.* J Biol Chem, 2000. **275**(50): p. 39569-78.

134. Ley, K., *Integration of inflammatory signals by rolling neutrophils.* Immunol Rev, 2002. **186**: p. 8-18.

135. Ley, K., *The role of selectins in inflammation and disease.* Trends Mol Med, 2003. **9**(6): p. 263-8.

136. Ley, K., et al., *Getting to the site of inflammation: the leukocyte adhesion cascade updated.* Nat Rev Immunol, 2007. **7**(9): p. 678-89.

137. Ley, K., T.F. Tedder, and G.S. Kansas, *L-Selectin Can Mediate Leukocyte Rolling in Untreated Mesenteric Venules in-Vivo Independent of E-Selection or P-Selectin.* Blood, 1993. **82**(5): p. 1632-1638.

138. Li, F., et al., *Post-translational modifications of recombinant P-selectin glycoprotein ligand-1 required for binding to P- and E-selectin.* J Biol Chem, 1996. **271**(6): p. 3255-64.

139. Li Jeon, N., et al., *Neutrophil chemotaxis in linear and complex gradients of interleukin-8 formed in a microfabricated device.* Nature biotechnology, 2002. **20**(8): p. 826-30.

140. Long, Q., et al., *Reconstruction of blood flow patterns in a human carotid bifurcation: a combined CFD and MRI study.* J Magn Reson Imaging, 2000. **11**(3): p. 299-311.

141. Lopes-Virella, M.F. and G. Virella, *Immune mechanisms of atherosclerosis in diabetes mellitus.* Diabetes, 1992. **41 Suppl 2**: p. 86-91.

142. Lu, H., et al., *Microfluidic Shear Devices for Quantitative Analysis of Cell Adhesion.* Analytical Chemistry, 2004. **76**(18): p. 5257-5264.

143. Ma, X.L., et al., *Monoclonal antibody to L-selectin attenuates neutrophil accumulation and protects ischemic reperfused cat myocardium.* Circulation, 1993. **88**(2): p. 649-58.

144. Majstoravich, S., et al., *Lymphocyte microvilli are dynamic, actin-dependent structures that do not require Wiskott-Aldrich syndrome protein (WASp) for their morphology.* Blood, 2004. **104**(5): p. 1396-403.

145. Malek, A.M., S.L. Alper, and S. Izumo, *Hemodynamic shear stress and its role in atherosclerosis.* JAMA : the journal of the American Medical Association, 1999. **282**(21): p. 2035-42.

146. Mallat, Z., et al., *Shed membrane microparticles with procoagulant potential in human atherosclerotic plaques: a role for apoptosis in plaque thrombogenicity.* Circulation, 1999. **99**(3): p. 348-53.

147. Marcus, W.D. and R.M. Hochmuth, *Experimental studies of membrane tethers formed from human neutrophils.* Annals of Biomedical Engineering, 2002. **30**(10): p. 1273-80.

148. Marshall, B.T., et al., *Direct observation of catch bonds involving cell-adhesion molecules.* Nature, 2003. **423**(6936): p. 190-3.

149. McEver, R.P., *Selectins: novel receptors that mediate leukocyte adhesion during inflammation.* Thromb Haemost, 1991. **65**(3): p. 223-8.

150. McEver, R.P., *Selectin-carbohydrate interactions during inflammation and metastasis.* Glycoconj J, 1997. **14**(5): p. 585-91.

151. McEver, R.P., *Adhesive interactions of leukocytes, platelets, and the vessel wall during hemostasis and inflammation.* Thrombosis and haemostasis, 2001. **86**(3): p. 746-56.

152. McEver, R.P., et al., *GMP-140, a platelet alpha-granule membrane protein, is also synthesized by vascular endothelial cells and is localized in Weibel-Palade bodies.* The Journal of clinical investigation, 1989. **84**(1): p. 92-9.

153. McEver, R.P. and M.N. Martin, *A monoclonal antibody to a membrane glycoprotein binds only to activated platelets.* J Biol Chem, 1984. **259**(15): p. 9799-804.

154. McEver, R.P. and C. Zhu, *Chapter 7 Biophysical Regulation of Selectin-Ligand Interactions Under Flow*, in *Current Topics in Membranes*, L. Klaus, Editor. 2009, Academic Press. p. 195-220.

155. McKinney, V.Z., K.D. Rinker, and G.A. Truskey, *Normal and shear stresses influence the spatial distribution of intracellular adhesion molecule-1 expression in human umbilical vein endothelial cells exposed to sudden expansion flow.* J Biomech, 2006. **39**(5): p. 806-17.

156. Melnick, M., *Pattern of Cell Rolling and Adhesion at Bifurcations*, in *Department of Chemical, Biological and Materials Engineering*. 2004, University of Oklahoma: Norman, OK.

157. Meng, H., et al., *Complex hemodynamics at the apex of an arterial bifurcation induces vascular remodeling resembling cerebral aneurysm initiation.* Stroke, 2007. **38**(6): p. 1924-31.

158. Migliorini, C., et al., *Red blood cells augment leukocyte rolling in a virtual blood vessel.* Biophysical Journal, 2002. **83**(4): p. 1834-1841.

159. Milner, J.S., et al., *Hemodynamics of human carotid artery bifurcations: computational studies with models reconstructed from magnetic resonance imaging of normal subjects.* J Vasc Surg, 1998. **28**(1): p. 143-56.

160. Miner, J.J., et al., *Separable requirements for cytoplasmic domain of PSGL-1 in leukocyte rolling and signaling under flow.* Blood, 2008. **112**(5): p. 2035-45.

161. Mitchell, D.J., et al., *Importance of L-selectin-dependent leukocyte-leukocyte interactions in human whole blood.* Blood, 2000. **95**(9): p. 2954-9.

162. Moore, K.L., et al., *P-Selectin Glycoprotein Ligand-1 Mediates Rolling of Human Neutrophils on P-Selectin.* Journal of Cell Biology, 1995. **128**(4): p. 661-671.

163. Moore, K.L., et al., *Identification of a specific glycoprotein ligand for P-selectin (CD62) on myeloid cells.* The Journal of cell biology, 1992. **118**(2): p. 445-56.

164. Morrissey, J.H., *Tissue factor: an enzyme cofactor and a true receptor.* Thrombosis and haemostasis, 2001. **86**(1): p. 66-74.

165. Morrissey, J.H., H. Fakhrai, and T.S. Edgington, *Molecular cloning of the cDNA for tissue factor, the cellular receptor for the initiation of the coagulation protease cascade.* Cell, 1987. **50**(1): p. 129-35.

166. Murthy, S.K., et al., *Effect of flow and surface conditions on human lymphocyte isolation using microfluidic chambers.* Langmuir, 2004. **20**(26): p. 11649-55.

167. Myers, D.D., et al., *P-selectin and leukocyte microparticles are associated with venous thrombogenesis.* J Vasc Surg, 2003. **38**(5): p. 1075-89.

168. N'dri, N.A., W. Shyy, and R. Tran-Soy-Tay, *Computational modeling of cell adhesion and movement using a continuum-kinetics approach.* Biophysical Journal, 2003. **85**(4): p. 2273-2286.

169. Nagel, T., et al., *Shear stress selectively upregulates intercellular adhesion molecule-1 expression in cultured human vascular endothelial cells.* The Journal of clinical investigation, 1994. **94**(2): p. 885-91.

170. Nakashima, Y., et al., *ApoE-deficient mice develop lesions of all phases of atherosclerosis throughout the arterial tree.* Arterioscler Thromb, 1994. **14**(1): p. 133-40.

171. Nalayanda, D.D., M. Kalukanimuttam, and D.W. Schmidtke, *Micropatterned surfaces for controlling cell adhesion and rolling under flow.* Biomedical Microdevices, 2007. **9**(2): p. 207-14.

172. Neeves, K.B., et al., *Microfluidic focal thrombosis model for measuring murine platelet deposition and stability: PAR4 signaling enhances shear-resistance of platelet aggregates.* J Thromb Haemost, 2008. **6**(12): p. 2193-201.

173. Nixon, A.M., M. Gunel, and B.E. Sumpio, *The critical role of hemodynamics in the development of cerebral vascular disease.* Journal of Neurosurgery, 2010. **112**(6): p. 1240-1253.

174. Norman, K.E., et al., *Leukocyte Rolling in-Vivo Is Mediated by P-Selectin Glycoprotein Ligand-1.* Blood, 1995. **86**(12): p. 4417-4421.

175. Oh, H. and S.L. Diamond, *Ethanol enhances neutrophil membrane tether growth and slows rolling on P-selectin but reduces capture from flow and firm arrest on IL-1-treated endothelium.* J Immunol, 2008. **181**(4): p. 2472-82.

176. Ojha, M., *Wall shear stress temporal gradient and anastomotic intimal hyperplasia.* Circ Res, 1994. **74**(6): p. 1227-31.

177. Onai, Y., et al., *Blockade of cell adhesion by a small molecule selectin antagonist attenuates myocardial ischemia/reperfusion injury.* Eur J Pharmacol, 2003. **481**(2-3): p. 217-25.

178. Osborn, L., *Leukocyte adhesion to endothelium in inflammation.* Cell, 1990. **62**(1): p. 3-6.

179. Palabrica, T., et al., *Leukocyte accumulation promoting fibrin deposition is mediated in vivo by P-selectin on adherent platelets.* Nature, 1992. **359**(6398): p. 848-51.

180. Papaharilaou, Y., D.J. Doorly, and S.J. Sherwin, *The influence of out-of-plane geometry on pulsatile flow within a distal end-to-side anastomosis.* J Biomech, 2002. **35**(9): p. 1225-39.

181. Pappu, V., S.K. Doddi, and P. Bagchi, *A computational study of leukocyte adhesion and its effect on flow pattern in microvessels.* Journal of Theoretical Biology, 2008. **254**(2): p. 483-498.

182. Park, E.Y., et al., *Comparison of PSGL-1 microbead and neutrophil rolling: microvillus elongation stabilizes P-selectin bond clusters.* Biophys J, 2002. **82**(4): p. 1835-47.

183. Park, S.T., et al., *Atherosclerotic carotid stenoses of apical versus body lesions in high-risk carotid stenting patients.* Am J Neuroradiol, 2010. **31**(6): p. 1106-12.

184. Patel, K.D., et al., *Neutrophils use both shared and distinct mechanisms to adhere to selectins under static and flow conditions.* The Journal of clinical investigation, 1995. **96**(4): p. 1887-96.

185. Patel, K.D., M.U. Nollert, and R.P. McEver, *P-selectin must extend a sufficient length from the plasma membrane to mediate rolling of neutrophils.* J Cell Biol, 1995. **131**(6 Pt 2): p. 1893-902.

186. Pawar, P., et al., *Roles of cell and microvillus deformation and receptor-ligand binding kinetics in cell rolling.* Am J Physiol Heart Circ Physiol, 2008. **295**(4): p. H1439-50.

187. Pearson, M.J. and H.H. Lipowsky, *Influence of erythrocyte aggregation on leukocyte margination in postcapillary venules of rat mesentery.* American Journal of Physiology-Heart and Circulatory Physiology, 2000. **279**(4): p. H1460-H1471.

188. Pedersen, E.M., A.P. Yoganathan, and X.P. Lefebvre, *Pulsatile Flow Visualization in a Model of the Human Abdominal-Aorta and Aortic Bifurcation.* J Biomech, 1992. **25**(8): p. 935-944.

189. Pierres, A., et al., *How cells tiptoe on adhesive surfaces before sticking.* Biophys J, 2008. **94**(10): p. 4114-22.

190. Pierres, A., et al., *Cell membrane alignment along adhesive surfaces: contribution of active and passive cell processes.* Biophys J, 2003. **84**(3): p. 2058-70.

191. Polley, M.J., et al., *CD62 and endothelial cell-leukocyte adhesion molecule 1 (ELAM-1) recognize the same carbohydrate ligand, sialyl-Lewis x.* Proc Natl Acad Sci U S A, 1991. **88**(14): p. 6224-8.

192. Pospieszalska, M.K. and K. Ley, *Dynamics of Microvillus Extension and Tether Formation in Rolling Leukocytes.* Cell Mol Bioeng, 2009. **2**(2): p. 207-217.

193. Pospieszalska, M.K., et al., *Event-tracking model of adhesion identifies load-bearing bonds in rolling leukocytes.* Microcirculation, 2009. **16**(2): p. 115-30.

194. Pozrikidis, C., *Effect of pressure gradient on viscous shear flow past an axisymmetric depression or protuberance on a plane wall.* Computers & Fluids, 2000. **29**(6): p. 617-637.

195. Prabhakarpandian, B., et al., *Synthetic microvascular networks for quantitative analysis of particle adhesion.* Biomed Microdev, 2008. **10**(4): p. 585-95.

196. Prabhakarpandian, B., et al., *Microfluidic devices for modeling cell-cell and particle-cell interactions in the microvasculature.* Microvasc Res, 2011. **82**(3): p. 210-20.

197. Ramachandran, V., et al., *Dynamic alterations of membrane tethers stabilize leukocyte rolling on P-selectin.* Proc. Natl. Acad. Sci. U.S.A., 2004. **101**(37): p. 13519-24.

198. Ramos, C.L., et al., *Direct demonstration of P-selectin- and VCAM-1-dependent mononuclear cell rolling in early atherosclerotic lesions of apolipoprotein E-deficient mice.* Circ Res, 1999. **84**(11): p. 1237-44.

199. Ranjan, V., Z. Xiao, and S.L. Diamond, *Constitutive NOS expression in cultured endothelial cells is elevated by fluid shear stress.* Am J Physiol, 1995. **269**(2 Pt 2): p. H550-5.

200. Raucher, D. and M.P. Sheetz, *Characteristics of a membrane reservoir buffering membrane tension.* Biophys J, 1999. **77**(4): p. 1992-2002.

201. Reininger, A.J., et al., *Mechanism of platelet adhesion to von Willebrand factor and microparticle formation under high shear stress.* Blood, 2006. **107**(9): p. 3537-3545.

202. Rinker, K.D., et al., *Linoleic acid increases monocyte deformation and adhesion to endothelium.* Atherosclerosis, 2004. **177**(2): p. 275-85.

203. Rinko, L.J., M.B. Lawrence, and W.H. Guilford, *The molecular mechanics of P- and L-selectin lectin domains binding to PSGL-1.* Biophys J, 2004. **86**(1 Pt 1): p. 544-54.

204. Ritter, L.S., et al., *Leukocyte accumulation and hemodynamic changes in the cerebral microcirculation during early reperfusion after stroke.* Stroke, 2000. **31**(5): p. 1153-61.

205. Roach, M.R., *Biophysical analyses of blood vessel walls and blood flow.* Annu Rev Physiol, 1977. **39**: p. 51-71.

206. Rodgers, S.D., R.T. Camphausen, and D.A. Hammer, *Sialyl Lewis(x)-mediated, PSGL-1-independent rolling adhesion on P-selectin.* Biophys J, 2000. **79**(2): p. 694-706.

207. Rodgers, S.D., R.T. Camphausen, and D.A. Hammer, *Tyrosine sulfation enhances but is not required for PSGL-1 rolling adhesion on P-selectin.* Biophys J, 2001. **81**(4): p. 2001-9.

208. Rosenbluth, M.J., W.A. Lam, and D.A. Fletcher, *Analyzing cell mechanics in hematologic diseases with microfluidic biophysical flow cytometry.* Lab Chip, 2008. **8**(7): p. 1062-70.

209. Rosenfeld, M.E., et al., *Fatty streak initiation in Watanabe Heritable Hyperlipemic and comparably hypercholesterolemic fat-fed rabbits.* Arteriosclerosis, 1987. **7**(1): p. 9-23.

210. Ross, R., *Atherosclerosis--an inflammatory disease.* N Engl J Med, 1999. **340**(2): p. 115-26.

211. Rouleau, L., et al., *Neutrophil adhesion on endothelial cells in a novel asymmetric stenosis model: effect of wall shear stress gradients.* Ann Biomed Eng, 2010. **38**(9): p. 2791-804.

212. Ruehl, M.L., et al., *Protective effects of inhibiting both blood and vascular selectins after stroke and reperfusion.* Neurol Res, 2002. **24**(3): p. 226-32.

213. Saadi, W., et al., *A parallel-gradient microfluidic chamber for quantitative analysis of breast cancer cell chemotaxis.* Biomedical Microdevices, 2006. **8**(2): p. 109-118.

214. Sarvepalli, D.P., D.W. Schmidtke, and M.U. Nollert, *Design considerations for a microfluidic device to quantify the platelet adhesion to collagen at physiological shear rates.* Ann Biomed Eng, 2009. **37**(7): p. 1331-41.

215. Schaff, U.Y., et al., *Vascular mimetics based on microfluidics for imaging the leukocyte--endothelial inflammatory response.* Lab Chip, 2007. **7**(4): p. 448-56.

216. Schaff, U.Y., et al., *Calcium flux in neutrophils synchronizes beta2 integrin adhesive and signaling events that guide inflammatory recruitment.* Ann Biomed Eng, 2008. **36**(4): p. 632-46.

217. Schmid-Schonbein, G.W., et al., *Passive mechanical properties of human leukocytes.* Biophys J, 1981. **36**(1): p. 243-56.

218. Schmid-Schonbein, G.W., et al., *Interaction of Leukocytes and Erythrocytes in Capillary and Post-Capillary Vessels.* Microvascular research, 1980. **19**(1): p. 45-70.

219. Schmidtke, D.W. and S.L. Diamond, *Direct observation of membrane tethers formed during neutrophil attachment to platelets or P-selectin under physiological flow.* J Cell Biol, 2000. **149**(3): p. 719-30.

220. Sengupta, K., et al., *Spreading of neutrophils: from activation to migration.* Biophys J, 2006. **91**(12): p. 4638-48.

221. Setiadi, H. and R.P. McEver, *Clustering endothelial E-selectin in clathrin-coated pits and lipid rafts enhances leukocyte adhesion under flow.* Blood, 2008. **111**(4): p. 1989-98.

222. Setiadi, H., et al., *Interactions of the cytoplasmic domain of P-selectin with clathrin-coated pits enhance leukocyte adhesion under flow.* Journal of Cell Biology, 1998. **142**(3): p. 859-871.

223. Shao, J.Y. and R.M. Hochmuth, *Micropipette suction for measuring piconewton forces of adhesion and tether formation from neutrophil membranes.* Biophys J, 1996. **71**(5): p. 2892-901.

224. Shao, J.Y., H.P. Ting-Beall, and R.M. Hochmuth, *Static and dynamic lengths of neutrophil microvilli.* Proc. Natl. Acad. Sci. U.S.A., 1998. **95**(12): p. 6797-802.

225. Simon, D.I., et al., *Platelet glycoprotein ibalpha is a counterreceptor for the leukocyte integrin Mac-1 (CD11b/CD18).* The Journal of experimental medicine, 2000. **192**(2): p. 193-204.

226. Simon, D.I., et al., *Decreased neointimal formation in Mac-1(-/-) mice reveals a role for inflammation in vascular repair after angioplasty.* The Journal of clinical investigation, 2000. **105**(3): p. 293-300.

227. Sin, A., et al., *Enrichment using antibody-coated microfluidic chambers in shear flow: model mixtures of human lymphocytes.* Biotechnol Bioeng, 2005. **91**(7): p. 816-26.

228. Skilbeck, C., et al., *Population of the vessel wall by leukocytes binding to P-selectin in a model of disturbed arterial flow.* Arteriosclerosis, thrombosis, and vascular biology, 2001. **21**(8): p. 1294-300.

229. Skilbeck, C.A., et al., *Disturbed flow promotes deposition of leucocytes from flowing whole blood in a model of a damaged vessel wall.* Br J Haematol, 2004. **126**(3): p. 418-27.

230. Smith, M.L., et al., *Viscosity-independent velocity of neutrophils rolling on p-selectin in vitro or in vivo.* Microcirculation, 2002. **9**(6): p. 523-36.

231. Smith, M.L., et al., *Viscosity-independent velocity of neutrophils rolling on P-selectin in vitro or in vivo.* Microcirculation, 2002. **9**(6): p. 523-536.

232. Sperandio, M., et al., *P-selectin glycoprotein ligand-1 mediates L-selectin-dependent leukocyte rolling in venules.* The Journal of experimental medicine, 2003. **197**(10): p. 1355-63.

233. Springer, T.A., *Traffic signals for lymphocyte recirculation and leukocyte emigration: the multistep paradigm.* Cell, 1994. **76**(2): p. 301-14.

234. Suh, S.H., et al., *Significance of hemodynamic effects on the generation of atherosclerosis.* Journal of Mechanical Science and Technology, 2005. **19**(3): p. 836-845.

235. Sun, C.H., C. Migliorini, and L.L. Munn, *Red blood cells initiate leukocyte rolling in postcapillary expansions: A lattice Boltzmann analysis.* Biophysical Journal, 2003. **85**(1): p. 208-222.

236. Sundd, P., et al., *Quantitative dynamic footprinting microscopy reveals mechanisms of neutrophil rolling.* Nat Methods, 2010. **7**(10): p. 821-4.

237. Svindland, A., *The localization of sudanophilic and fibrous plaques in the main left coronary bifurcation.* Atherosclerosis, 1983. **48**(2): p. 139-45.

238. Tedder, T.F., et al., *Isolation and chromosomal localization of cDNAs encoding a novel human lymphocyte cell surface molecule, LAM-1. Homology with the mouse lymphocyte homing receptor and other human adhesion proteins.* J Exp Med, 1989. **170**(1): p. 123-33.

239. Tempelman, L.A., S. Park, and D.A. Hammer, *Motion of Model Leukocytes near a Wall in Simple Shear Flow.* Biotechnology Progress, 1994. **10**(1): p. 97-108.

240. Truskey, G.A., et al., *Characterization of a sudden expansion flow chamber to study the response of endothelium to flow recirculation.* J Biomech Eng, 1995. **117**(2): p. 203-10.

241. Truskey, G.A. and J.S. Pirone, *The effect of fluid shear stress upon cell adhesion to fibronectin-treated surfaces.* Journal of Biomedical Materials Research, 1990. **24**(10): p. 1333-1353.

242. Tsai, M.A., R.S. Frank, and R.E. Waugh, *Passive mechanical behavior of human neutrophils: power-law fluid.* Biophys J, 1993. **65**(5): p. 2078-88.

243. Tsao, P.S., et al., *Exposure to shear stress alters endothelial adhesiveness. Role of nitric oxide.* Circulation, 1995. **92**(12): p. 3513-9.

244. Tseng, Y., et al., *Micro-organization and visco-elasticity of the interphase nucleus revealed by particle nanotracking.* J Cell Sci, 2004. **117**(Pt 10): p. 2159-67.

245. Urschel, K., et al., *Role of shear stress patterns in the TNF-alpha-induced atherogenic protein expression and monocytic cell adhesion to endothelium.* Clin Hemorheol Microcirc, 2010. **46**(2-3): p. 203-10.

246. Ushiyama, S., et al., *Structural and functional characterization of monomeric soluble P-selectin and comparison with membrane P-selectin.* J Biol Chem, 1993. **268**(20): p. 15229-37.

247. van der Wal, A.C., et al., *Site of intimal rupture or erosion of thrombosed coronary atherosclerotic plaques is characterized by an inflammatory process irrespective of the dominant plaque morphology.* Circulation, 1994. **89**(1): p. 36-44.

248. Vestweber, D. and J.E. Blanks, *Mechanisms that regulate the function of the selectins and their ligands.* Physiol Rev, 1999. **79**(1): p. 181-213.

249. Walcheck, B., et al., *Neutrophil rolling altered by inhibition of L-selectin shedding in vitro.* Nature, 1996. **380**(6576): p. 720-3.

250. Waugh, R.E. and R.M. Hochmuth, *Mechanical Equilibrium of Thick, Hollow, Liquid Membrane Cylinders.* Biophysical Journal, 1987. **52**(3): p. 391-400.

251. Waugh, R.E., et al., *Membrane instability in late-stage erythropoiesis.* Blood, 2001. **97**(6): p. 1869-75.

252. Wayman, A.M., et al., *Triphasic force dependence of E-selectin/ligand dissociation governs cell rolling under flow.* Biophys J, 2010. **99**(4): p. 1166-74.

253. Weber, C. and T.A. Springer, *Neutrophil accumulation on activated, surface-adherent platelets in flow is mediated by interaction of Mac-1 with fibrinogen bound to alphaIIbbeta3 and stimulated by platelet-activating factor.* The Journal of clinical investigation, 1997. **100**(8): p. 2085-93.

254. Westrick, R.J., et al., *Deficiency of tissue factor pathway inhibitor promotes atherosclerosis and thrombosis in mice.* Circulation, 2001. **103**(25): p. 3044-6.

255. White, C.R., et al., *Temporal gradients in shear, but not spatial gradients, stimulate endothelial cell proliferation.* Circulation, 2001. **103**(20): p. 2508-13.

256. White, C.R., et al., *Temporal gradients in shear, but not spatial gradients, stimulate ERK1/2 activation in human endothelial cells.* Am J Physiol Heart Circ Physiol, 2005. **289**(6): p. H2350-5.

257. Williams, M., *The Role of Membrane Tether Formation in Neutrophil rolling on Selectin Coated Surfaces*, in *Department of Chemical, Biological and Materials Engineering*. 2003, University of Oklahoma: Norman, OK.

258. Xia, L., et al., *P-selectin glycoprotein ligand-1-deficient mice have impaired leukocyte tethering to E-selectin under flow.* The Journal of clinical investigation, 2002. **109**(7): p. 939-50.

259. Yago, T., et al., *Distinct molecular and cellular contributions to stabilizing selectin-mediated rolling under flow.* J Cell Biol, 2002. **158**(4): p. 787-799.

260. Yago, T., et al., *Catch bonds govern adhesion through L-selectin at threshold shear.* J Cell Biol, 2004. **166**(6): p. 913-23.

261. Yago, T., et al., *Transport governs flow-enhanced cell tethering through L-selectin at threshold shear.* Biophys J, 2007. **92**(1): p. 330-42.

262. Yang, J., et al., *Targeted gene disruption demonstrates that P-selectin glycoprotein ligand 1 (PSGL-1) is required for P-selectin-mediated but not E-selectin-mediated neutrophil rolling and migration.* The Journal of experimental medicine, 1999. **190**(12): p. 1769-82.

263. Yang, X., et al., *Traffic of leukocytes in microfluidic channels with rectangular and rounded cross-sections.* Lab Chip, 2011. **11**(19): p. 3231-40.

264. Zarbock, A., C.A. Lowell, and K. Ley, *Spleen tyrosine kinase Syk is necessary for E-selectin-induced alpha(L)beta(2) integrin-mediated rolling on intercellular adhesion molecule-1.* Immunity, 2007. **26**(6): p. 773-83.

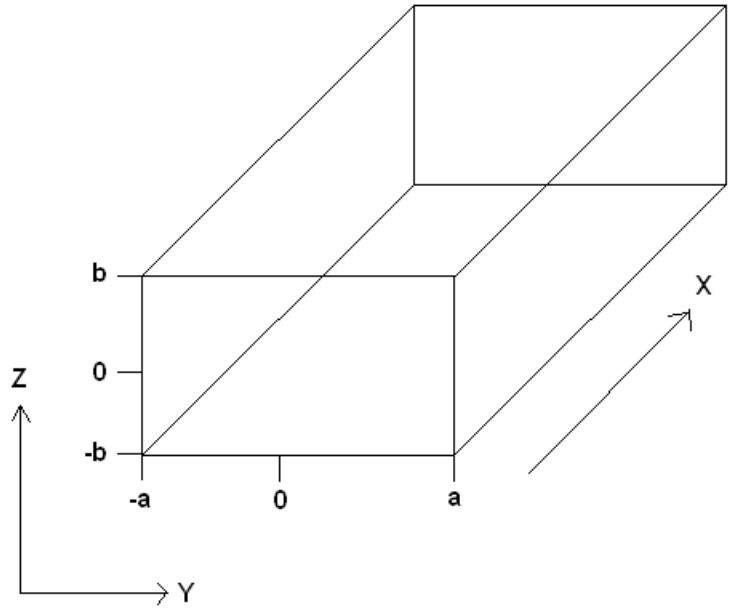
265. Zarins, C.K., et al., *Carotid bifurcation atherosclerosis. Quantitative correlation of plaque localization with flow velocity profiles and wall shear stress.* Circ Res, 1983. **53**(4): p. 502-14.

266. Zhao, S.Z., et al., *Blood flow and vessel mechanics in a physiologically realistic model of a human carotid arterial bifurcation.* J Biomech, 2000. **33**(8): p. 975-84.

267. Zhelev, D.V., D. Needham, and R.M. Hochmuth, *Role of the membrane cortex in neutrophil deformation in small pipets.* Biophys J, 1994. **67**(2): p. 696-705.

Appendix A: Mathematical description of flow in a rectangular channel

For a rectangular channel…



where a > b, height (H) = 2b and width (W) = 2a…

$$\rho\left(\frac{\partial v_x}{\partial t}+v_x\frac{\partial v_x}{\partial x}+v_y\frac{\partial v_x}{\partial y}+v_z\frac{\partial v_x}{\partial z}\right)=-\frac{dP}{dx}+\mu\left(\frac{\partial^2 v_x}{\partial x^2}+\frac{\partial^2 v_x}{\partial y^2}+\frac{\partial^2 v_x}{\partial z^2}\right)+\rho g_x$$

Assumptions

1. Steady State
2. Incompressible Flow
3. Laminar Flow
4. No gravity in x direction

$$\rho\left(\cancel{\frac{\partial v_x}{\partial t}}^{1}+v_x\cancel{\frac{\partial v_x}{\partial x}}^{2}+v_y\cancel{\frac{\partial v_x}{\partial y}}^{3}+v_z\cancel{\frac{\partial v_x}{\partial z}}^{3}\right)=-\frac{dP}{dx}+\mu\left(\cancel{\frac{\partial^2 v_x}{\partial x^2}}^{2}+\frac{\partial^2 v_x}{\partial y^2}+\frac{\partial^2 v_x}{\partial z^2}\right)+\cancel{\rho g_x}^{4}$$

This implies that,

$$o = -\frac{dP}{dx} + \mu\left(\frac{\partial^2 v_x}{\partial y^2} + \frac{\partial^2 v_x}{\partial z^2}\right)$$

Rearranging gives,

$$\frac{1}{\mu}\frac{dP}{dx} = \left(\frac{\partial^2 v_x}{\partial y^2} + \frac{\partial^2 v_x}{\partial z^2}\right)$$

Solving this differential equation for v_x gives the following equation,

$$v_x = \frac{1}{2}\frac{\Delta P}{\mu L}\left(z^2 - b^2\right) + \sum_{n=0}^{\infty} A_n \cos\frac{(2n+1)\pi z}{2b}\cosh\frac{(2n+1)\pi y}{2b}$$

where b = H/2 and a = W/2. To solve for A_n, use the boundary condition of $v_x = 0$ at y = a and rearrange to get,

$$-\frac{1}{2}\frac{\Delta P}{\mu L}\left(z^2 - b^2\right) = \sum_{n=0}^{\infty} A_n \cos\frac{(2n+1)\pi z}{2b}\cosh\frac{(2n+1)\pi a}{2b}$$

From here, you are solving for the Fourier coefficient, A_n, using the formula,

$$A_n = \frac{\frac{1}{b}\int_{-b}^{b} -\frac{1}{2}\frac{\Delta P}{\mu L}\left(z^2 - b^2\right)\cos\frac{(2n+1)\pi z}{2b}}{\cosh\frac{(2n+1)\pi a}{2b}}$$

Performing the integration results in,

$$A_n = \frac{16b^2\left(\frac{\Delta P}{\mu L}\right)(-1)^n}{[(2n+1)\pi]^3 \cosh\left(\frac{(2n+1)\pi a}{2b}\right)}$$

Now we can solve for the total flow rate and the shear rate.

For the volumetric flow rate,

$$Q = \int_{-a}^{a}\int_{-b}^{b} v_x dz dy$$

and for the wall shear rates,

$$\gamma_y = \frac{\partial v_x}{\partial y} \quad \text{and} \quad \gamma_z = \frac{\partial v_x}{\partial z}$$

Since the series

$$\sum_{n=0}^{\infty} \frac{16b^2\left(\frac{\Delta P}{\mu L}\right)(-1)^n}{[(2n+1)\pi]^3 \cosh\left(\frac{(2n+1)\pi a}{2b}\right)} \cos\frac{(2n+1)\pi z}{2b} \cosh\frac{(2n+1)\pi a}{2b}$$

converges to 0 as n approaches infinity, it can be neglected in the solution of Q and γ_y and γ_z if a is sufficiently larger than b. When this condition is met, the wall shear rate along the width of the channel is nearly uniform over almost the entire width.

Given that we can neglect the series term, the equation for the volumetric flow rate reduces to,

$$Q = \int_{-a}^{a}\int_{-b}^{b} \frac{1}{2}\frac{\Delta P}{\mu L}\left(z^2 - b^2\right) dz dy$$

Performing the integration results in,

$$Q=\frac{-4\Delta P b^3 a}{3\mu L}$$

This formula can be rearranged to solve for ΔP as follows,

$$\Delta P=\frac{-3Q\mu L}{4b^3 a}$$

The equation for shear rate in the z-direction now becomes,

$$\gamma_z=\frac{\partial v_x}{\partial z}=\frac{\partial}{\partial z}\left(\frac{3Q}{8b^3 a}\left(z^2-b^2\right)\right)$$

which results in,

$$\gamma_z=\frac{3Qz}{4b^3 a}$$

or for the wall shear rate (z = ±b),

$$\gamma_{z_w}=\frac{3Q}{4b^2 a}$$

Remember that a = W/2 and b = H/2. Therefore,

$$\gamma_{z_w}=\frac{3Q\mu}{4b^2 a}=\frac{3Q\mu}{4\left(\frac{H}{2}\right)^2\left(\frac{W}{2}\right)}=\frac{3Q\mu}{4\left(\frac{H^2 W}{8}\right)}=\frac{6Q\mu}{H^2 W}$$

Appendix B: Neutrophil Isolation Protocols

Dextran Sedimentation Protocol

- Add 7.5 mL dextran to a syringe containing 15 mL whole blood. Invert syringe and allow to sit for 1 h.
- Following sedimentation, the top layer will contain leukocytes, platelets and plasma and some RBCs. This layer should be removed and spun at 500 g for 10 min.
- Remove supernatant. RBCs contained in pellet can be lysed by adding 10 mL of 0.2% NaCl followed immediately by 10 mL of 1.6% NaCl. Spin at 500 g for 5 min.
- Remove supernatant. Resuspend pellet in 5 mL of 0.5% HSA/HBSS.
- Layer new suspension on top of 6 mL Histopaque 1077. Spin at 500 g for 30 min.
- Remove supernatant. Resuspend pellet in 5 mL of 0.5% HSA/HBSS. Spin at 500 g for 5 min. Repeat two more times.
- Count cells with hemocytometer. Dilute to desired concentration.

Lympholyte Separation Protocol

- Layer 5 mL of whole blood on top of 5 mL Lympholyte-poly. Spin at 400 g for 30 min.
- Following the spin, there will be two layers of leukocytes visible. The first layer will be mononuclear leukocytes and should be discarded. The second

layer is granulocytes. Remove this layer and dilute it first with 5 mL 0.4 % NaCl and then with 10 mL HBSS. Spin at 500 g for 10 min.

- Remove supernatant. If RBCs were collected with granulocyte layer, they can be lysed by adding 10 mL of 0.2% NaCl followed by 10 mL of 1.6% NaCl. Spin at 500 g for 5 min.
- Remove supernatant. Resuspend pellet in 5 mL 0.5% HSA/HBSS. Spin at 500 g for 5 min. Repeat two more times.
- Count cells with hemocytometer. Dilute to desired concentration.

Appendix C: Photolithography Protocol

- Glass substrates for photolithography must first be cleaned using the following organic series: TCE, methanol, acetone. Sonicate a substrate in 100 mL of each chemical for 5 min. Rinse by sonicating in DI H_2O for 5 min. Substrates should be dried with compressed air and then allowed to sit in an oven for 10 min to fully dry.
- Once substrates are dry, photoresist can be spun onto them using the spin coater with the following parameters based on desired template size. Note that SU-8 photoresists must be preceded by a layer of Omnicoat spun at 3000 rpm for 30 s.

Size (μm x μm, W x H)	Photoresist	Spin Speeds (rpm)*	UV Exposure Time (s)
200 x 20	SU-8 2015	500/2000	15
300 x 30	SU-8 2015	500/1300	20
750 x 75	KMPR 1050	500/1700	45
1000 x 100	KMPR 1050	500/1000	60
1500 x 150	SU-8 2100	500/2000	90

*Photoresist was spun onto substrates using a two step process (spread cycle/spin cycle).

- After photoresist is spun onto substrates, it must be heated to drive out moisture. SU-8 resists are heated at 65ºC for 10 min and 95ºC for 30 min. KMPR resists are heated at 100ºC for 10 min. Substrates must be allowed to cool to room temperature before UV exposure.
- Following UV exposure, substrates are again heated to catalyze the curing process. SU-8 resists are heated at 65º for 1 min and 95ºC for 10 min. KMPR resists are heated at 100ºC for 5 min. Substrates must be allowed to cool to room temperature before developing.

- SU-8 and KMPR resists can both be developed with SU-8 developer. Develop by sonicating in 25 mL of developer for 60 – 120 s.
- After sonication, rinse excess developer away with isopropyl alcohol and dry template with compressed air.
- Examine template under a microscope. If it appears the template is peeling away from the substrate, bake it on a hot plate set to 125ºC for 5 min and allow it to cool to room temperature.

Note: Bake times are dependent on the ambient humidity. Photolithography done on extremely humid days may require longer bake times before UV exposure.